



UNIVERSITEIT•STELLENBOSCH•UNIVERSITY
jou kennisvenoot • your knowledge partner

10 kW L-Band Planar Power Combiner

by

Gerhardus Johannes Fourie

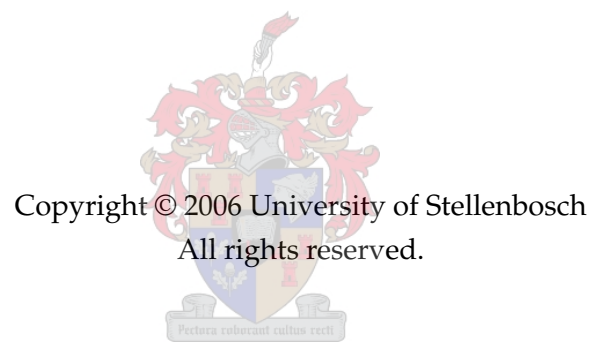


*Thesis presented at the University of Stellenbosch in
partial fulfilment of the requirements for the degree of*

Master of Science in Electronic Engineering

Supervisors: Dr. C. van Niekerk and Prof. P.W. van der Walt

April 2006



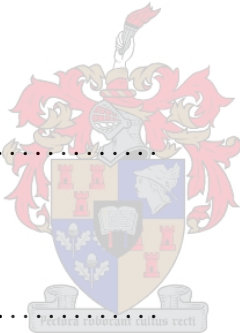
Declaration

I, the undersigned, hereby declare that the work contained in this thesis is my own original work and that I have not previously in its entirety or in part submitted it at any university for a degree.

Signature:

G.J. Fourie

Date:



Abstract

This thesis relates to the design and characterization of a 10 kW L-band power combiner consisting of 8 input ports. The design is implemented in a non-radial planar transmission line architecture and operates between 1.2 and 1.4 GHz.

Because of the ultra high power requirements for the combiner, special attention is given to the power handling capabilities of the transmission lines and the other components involved. Simulated S-parameter models of connector to stripline transitions and a one to four-way junction, as well as measured S-parameter models of high power terminations are incorporated in the final design.

A 10 kW combiner was built and measured at low power only due to time constraints and the limited availability of high power sources. Satisfactory results were obtained in terms of the graceful degradation of unit amplifiers, port mismatches and power combining efficiency.



Opsomming

Hierdie tesis handel oor die ontwerp en meet van 'n 10 kW L-band drywingskombineerder. Die kombineerder ontwerp beskik oor 8 intree poorte en word in 'n nie-radiale planêre transmisielyn argitektuur geïmplementeer. Dit word ook gespesifiseer om tussen 1.2 en 1.4 GHz te werk.

As gevolg van die ultra hoë drywingsvermoë van die kombineerder, word spesiale aandag aan transmisielyne en ander komponente gegee in terme van hulle vermoë om baie hoë drywing te kan hanteer. Gesimuleerde S-parameter modelle van konnektor oorgange en een na vier-poort transmisielyn verbindings, asook gemete S-parameter modelle van hoëdrywing terminasies word in die finale ontwerp gebruik.

'n Prototipe van die 10 kW kombineerder was gebou en gemeet by lae drywing. Geen hoëdrywing toetse kon uitgevoer word nie as gevolg van die gebrek aan tyd en beskikbare hoë drywingsbronne. Bevredigende resultate is verkry in terme van die stelselmatige degradasie van eenheidversterkers, poort refleksies en die kombineringsdoeltreffendheid van die kombineerder.

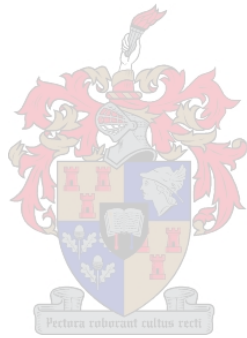
Acknowledgements

I would like to express my sincere gratitude to the following people and organisations who have contributed to making this work possible:

- Wessel Croukamp en Lincoln Saunders for constructing the prototype and all the other designs
- Ashley Cupido for manufacturing of the printed circuit boards
- DuPont and Advanced Polymers for providing Teflon™ samples
- Dries van Schalkwyk and Applied Wave Research for the use of Microwave Office
- EM Software & Systems - S.A. (Pty) Ltd for the use of FEKO
- Computer Simulated Technology for the use of Microwave Studio
- Dr C. van Niekerk of the University of Stellenbosch and Prof P.W. van der Walt of Reutech Radar Systems (Pty) Ltd as my co-supervisors
- Reutech Radar Systems for providing the opportunity and funding for this thesis
- Willem Burger and Dr C. van Niekerk for providing the presented photographs

Contents

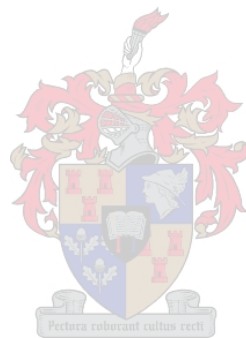
Declaration	ii
Abstract	iii
Opsomming	iv
Acknowledgements	v
Contents	vi
List of Figures	x
List of Tables	xv
1 Introduction	1
2 Power Combiners	3
2.1 Introduction	3
2.2 Wilkinson Power Combiners	3
2.2.1 High Power Resistor Measurement and Modeling	5
2.3 Gysel Power Combiner	10
2.3.1 High Power Termination Measurement and Modeling	13
2.3.2 Power Rating of Isolation Terminations	15
2.3.3 1.3 GHz Gysel Power Combiner Design	15



2.4	Fork-Type Power Combiner	16
2.4.1	Isolation Network Power Rating	23
2.4.2	Improving Bandwidth, Matching and Isolation	23
2.5	Conclusion	23
3	Four-Way Combiner Junction Design	24
3.1	Introduction	24
3.2	Possible Explanations for Poor Junction Performance	25
3.3	Four-Way Junction Analysis	25
3.3.1	Junctions Implemented in Microstrip	26
3.3.2	Junctions Implemented in Stripline or Shielded Microstrip	29
3.3.3	Improved MATLAB Drawn Junction Implemented in Stripline	31
3.4	Practical Design and Measurement	32
3.5	Conclusion	36
4	Power Handling Capability	38
4.1	Introduction	38
4.2	Peak Power Handling Capability of Shielded Microstrip	39
4.3	Average Power Handling Capability of Stripline and Shielded Microstrip	40
4.3.1	Stripline Transmission Line Losses	41
4.3.2	Impact of Conductor Surface Profile	42
4.3.3	Strip Transmission Line Heating	43
4.3.4	Thermal Performance Comparison	43
4.4	Power Handling Capability of Coaxial Connectors	45
4.5	Power Handling Capability of Resistors and Terminations	46
4.6	Conclusion	46
5	10 kW L-Band 8-Way Planar Power Combiner Design	48

5.1	Introduction	48
5.2	Basic Theoretical Design	49
5.3	Practical Design Considerations	50
5.3.1	Substrate	50
5.3.2	Transmission Lines Configurations, Temperatures and Voltage Breakdown	51
5.3.3	Connectors	53
5.3.4	Solder	54
5.3.5	Terminations	54
5.4	Prototype Design	55
5.4.1	Altered Theoretical Design	55
5.4.2	7/16-Type Connector Transition Design	56
5.4.3	N-Type Connector Transition Design	58
5.4.4	Junction Design	59
5.4.5	Layout and Microwave Analysis	60
5.5	Conclusion	65
6	Performance Evaluation	68
6.1	Introduction	68
6.2	S-Parameter Measurement of the 8-Way Power Combiner During Normal Operation	68
6.3	S-Parameter Measurement of the 8-Way Power Combiner During Fault Conditions	73
6.4	Conclusion	75
7	Conclusions	77
	Appendices	79
A	MATLAB Code for Drawn DXF Junction	80

<i>CONTENTS</i>	ix
B Thermal Performance Calculation MATLAB Code	85
C Taconic Product Guide	89
List of References	92



List of Figures

2.1	Transmission line schematic of the Wilkinson power combiner.	4
2.2	L-band Wilkinson power combiner frequency response. Marker m1 shows the perfect power division at centre frequency. Marker m2 shows the excellent isolation and matching of the device.	5
2.3	Basic chip resistor mounted on a flange.	6
2.4	Basic model of a chip resistor.	7
2.5	Resistor DUT block.	7
2.6	Model created of a 150 W 100 Ω resistor.	8
2.7	S_{21} of modeled vs measured resistor.	8
2.8	S_{22} of modeled vs measured resistor.	9
2.9	Poor S-parameters of a Wilkinson combiner simulated with the measured 150 W 100 Ω resistor. The top marker shows the transmission response at a maximum of 4.1 dB (1 dB worse then before).	9
2.10	A typical Gysel isolation network for a two-way combiner.	10
2.11	Symmetric form of the Gysel power combiner.	11
2.12	Gysel combiner circuit for even mode excitation.	11
2.13	Gysel combiner circuit for odd mode excitation.	12
2.14	Circuit schematic of a basic two-way Gysel power combiner.	12
2.15	L-Band Gysel power combiner frequency response. The horizontal marker shows the minimum port reflections and isolation between the ports. Marker m2 shows the perfect division of the power.	13
2.16	TRL termination (DUT) block with the two terminations.	14

2.17	Close-up photo of the 100 W, 50 Ω termination with the bent tab.	14
2.18	Bent and Flat Tab Termination Measurement.	15
2.19	Physical layout of a 50 Ω termination (left) with a equivalent model (right).	16
2.20	A comparison between a measured and modeled 100 W, 50 Ω termination on an enlarged Smith Chart.	17
2.21	Circuit schematic of a Gysel power combiner implementing 100 W, 50 Ω measured termination models.	17
2.22	S-parameters of Gysel power combiner with measured isolation terminations. The horizontal marker shows the minimum isolation between ports and and the maximum port reflections. Marker m2 shows that equal power division still takes place. .	18
2.23	Built L-band Gysel power combiner with top shield removed.	18
2.24	Measured vs simulated port reflections of a two-way Gysel power combiner.	19
2.25	Measured vs simulated transmission response of a two-way Gysel power combiner.	19
2.26	Measured vs simulated port isolation of a two-way Gysel power combiner.	20
2.27	4-Way fork-type combiner.	20
2.28	Schematic of a 4-way fork-type combiner using resistors.	21
2.29	Port matching and isolation for a 4-way fork-type combiner using resistors.	21
2.30	Schematic four-way fork-type combiner using terminations.	22
2.31	Port matching and isolation of a four-way fork-type combiner using terminations. .	22
3.1	TEM electric field and current distribution on microstrip.	25
3.2	Theoretical binomial matching transformer to be used for analysis.	26
3.3	Surface current of a binomial transformer junction simulated in FEKO using a 1.524 mm substrate.	27
3.4	Complete binomial matching transformer consisting of the junction and completed quarter-wave transmission lines.	27
3.5	Surface current of a binomial transformer junction simulated in FEKO using a 0.5 mm substrate.	29

3.6	Surface current of a binomial transformer junction simulated in FEKO using a stripline architecture. Groundplane spacing = 3.048 mm and $\epsilon_r = 3$	30
3.7	Basic junction drawn with the MATLAB code.	31
3.8	Surface current of a binomial transformer junction drawn with MATLAB and simulated in FEKO.	33
3.9	Four-way divider with the top shield removed.	34
3.10	Four-way junction simulated in CST Microwave Studio using discrete ports at the outputs.	35
3.11	Transmission response comparison between a measured and simulated four-way divider.	35
3.12	Input reflection comparison between a measured and simulated four-way divider.	36
4.1	Shielded microstrip dimensions as defined by [1].	40
4.2	Shielded microstrip breakdown voltage design graph at 760 Torr as given by [1].	41
5.1	Circuit diagram of an ideal 8-way power combiner consisting of a four-way fork-type combiner and four two-way Gysel combiners.	49
5.2	Optimised isolation network for a four-way fork-type combiner.	50
5.3	Isolation network for a Gysel combiner.	50
5.4	Transmission response, port reflections and isolation of an ideal 8-way combiner.	50
5.5	Stripline (left) and shielded microstrip (right) implementation and dimensions.	52
5.6	Lowering impedances with the use of a second order transformer.	55
5.7	Practical theoretical design schematic using a second order transformer and 180° extension sections.	56
5.8	7/16-Type connector representation with a custom made contact pin.	57
5.9	7/16-Type connector centre cutplane representation with custom made contact pin.	57
5.10	7/16-Type connector implementation to avoid voltage breakdown and to ensure good heat flow.	58
5.11	Foam and Teflon™ washer simulated with CST Microwave Studio.	58
5.12	S_{11} of foam and Teflon™ isolation configuration.	59

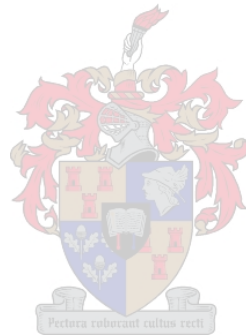
5.13	7/16-Type connector transition simulated in CST Microwave Studio.	59
5.14	Isolating enclosure and Teflon TM washer (left). 7/16 Connector with foam washer and contact pin (right).	60
5.15	N-Type connector transition simulated in CST Microwave Studio.	60
5.16	S_{11} of N-type connector transition simulated in CST Microwave Studio.	61
5.17	Four-way junction simulated in Feko with meshing triangles shown.	61
5.18	Transmission response of inner and outer strips.	62
5.19	Phase response of inner and outer strips.	62
5.20	Circuit layout of the 8-way combiner design.	63
5.21	8-Way combiner port reflections. Markers m1 and m2 give the maximum port reflections of the input ports and output port respectively.	64
5.22	8-Way combiner transmission response. Markers m1 and m2 give the minimum transmission response of the inner and outer Gysel sections respectively.	64
5.23	8-Way combiner port isolation with marker m1 showing the minimum isolation mark.	65
5.24	8-Way power combiner design output power assuming 125 W unit amplifiers.	65
5.25	Average output power when a unit amplifier fails at one of the centre Gysel sections.	66
5.26	Average output power when a unit amplifier fails at one of the outer Gysel sections.	66
5.27	Average output power when a whole middle Gysel section fails.	66
5.28	Average output power when a whole outer Gysel section fails.	66
5.29	3D Representation of the 8-way power combiner design with the top ground cover removed.	67
6.1	8-Way power combiner circuit with top shield removed.	69
6.2	Measured port reflections of the 8-way power combiner.	70
6.3	Comparison between measured and simulated transmission response of the 8-way power combiner.	71
6.4	Measured phase response of the 8-way power combiner	71
6.5	Comparison between the measured and simulated input port isolation of the 8-way power combiner	72

6.6 Comparison between the simulated output power and the calculated output power from the S-parameter measurement for the case where no Gysel combiner port fails. 73

6.7 Comparison between the simulated output power and the calculated output power from the S-parameter measurement for the case where an outer Gysel combiner port fails. 74

6.8 Comparison between the simulated output power and the calculated output power from the S-parameter measurement for the case where a centre Gysel combiner port fails. 74

6.9 Comparison between the simulated output power and the calculated output power from the S-parameter measurement for the case where the input unit amplifiers of a whole Gysel section fails. 75



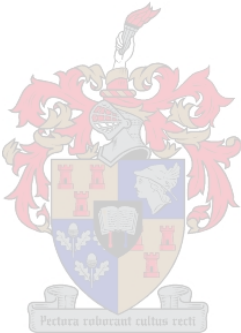
List of Tables

3.1	Analysis results of the binomial transformer implemented in 1.524 mm thick microstrip	27
3.2	Coupled line values used for approximating the splitting lines. Point of separation starts on the left.	28
3.3	Binomial matching transformer results of Microwave Office approximated design using coupling line models.	28
3.4	Analysis results of binomial transformer implemented in 0.5 mm thick microstrip.	29
3.5	Analysis results of binomial transformer implemented in 3.048 mm thick stripline.	30
3.6	Analysis results of binomial transformer implemented in stripline with a ground plane spacing of 3.048 mm using a junction drawn using MATLAB code.	34
3.7	Performance comparison between the measured and simulated matching transformer.	36
4.1	Thermal performance example comparison: 18 μm copper.	44
4.2	Thermal performance example comparison: 35 μm copper	45
4.3	Typical average power and voltage ratings of high power coaxial connectors [2].	46
5.1	Material and dimension properties of Taconic TLY-5 substrate to be used for the design.	51
5.2	Maximum line impedances capable of handling the power at the different combining sections.	52
5.3	Maximum power dissipation in isolation terminations when a single unit amplifier fails.	54
5.4	Maximum power dissipation in isolation terminations when two adjacent unit amplifiers situated on the outside fail.	54

5.5 Simulated effect of various fault conditions on the performance of the designed power combiner. 66

6.1 Maximum port reflections of the 8-way power combiner. 70

6.2 Measured performance specifications of constructed combiner including various fault conditions. 76



Chapter 1

Introduction

Many applications require microwave power sources with output levels which are higher than what a single amplifier unit can deliver. This problem is resolved through the utilization of power combiners which are used to combine the output power of several devices or amplifiers.

Power combining methods range from complex spatial techniques [3],[4] to the more commonly used transmission line techniques. Spatial power combiners implement antenna arrays and are limited to only a few hundred Watt due to size and heat dissipation problems. These combiners are limited to frequencies in the millimeter range and above, due to their limited size and improved efficiency at these higher frequencies.

Transmission line combiners have become the most popular type of combiner for L and S-band frequencies, and are known to be capable of handling several kilowatts of power [5],[6]. These types of combiners consist of planar radial [7],[6],[8],[9], planar non-radial [8],[10],[11],[12][5], and coaxial combiners [13]. The primary reason for the popularity of these combiners, lie in their relative ease of fabrication and ease of integration with other passive and active microwave devices. This is especially true in the case of the planar power combiners constructed out of strip or microstrip transmission lines. Transmission line combiners are purely passive circuits and are implemented with well known networks such as the Wilkinson [14], Gysel [7] and N-way fork-type [12] combiners.

Radial power combiners and coaxial combiners have very good performance due to their perfect symmetry and are most commonly used in high power applications. Due to the unconventional shape and port arrangements of these type of dividers, physical integration with other systems is more difficult than with planar fork-type combiners.

While non-radial planar combiners with only a few ports are fairly easy to design and show good performance, non-radial combiners with several ports have problems with size, complexity and poorer performance. These problems are amplified considerably when implementing designs for ultra high power applications.

The aim of this study is to design and construct a working 8-way 10 kW L-band power combiner capable of operating at temperatures as high as 65°C and at altitudes as high as 3000m above sea level. The average power rating of the combiner is specified as 1 kW. This combiner will be implemented in a non-radial planar configuration.

Chapter 2 opens the study by looking at various planar combiner configurations and their respective implementation difficulties, especially at high power. Models of high power resistors and terminations are also constructed and their performance investigated.

Chapter 3 examines the performance of a few one to n-way junctions with the intention to create and model an acceptable n-way junction. These junctions are commonly used in n-way combiners and have performance problems due to discontinuities at the point of separation.

Chapter 4 looks at an important aspect of any high power design, namely the power handling capabilities of the components to be used. By predicting the power handling capability of all components, a measure of the combiner's theoretical power rating can be created.

In Chapter 5 a practical prototype combiner is designed and simulated with special attention to the power handling capability, while Chapter 6 presents the measured performance of a built prototype.



Chapter 2

Power Combiners

2.1 Introduction

Power combiners are passive microwave components used for power combining or power division. The simplest power combiners are three-port networks with two input ports and one output port. A passive combiner implies that the component is reciprocal and it is shown (Pozar [15],p309) that a three-port network cannot be lossless, reciprocal and matched at all ports. If a combiner contains lossy components it can be made to be matched at all ports, although the input ports may not be isolated.

Except for the basic requirement of any n-way combiner which is to obtain n-times the output power of a single amplifier, combiners should also be able to fail gracefully. This means that when one or more unit amplifiers fail, it should not significantly affect the power combining of the the remaining amplifier units. Also, if arbitrary failures of unit amplifiers occur, such failures should not affect the impedances seen at the other ports.

Power combiners such as the Wilkinson [14], Gysel [7] and N-way fork-type [12] form the basis of most transmission line combiners and are covered in Sections 2.2, 2.3 and 2.4 respectively.

Imperfect components in circuits can have a significant effect on performance and need to be considered in a thorough design. Section 2.2.1 shows the effect of a high power, thermally floating resistor on the performance of a Wilkinson power combiner while section 2.3.1 shows the effect of a high power termination on the performance of a Gysel power combiner.

2.2 Wilkinson Power Combiners

Wilkinson power combiners [14] make use of the fact that a lossy three-port network can be made to have all the ports matched with isolation between the ports. These N-port networks

(N inputs/ 1 output) implement isolation resistors between the input ports and have the useful property of being lossless when the input ports are matched. Only the reflected power is dissipated in the isolation resistor.

The combiner will be lossless when an equal amount of power is applied at the two inputs. Even when the two input levels are not closely matched in power, only a small penalty is paid in output power. It is shown by [16] that when the input signals differ by as much as 1 dB, combining efficiency will still be 97 % with

$$\text{combining efficiency percentage} = \frac{\text{total output power}}{\text{total input power}} \times 100. \quad (2.2.1)$$

The simplest Wilkinson combiner is the a single-section 2-way and consists of two 70.7Ω quarter-wavelength transformers with a 100Ω resistor between them (Figure 2.1). A complete analysis of this combiner can be done with even-odd mode analysis and is shown in ([15],p320). The 2-way Wilkinson combiner is quite useful for limited bandwidth applications and with additional quarter wave transformers the useful bandwidth can be improved. Figure 2.2 shows the frequency response of a L-band Wilkinson combiner.

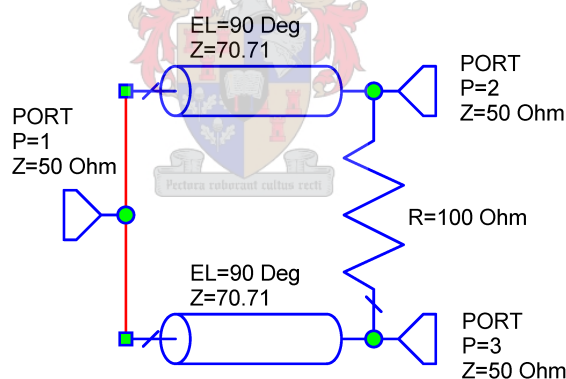


Figure 2.1: Transmission line schematic of the Wilkinson power combiner.

With these characteristics mentioned, the Wilkinson seems to be an attractive choice for a combiner. This is only true for low power applications with $N = 2$ or radial combiners. Implementation of these types of combiners for N larger than 2 in non-radial planar form are difficult and require crossovers to keep the design completely symmetric with respect to every port. The close placement of all the resistors also creates thermal and layout problems in practice.

Consequently, a corporate branch structure can be used as an alternative which uses a network of two-way combiners. The disadvantage of the corporate structure is that it is very lossy for a large value of N and that it can become quite large [9]. Input/output ports are also limited to an even number.

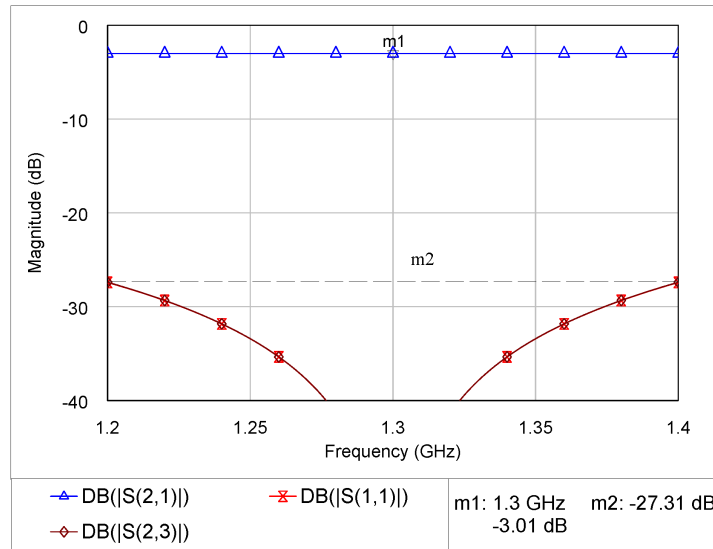


Figure 2.2: L-band Wilkinson power combiner frequency response. Marker m1 shows the perfect power division at centre frequency. Marker m2 shows the excellent isolation and matching of the device.

When realized as a three-port network, the combiner still has a problem with the implementation of high power isolation resistors. The performance of a Wilkinson combiner can be significantly reduced if non-ideal isolation resistors are used.

2.2.1 High Power Resistor Measurement and Modeling

For high power Wilkinson combiner applications, high power resistors are needed to absorb reflected power whenever a fault occurs. Thermally floating isolation resistors however are not suitable for high power applications. These high power resistors are extremely capacitive due to the proximity of the resistive film to ground. Figure 2.3 shows a picture of a basic chip resistor mounted on a flange.

The small distance between the resistive film and ground, is necessary to ensure low temperature rise. This derivation can be made from the basic formulas for one-dimensional steady state heat flow and one-dimensional capacitance.

$$T - T_A = \Delta T = P \frac{D}{kA} \quad (^\circ\text{C}) \quad (2.2.2)$$

where

- T = Temperature of film ($^\circ\text{C}$)
- T_A = Ambient temperature ($^\circ\text{C}$)
- P = Power dissipated in film (W)
- D = Substrate thickness (m)
- A = Area of film (m^2)

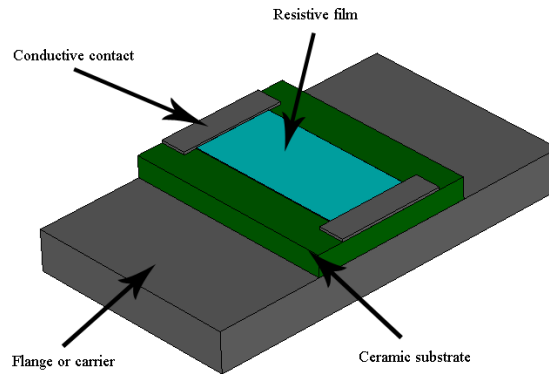


Figure 2.3: Basic chip resistor mounted on a flange.

k = Thermal conductivity of substrate ($\text{W}/\text{m}/^\circ\text{C}$)

For the same temperature rise, the higher the power dissipation, the thinner the substrate thickness has to be assuming that all other dimension are kept the same. The relation between the power dissipation capability of a resistor and the capacitance to ground is given by

$$C_g = 8.85 \frac{A\epsilon}{D} \quad (\text{pF}) \quad (2.2.3)$$

where

C_g = Capacitance to ground (pF)

ϵ = relative dielectric constant

which shows that, the thinner the substrate, the greater the film capacitance to ground.

Considering the layout of the resistor shown in Figure 2.3, a basic model of a chip resistor can be constructed as shown in Figure 2.4.

To investigate the capacitive nature of a high power resistor, a 150 W, 100 Ω flanged resistor (Barry Industries, RA1000-150-4S) is measured on a HP8510 network analyzer using a Thru-Reflect-Line (TRL) calibration technique [17]. The TRL calibration technique enables the reference plane of measurement to be shifted up to the contact tabs of the resistor.

Figure 2.5 shows a picture of the DUT (Device under test) block on which the resistor is mounted. A perspex press together with low permittivity foam ($\epsilon_r = 1.09$) is used to press the resistor tabs down onto the transmission lines.

With the measured S-parameters imported into Microwave Office, and by using the model

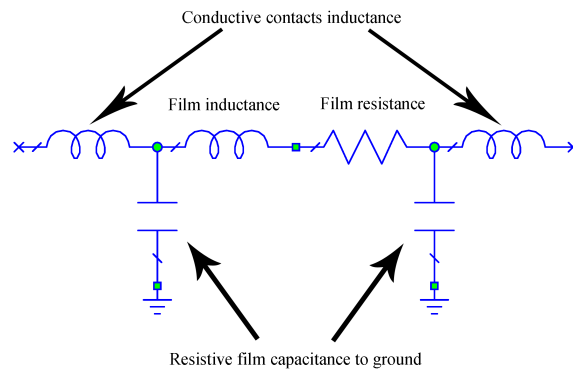


Figure 2.4: Basic model of a chip resistor.

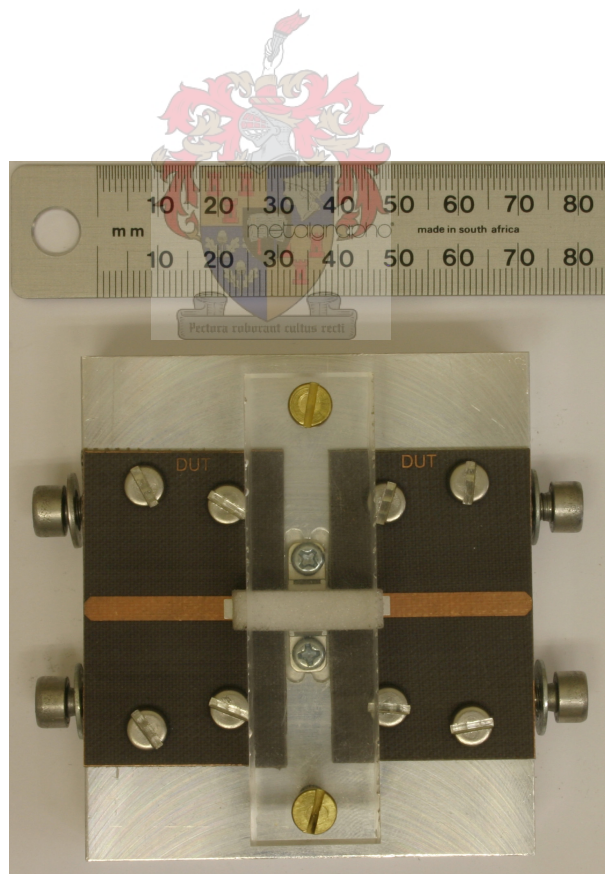


Figure 2.5: Resistor DUT block.

structure proposed in Figure 2.4, a simple model is created through parameter optimization. Figure 2.6 gives the component values of the resistor model while Figures 2.7 and 2.8 show the close comparison between the modeled and measured S_{21} and S_{22} S-parameters respectively.

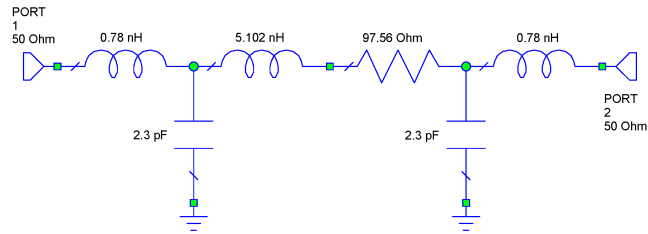


Figure 2.6: Model created of a 150 W 100 Ω resistor.

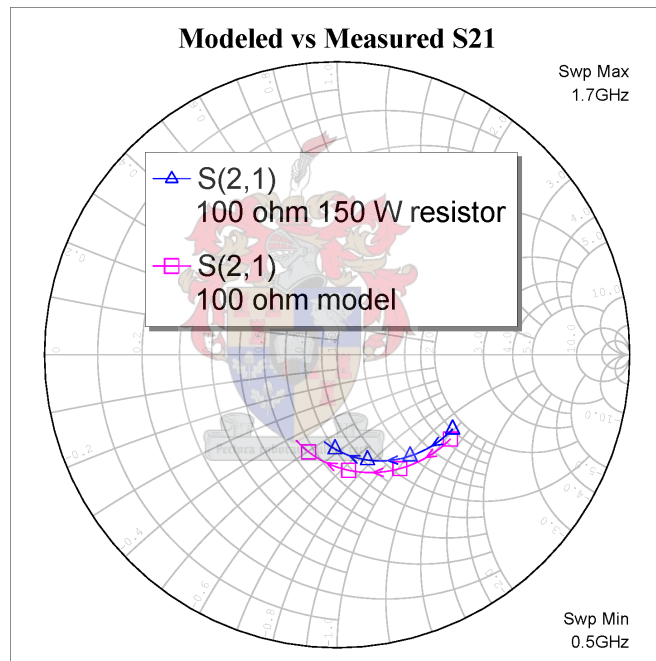


Figure 2.7: S_{21} of modeled vs measured resistor.

This simple model shows a total capacitance to ground of 4.6 pF which is expected considering the high power capability of the resistor. It should also be noted that a large film inductance of 5.1 nH is present in the model, added by the manufacturers to compensate for the unavoidable capacitance.

Current flow caused by the capacitance to ground result in losses and mismatched ports. To investigate the effect of such large capacitance on the performance of a 2-way Wilkinson power combiner, a simulation is performed in Microwave Office where the 100 Ω resistor is substituted with the 100 W 100 Ω S-parameter measurement.

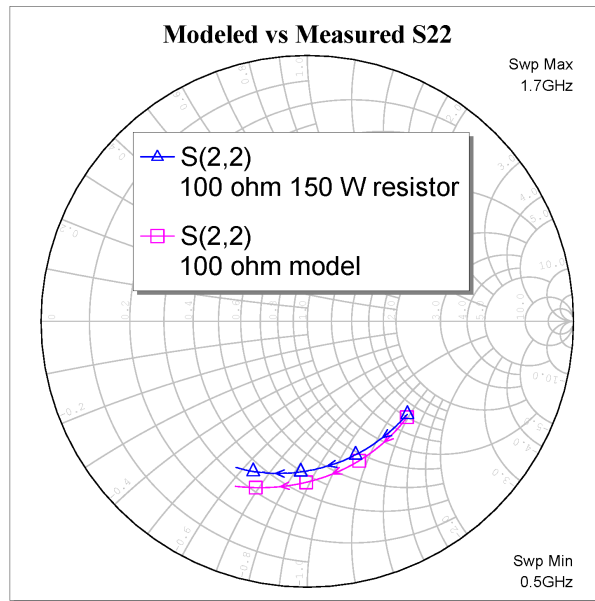


Figure 2.8: S_{22} of modeled vs measured resistor.

Figure 2.9 shows the poor S-parameter simulation results caused by the capacitive resistor. More than 1 dB of loss is introduced by the imperfect capacitive resistor while output mismatch is decreased to a poor 5.8 dB (21 dB more than the ideal case). These results show that high power resistors, having a large capacitance to ground, are not suitable for the Wilkinson power combiner configuration and alternative means must be looked at.

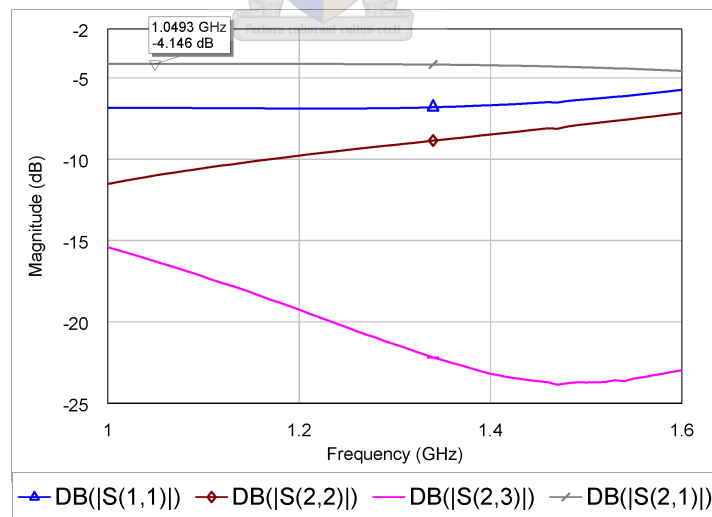


Figure 2.9: Poor S-parameters of a Wilkinson combiner simulated with the measured 150 W 100 Ω resistor. The top marker shows the transmission response at a maximum of 4.1 dB (1 dB worse than before).

2.3 Gysel Power Combiner

Section 2.2 showed that Wilkinson power combiners are not suitable for high power applications because of the high power capacitive resistors which must be used and the effect it has on performance. An alternative to the Wilkinson design is investigated in this chapter.

Gysel power combiners are similar to Wilkinson power combiners in the sense that both devices are constructed by quarter-wavelength transformers with isolation between them. The only difference between these two devices are the isolation networks.

Where the Wilkinson device uses a single resistor for isolation, the Gysel design's isolation network uses a combination of quarter-wavelength transmission lines and shunt-connected resistors as shown in Figure 2.10.

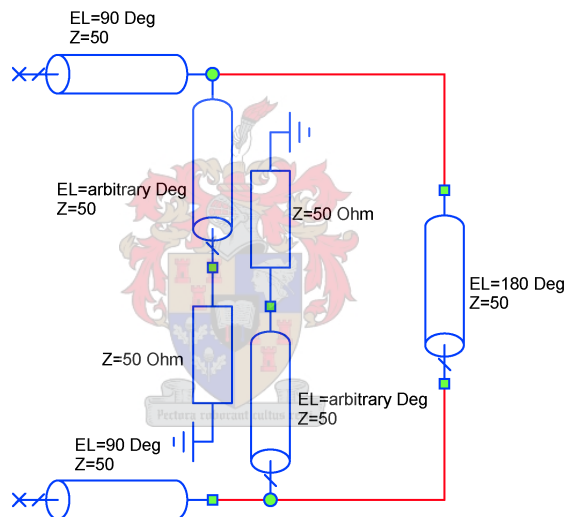


Figure 2.10: A typical Gysel isolation network for a two-way combiner.

The Gysel combiner has the distinct advantage that it uses two terminations for power dissipation instead of the single resistor as in the case of the Wilkinson design. The Gysel design also allows arbitrary lengths of transmission line before the terminations, providing more geometrical freedom for placing terminations. Both of these factors make the Gysel combiner more suitable for high power applications.

The matching and isolating properties of the Gysel power combiner are investigated through the use of even and odd mode analysis. The symmetric form of the Gysel combiner circuit is shown in Figure 2.11 where nodes A and B can either be short or open circuit nodes, depending on the mode of excitation.

For even mode operation, signals of equal excitation are applied to the two input ports and thus no current flows through nodes A and B and these nodes are thus replaced by open circuits.

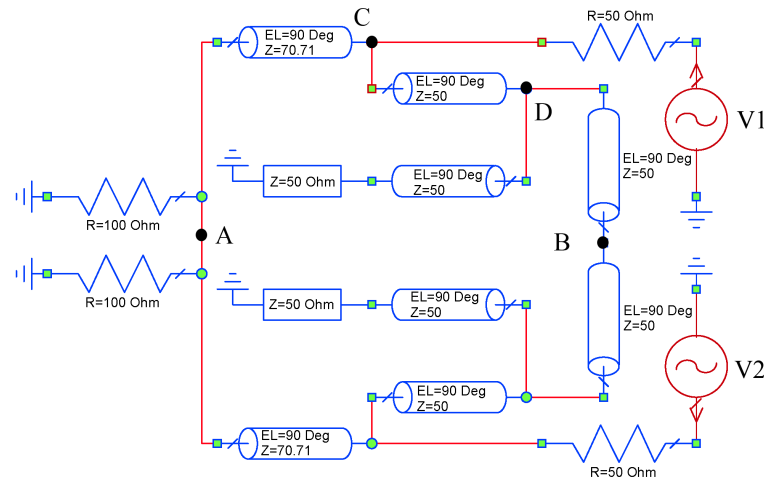


Figure 2.11: Symmetric form of the Gysel power combiner.

The open circuit point at B can now be transformed into a short circuit point at point D, due to the $\lambda/4$ long transmission line and again to an open circuit point at C. Figure 2.12 shows the even mode and resulting simplified even mode circuit of the combiner and shows that the isolation network is neglected during even mode operation. For this mode of excitation all power is delivered to the output of the combiner.

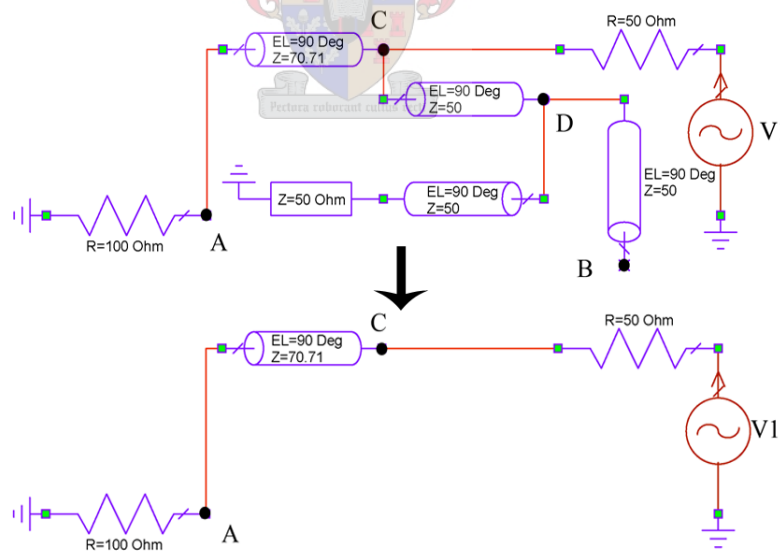


Figure 2.12: Gysel combiner circuit for even mode excitation.

For odd mode operation the isolating properties of the combiner is investigated by applying two excitation signals at the input ports with 180 degrees of phase difference between them. This results in a voltage null along the middle of the circuit which grounds nodes A and B. Due to $\lambda/4$ long transmission lines nodes A and B transform to open circuits at C and D as

shown in Figure 2.13. For odd mode excitation the ports are still matched while all power is now delivered to the isolation terminations.

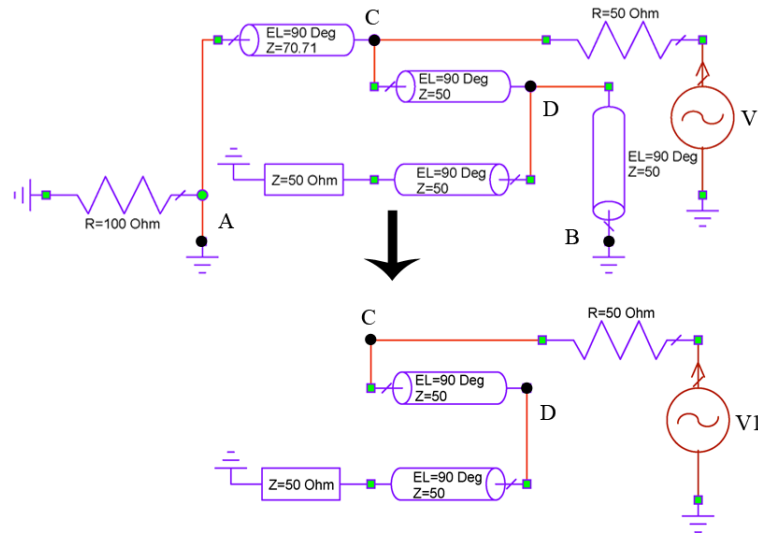


Figure 2.13: Gysel combiner circuit for odd mode excitation.

It should be noted that closed form solutions for optimum design parameters do not exist for the Gysel combiner. Computer aided optimization must be used to obtain parameter values to give minimum VSWR's for all ports and maximum isolation between input ports over the required bandwidth. The parameter value for the 180 degrees transmission line in the isolation network in Figure 2.10, was found through optimization using Microwave Office and serve as a good starting point.

Figures 2.14 and 2.15 show a transmission line circuit and the frequency response of a two-way, L-band Gysel power combiner designed through optimization. The frequency response shows the Gysel combiner to be nearly as good as a Wilkinson combiner.

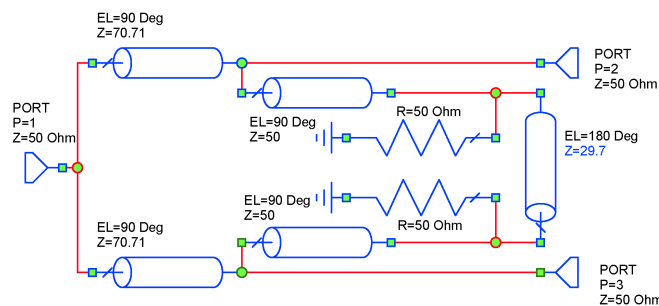


Figure 2.14: Circuit schematic of a basic two-way Gysel power combiner.

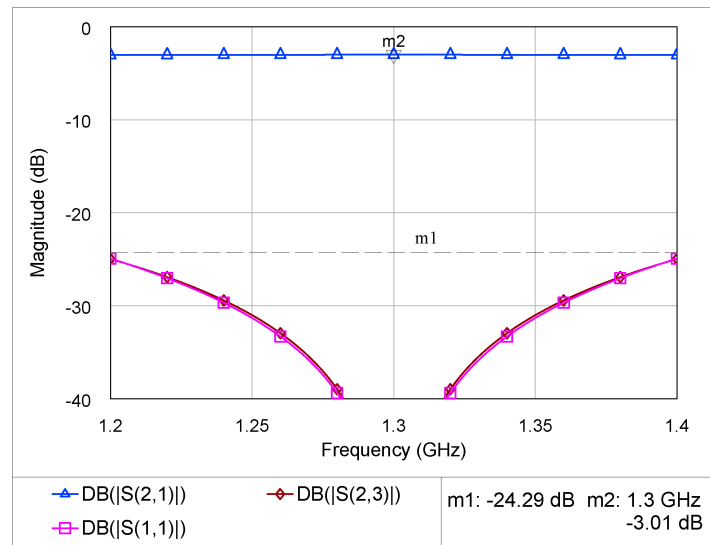


Figure 2.15: L-Band Gysel power combiner frequency response. The horizontal marker shows the minimum port reflections and isolation between the ports. Marker m2 shows the perfect division of the power.

The only negative aspects regarding the Gysel design is the larger configuration of the isolation network and the added layout complexity, adding extra discontinuities in the form of junctions and bends. Fortunately, modern analysis software however allows for accurate designs through the use of accurate discontinuity models.

2.3.1 High Power Termination Measurement and Modeling

To investigate the effectiveness and advantage of the Gysel design over the Wilkinson design, an analysis in Microwave Office is performed using the measured terminations as models for the isolation loads.

Two 100 W, 50 Ω flanged terminations (Barry Industries, T50R0-5-1S) are measured on a HP8510 network analyzer in the same manner as the resistor in Section 2.2.1 using a TRL calibration technique. Figure 2.16 shows the DUT block on which the terminations are mounted with the perspex press and foam used to press the termination tab down onto the transmission line.

Two tab configurations are tested using this DUT block. The left termination has a bent tab which will aid in heat strain relief due to thermal expansion when dissipating high power, while the right termination's tab is flat and is susceptible to fatigue. Figure 2.17 shows a close-up photo of the termination with the bent tab.

Measurement results of the two terminations on a Smith chart are shown in Figure 2.18. Both terminations show excellent performance up to 2 GHz.

As in Section 2.2.1, a model can be constructed for the termination shown in Figure 2.17. From

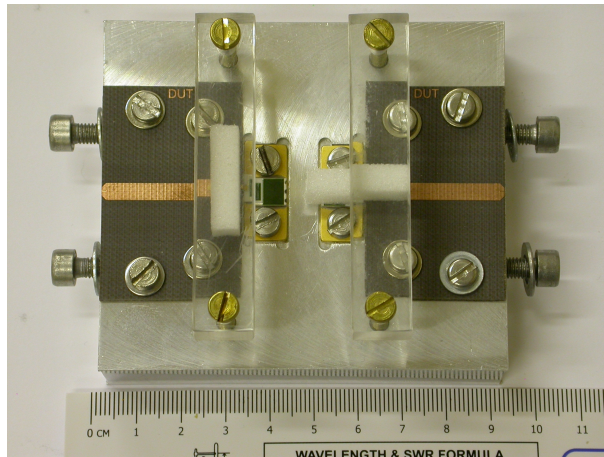


Figure 2.16: TRL termination (DUT) block with the two terminations.

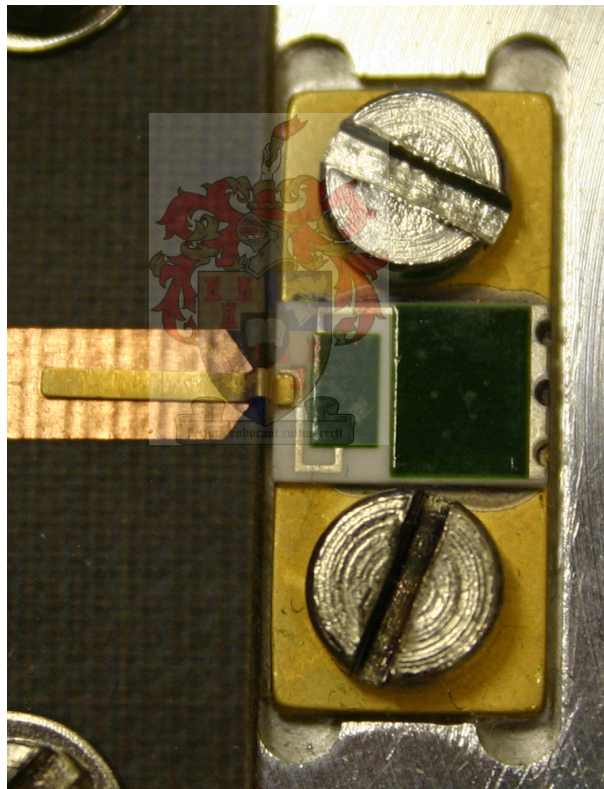


Figure 2.17: Close-up photo of the 100 W, 50 Ω termination with the bent tab.

Figure 2.17 it can be seen that the termination configuration differs from a typical resistor configuration in the sense that it has more than one section of resistive film and that there are long sections of conducting strips in between them. Considering these different sections of film and inductive conductors and assuming that each will have a capacitance to ground, a simple model is derived through optimization and is shown in Figure 2.19. Figure 2.20 shows the accuracy of the model between 0.6 GHz and 1.6 GHz on an enlarged Smith Chart.

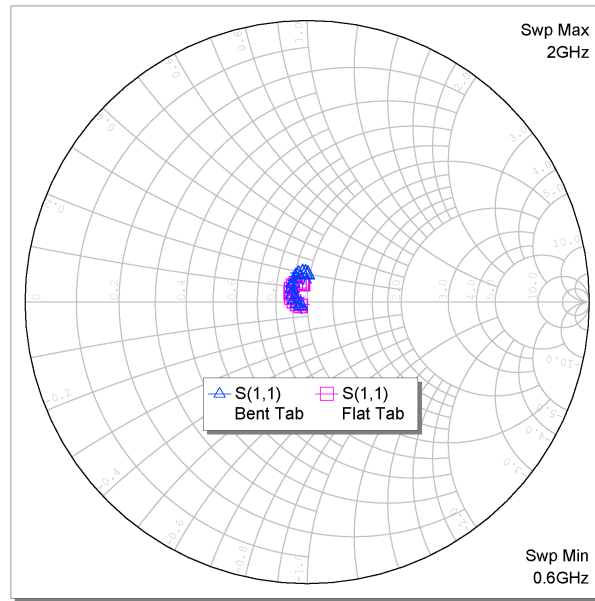


Figure 2.18: Bent and Flat Tab Termination Measurement.

An interesting point to note is that the physical layout suggests that the termination is actually built as a low-pass filter.

Now that the architecture of the termination is understood, a Gysel power combiner is analysed in Microwave Office using the measured S-parameters of the 100 W termination as models for the isolation loads. (Figure 2.21).

Figure 2.22 shows that excellent results are still achieved with isolation and port reflections are only 2.7 dB worse than the ideal case as shown in Figure 2.15, still being beneath 20 dB. This shows that the Gysel power combiner with its unique isolation network is more suitable for high power applications than the Wilkinson.

2.3.2 Power Rating of Isolation Terminations

When one of the inputs becomes an open circuit, the isolation network will dissipate half the incident power of the second input. This means that when working as a combiner each isolation termination in theory must be able to dissipate a quarter of the incident power levels.

2.3.3 1.3 GHz Gysel Power Combiner Design

To test the practical operation of a Gysel power combiner, a 1.3 GHz 2-way combiner is designed, built and measured by implementing a shielded microstrip design. Taconic TLY-5 ($\epsilon_r = 2.2$, $DF = 0.001$, height = 1.524 mm) substrate is used with a groundplane spacing equal to twice the substrate height. Figure 2.23 shows a photo of the combiner with the shield removed.

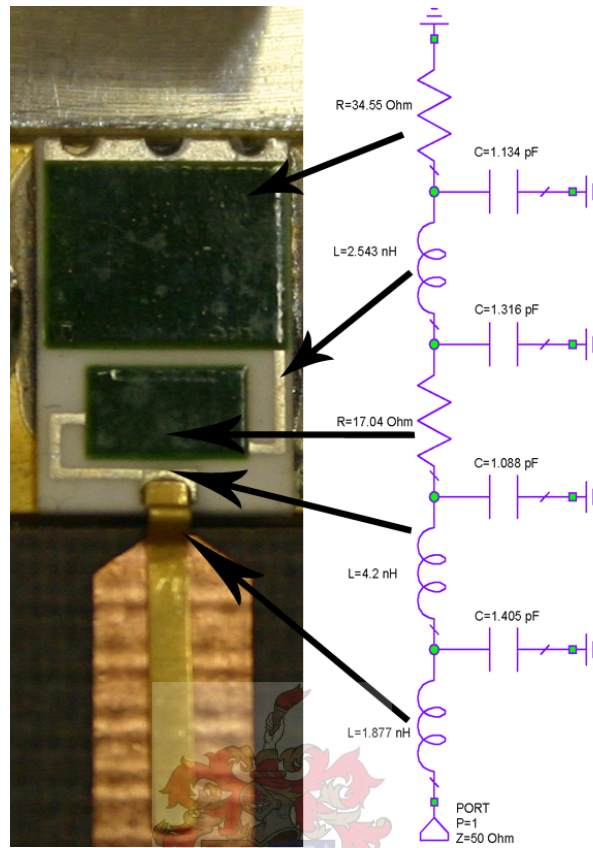


Figure 2.19: Physical layout of a $50\ \Omega$ termination (left) with an equivalent model (right).

A resistor is used in place of the two terminations for ease of construction and does not have an effect on the performance of the combiner.

Results show good comparison between the measured and analysed design considering that the imperfection of the 1206 surface mount resistor and connector discontinuities were not taken into account. Manufacturing tolerances may also cause small differences between the design and the measurement.

Figure 2.24 shows how well the port reflections of the measured and analysed design compare, with values below -20 dB. Figure 2.25 shows excellent transmission response over the whole frequency range with very little losses, while Figure 2.26 confirms that isolation between ports are better than 25 dB.

2.4 Fork-Type Power Combiner

Another type of combiner worth considering is a planar fork power combiner [12]. Although this type of combiner has the benefit of being completely planar, it has some disadvantages. For a large number of ports, it is very difficult to achieve simultaneous low port reflections, good

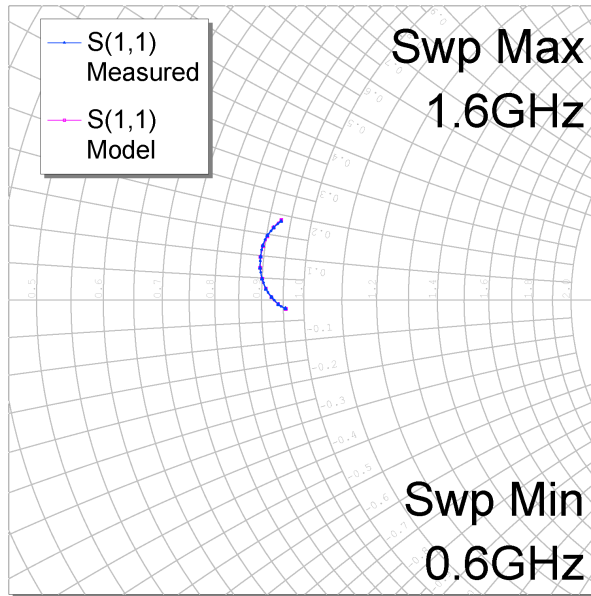


Figure 2.20: A comparison between a measured and modeled 100 W, 50 Ω termination on an enlarged Smith Chart.

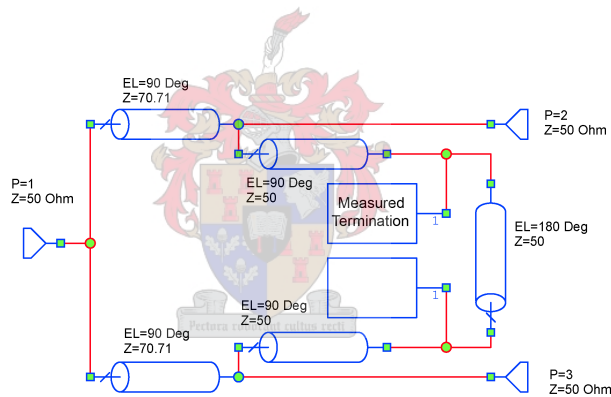


Figure 2.21: Circuit schematic of a Gysel power combiner implementing 100 W, 50 Ω measured termination models.

isolation and power balance between input ports. Figure 2.27 shows the schematic diagram of a 4-way fork-type power combiner as suggested by [12], where Z_0 represents single section quarter-wave transformers and is calculated with Equation 2.4.1.

$$Z_0 = \sqrt{nZ_1Z_2} \tag{2.4.1}$$

There are no design formulas given in the literature for the values of the isolation resistors (R_0) so as to optimize the match and isolation. Saleh [8] does however provide tables for determining the impedance values for optimum performance which were obtained through optimizing software.

Figure 2.28 shows the schematic diagram of a 4-way fork combiner using resistors in a Wilkinson-

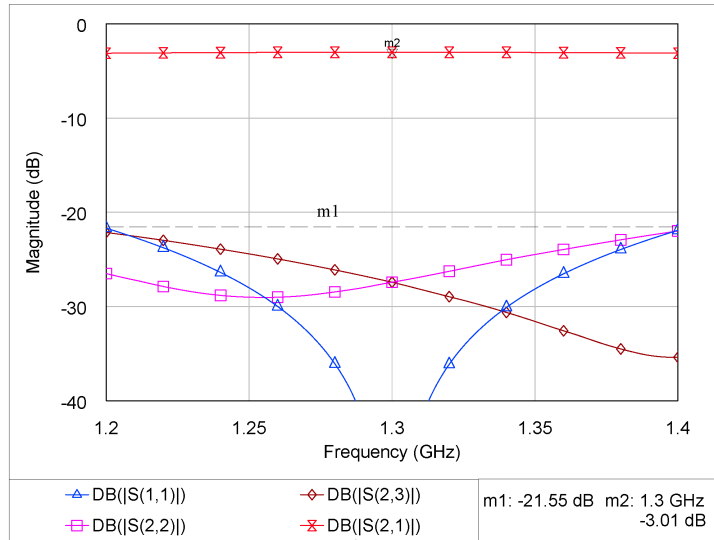


Figure 2.22: S-parameters of Gysel power combiner with measured isolation terminations. The horizontal marker shows the minimum isolation between ports and and the maximum port reflections. Marker m2 shows that equal power division still takes place.

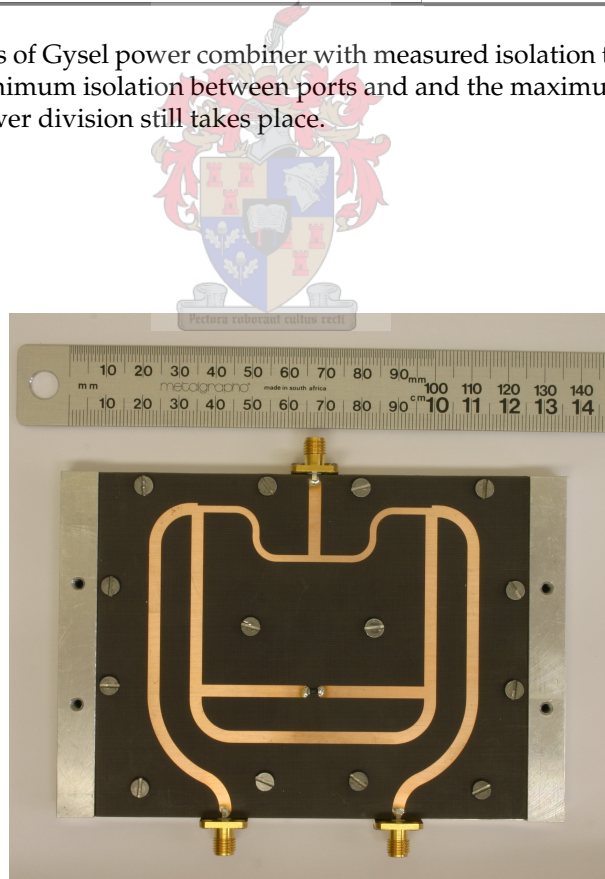


Figure 2.23: Built L-band Gysel power combiner with top shield removed.

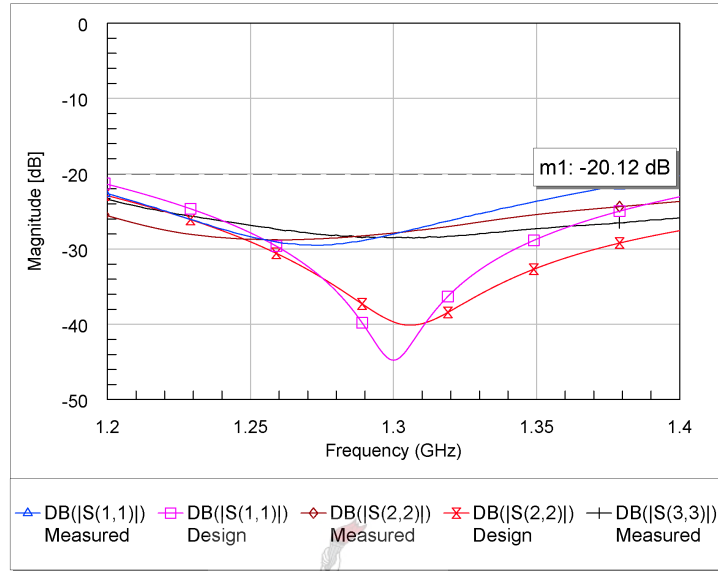


Figure 2.24: Measured vs simulated port reflections of a two-way Gysel power combiner.

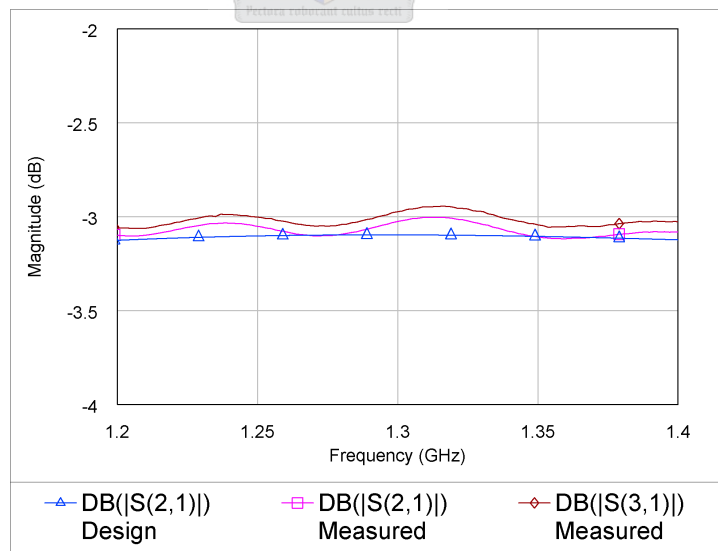


Figure 2.25: Measured vs simulated transmission response of a two-way Gysel power combiner.

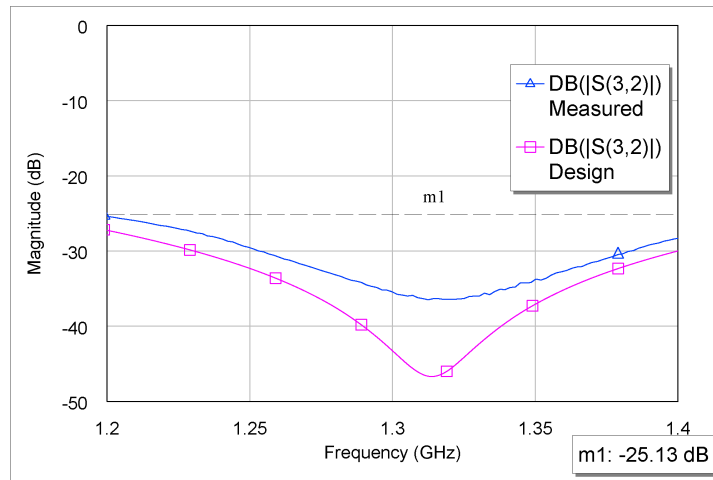


Figure 2.26: Measured vs simulated port isolation of a two-way Gysel power combiner.

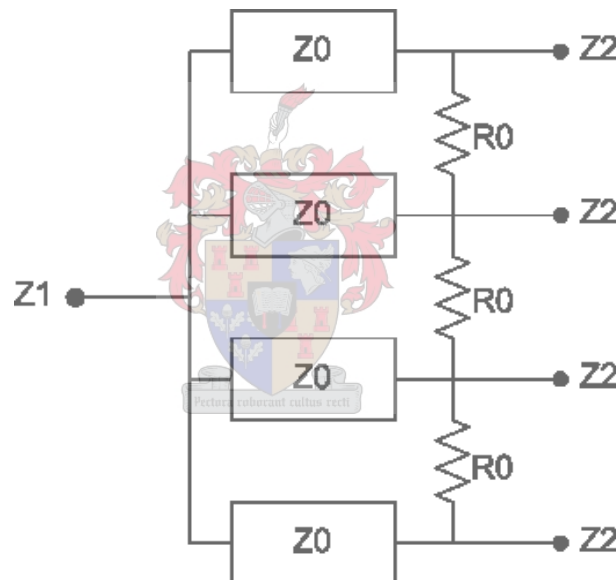


Figure 2.27: 4-Way fork-type combiner.

like configuration. The resistor values are obtained through optimization and provide optimum isolation and reflection. Figure 2.29 shows both the isolation and reflection of the input ports to be no more than -14 dB. Compared to the -27 dB (Figure 2.2) of the two-way Wilkinson combiner in Section 2.2, this fork-type combiner shows a decrease in port matching and isolation of 13 dB and which will degrade further as more ports are added.

Except for the planar structure, this type of configuration is almost equivalent to that of a N-way Wilkinson combiner. This means that there is no direct isolation resistors between the ports situated on the outsides.

As mentioned in Section 2.2.1, the thermally floating isolation resistors are not suitable for high power. A solution to this problem lies in using the same isolation configuration as used by

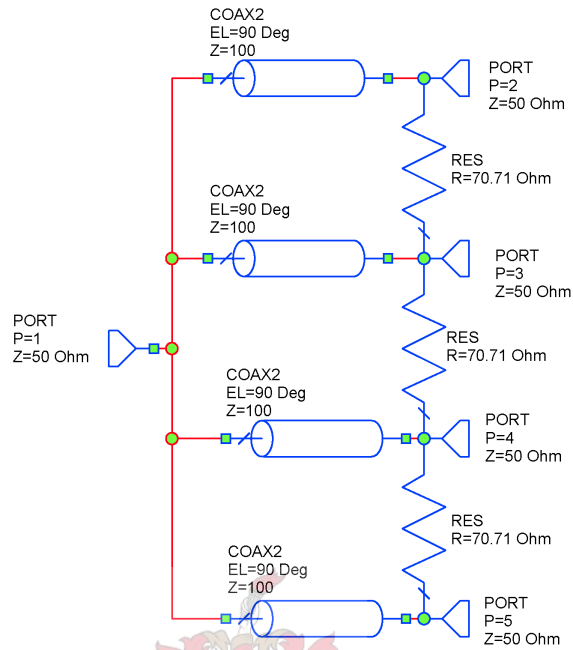


Figure 2.28: Schematic of a 4-way fork-type combiner using resistors.

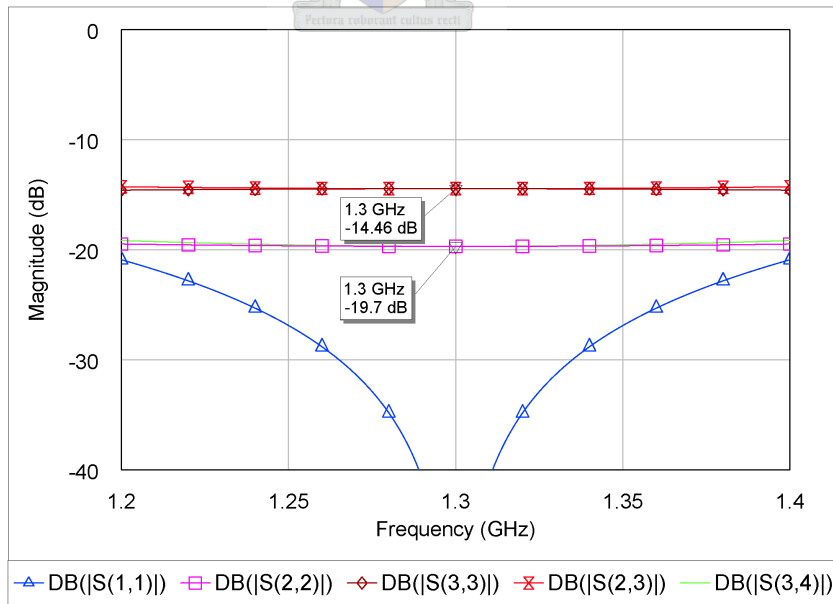


Figure 2.29: Port matching and isolation for a 4-way fork-type combiner using resistors.

a Gysel combiner. Figure 2.30 shows the schematic diagram of a 4-way fork combiner implementing a Gysel termination configuration. The port matching and isolation of this configuration is analysed in Microwave Office and is shown in Figure 2.31.

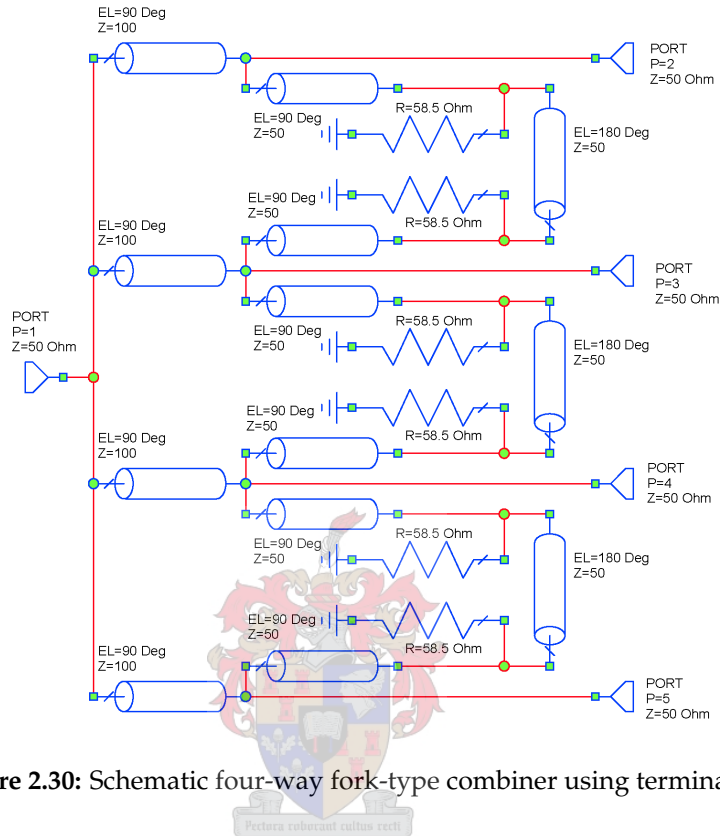


Figure 2.30: Schematic four-way fork-type combiner using terminations.

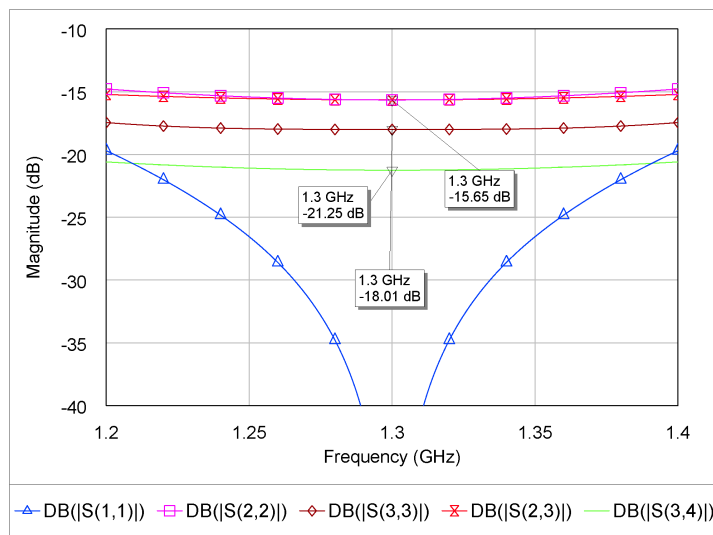


Figure 2.31: Port matching and isolation of a four-way fork-type combiner using terminations.

This configuration gives the same overall performance as the case with the ideal resistors and has the advantage that it is easier to realize in practice.

2.4.1 Isolation Network Power Rating

No design equations exist for determining the power rating of the isolation networks in a N-way fork-type combiner. Saleh, [8] provides a table for the isolation resistors power rating. Through a simple Microwave Office analysis, power ratings of isolation terminations can be established. It is found that for a four-way combiner each termination must be able to handle a factor of 0.46 the power level of the incident signals. This is much lower than the 0.74 factor for the single resistor isolation as given by [8].

2.4.2 Improving Bandwidth, Matching and Isolation

Matching, isolation and bandwidth of a N-way fork combiner can be improved considerably by using two stages [8] consisting of another 90° section and isolation sections. Adding a second stage improves the port matching and isolation from -14 dB to -28 dB. The realisation of this type of configuration still creates practical problems. For a large number of inputs, the structure layout becomes complex and large especially when implemented with termination isolation networks.

Output reflection bandwidth can also be improved by using a second order impedance transformer, instead of the single 90° transformer.



2.5 Conclusion

Several types of planar combiners have been investigated in this chapter. Bandwidth, isolation and mismatch are key performance factors to consider and it is found that in planar form it is extremely difficult to achieve an overall good performance for combiners with a large number of ports.

The amount of power to be combined or divided and power loss are factors in the selection of the type of combiner configuration implemented. High power thermally floating resistors are capacitive causing poor performance while circuits using terminations take up a lot of space. High power terminations and resistors were measured and modeled to investigate their performance and influences on different types of combiners.

Isolation networks implementing terminations seem to be the better choice.

Using a combination of the combining structures covered in this chapter, an adequate 8-way power combiner design is possible. Careful design is necessary to ensure good port matching, isolation and bandwidth.

Chapter 3

Four-Way Combiner Junction Design

3.1 Introduction

An important component in any combining or dividing network is the junctions where the lines combine or divide. Models of standard three-port and four-port junctions with 90° angles between the lines are present in most microwave CAD (Computer Aided Design) software packages and can accurately model the discontinuity reactances associated with them. If discontinuities of three-port junctions are found to be significant, these junctions can be compensated for through methods provided by [18]. These reactance discontinuities are more prominent at higher frequencies and can be compensated for, by removing a triangular portion from the junction.

Throughout this chapter the term divider instead of combiner will be used for the sake of easy explanation. The function of both of these designs are exactly the same.

Dividing circuits with a large number of outputs may need one-to-n-way splitting junctions with more than four ports, needing special attention when designing them for optimal performance. When these type of junctions are implemented, output lines are bound to influence each other through coupling and serious reactance discontinuities may occur. Current distribution at the point where the lines separate may also be a factor.

This chapter investigates the properties and performance of various one-to-four-way junctions. In section 3.2 the problems associated with junctions are explained, while section 3.3 provide examples of junctions implemented in microstrip and stripline. An example design is measured in Section 3.4 to test the results provided by the various simulations.

3.2 Possible Explanations for Poor Junction Performance

In practise, previous designs have shown that without careful design decisions a 5-way power divider's outputs can differ by up to 0.4 dB in magnitude and 17° in phase [10]. Explanations for this unequal power division can be derived by considering the electric field and current distribution on a microstrip line. For L-band frequencies and lower, the electric field and current distribution can be approximated to be the same as for pure TEM propagating modes (Figure 3.1 [19]). This suggests that when a microstrip line is divided lengthwise into three or more equal widths, more power will propagate along the outermost lines.

By considering the fringing fields at the edges of the outside lines, one could also think of the outermost lines having a lower characteristic impedance. When assuming that the line is implemented in microstrip, the effective change in line width will decrease the effective dielectric constant of the concerned line, which will result in the phase velocity of the line being increased. This means that a phase difference will occur between the centre and outermost lines.

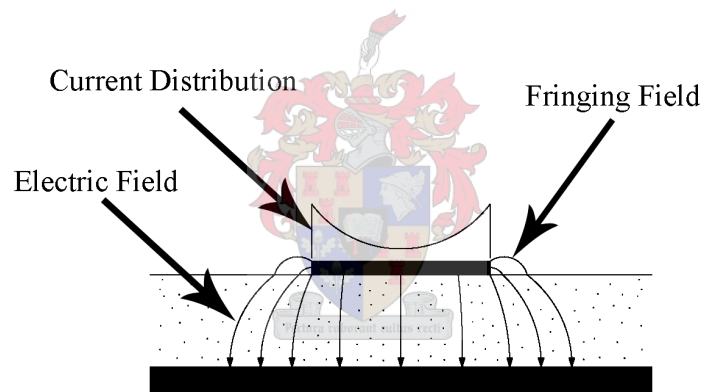


Figure 3.1: TEM electric field and current distribution on microstrip.

3.3 Four-Way Junction Analysis

A junction is normally implemented as part of a matching transformer, which is responsible for matching the input port to the various output ports. In most cases the input and output impedances are designed to have a characteristic impedance of 50Ω . To investigate the poor performance and properties of N-way junctions, various one-to-four-way junctions are simulated with FEKO and implemented in Microwave Office as part of a second order binomial matching transformer. By using this transformer with its maximally flat response (Pozar [15], p246), perfect matching should theoretically be achieved at the centre frequency of the design.

For the examples to follow, a second-order binomial matching transformer is chosen to function at a centre frequency of 1.3 GHz. Through the easy to use tables provided by Pozar [15] (p249), a theoretical four-way divider network is constructed as shown in Figure 3.2. This transformer uses a 35.26Ω and four 70.71Ω transmission lines to match a single 50Ω port to four 50Ω output ports.

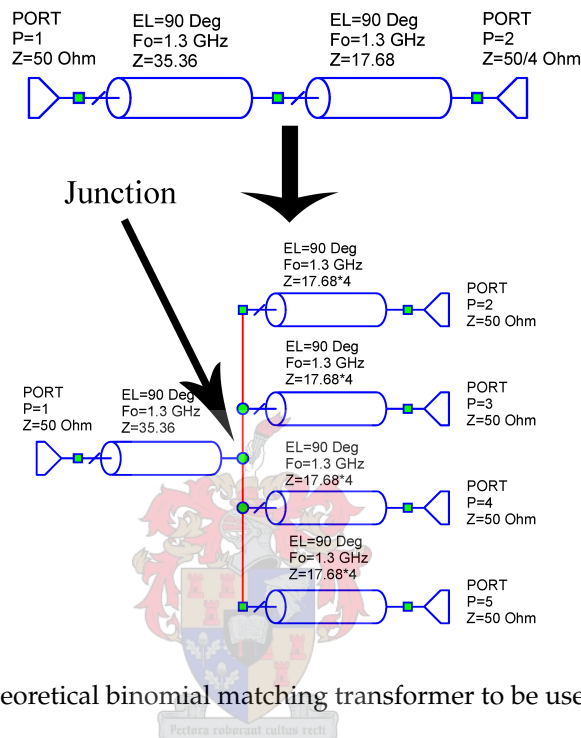


Figure 3.2: Theoretical binomial matching transformer to be used for analysis.

All simulations and analysis are performed only at the centre frequency where maximum performance should be achieved and a straightforward comparison can be made between the theoretical and simulated results. For the purpose of simulating a practical and realistic junction, lines are separated with an angle of 20° between each other. This creates sufficient room for isolation networks which are typically employed in high power applications. The substrate dielectric constant is chosen as $\epsilon = 3$.

3.3.1 Junctions Implemented in Microstrip

The first simulation consists of the binomial transformer implemented on a substrate with a relatively large thickness of 1.524 mm. Figure 3.3 shows the junction as simulated in FEKO, with the calculated surface current. It can clearly be seen that a quasi-TEM mode is present on the various lines. The effect of the coupling between the lines can also be observed by looking at the distribution of current.

By implementing the junction's S-parameter results of the electromagnetic simulation in Microwave Office, the complete matching transformer can be analysed. Perfect transmission lines

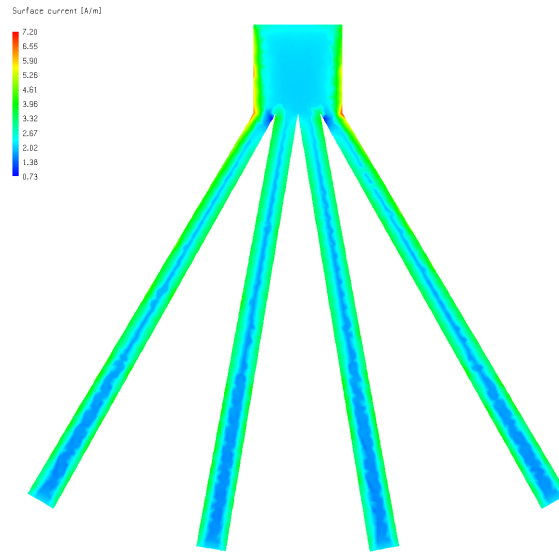


Figure 3.3: Surface current of a binomial transformer junction simulated in FEKO using a 1.524 mm substrate.

are added to complete the quarterwave sections (Figure 3.4) and the results are shown in Table 3.1.

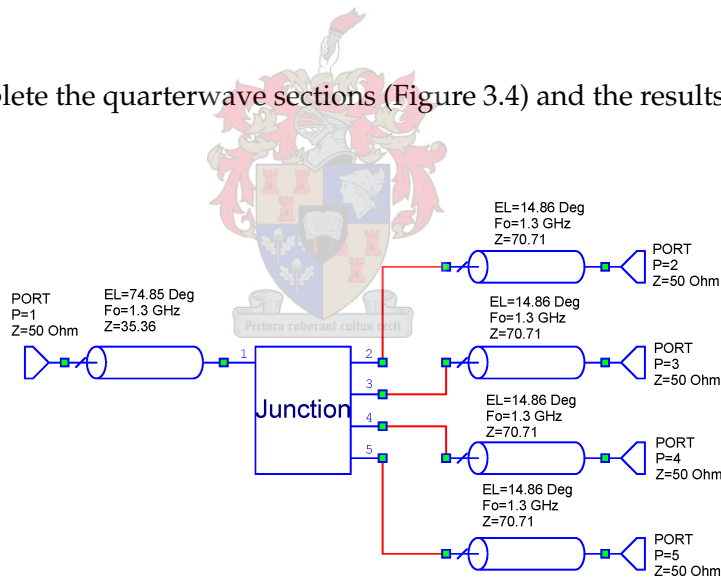


Figure 3.4: Complete binomial matching transformer consisting of the junction and completed quarter-wave transmission lines.

S-parameter	Magnitude (dB)	Phase (degrees)
S_{11}	-13	
S_{21}	-6.22	-179.4
S_{31}	-6.32	-180.8

Table 3.1: Analysis results of the binomial transformer implemented in 1.524 mm thick microstrip

The results are different from what is intuitively expected. The difference in the transmission response between the centre and outer strips are only 0.1 dB and phase difference is less than

Length (mm)	0.7875	0.7875	1.575	3.15	6.3	6.3	6.3	6.3
Spacing (mm)	0.275	0.55	1.1	2.2	4.4	6.6	8.8	10.1

Table 3.2: Coupled line values used for approximating the splitting lines. Point of separation starts on the left.

S-parameter	Magnitude (dB)	Phase (degrees)
S_{11}	-24	
S_{21}	-6.12	-180
S_{31}	-6.34	-182.2

Table 3.3: Binomial matching transformer results of Microwave Office approximated design using coupling line models.

2 degrees. The poor performance of the dividing transformer lies solely in the very poor input mismatch of -13 dB.

A quick comparative check is performed with Microwave Office to verify the validity of these results. By simulating the splitting junction through a series of coupled line models at various points along the lines, an indication of the performance can be found. Eight sections are used all together to create the splitting lines effect, with an increase in resolution nearer to the point of separation. Table 3.2 shows the line lengths and the spacing between the splitting lines over the complete length which was used for the test analysis, while Table 3.3 shows the analysis results from Microwave Office.

The simulation results of the transformer, using the approximated junction in Microwave Office, show that the results obtained from the electromagnetic simulation are valid. The phase difference and transmission difference between the ports of the approximated design is 2.2 degrees and 0.22 dB respectively and compares relatively well to the EM design. The port reflection is better than in the EM simulated design, but it should be remembered that the approximation does not account for current distribution at the point of separation and does not accurately consider the angle of the current flow of the coupling lines.

The results of the two simulations above show that the difference in power at the output ports is not as severe as initially thought. Input mismatch does however make this design very poor.

Another transformer design implemented in microstrip is now considered but this time a thinner substrate (0.5mm) is used to investigate the effect of substrate thickness on the design performance. Figure 3.5 gives the junction as simulated in FEKO with the calculated surface current showing. Results of the Microwave Office analysis, which includes the added transmission lines to complete the quarterwave sections, are shown in Table 3.4 .

The results of the transformer implemented in the thinner 0.5 mm substrate are very interesting. Very good input port matching is obtained while almost no difference in the transmission response or phase response is visible. This transformer has an all round good performance.

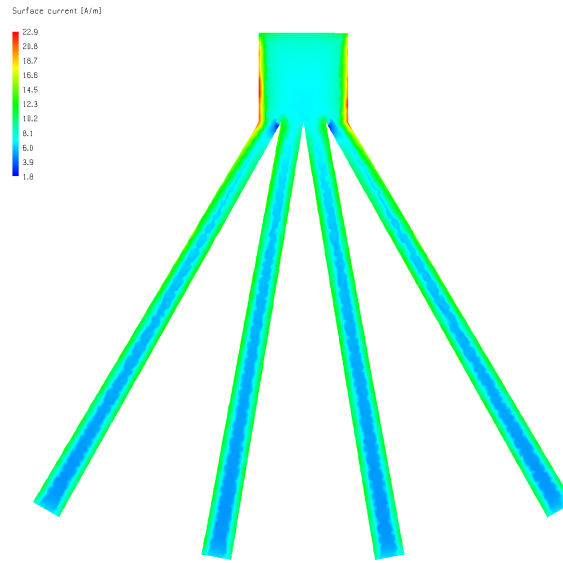


Figure 3.5: Surface current of a binomial transformer junction simulated in FEKO using a 0.5 mm substrate.

S-parameter	Magnitude (dB)	Phase (degrees)
S_{11}	-23.4	
S_{21}	-6.03	-179.3
S_{31}	-6.05	-179.8

Table 3.4: Analysis results of binomial transformer implemented in 0.5 mm thick microstrip.

Several important conclusions can be reached from the simulated results. The substrate thickness plays a major role in the performance of the splitting matching transformer. When it is implemented in a high power application, thicker substrates used for better thermal performance might give very poor results if special care is not take. Results were obtained from lines dividing into only four sections and worse results can be expected when implementing more outputs.

3.3.2 Junctions Implemented in Stripline or Shielded Microstrip

Solutions have been found for improved power division in dividers containing junctions with several output ports and have been implemented by [10]. This is especially important when designing high power circuits and will thus be implemented.

Section 3.2 explained the problem of the changing effective dielectric constant when using microstrip. A solution to the changing effective dielectric constant lies in the use of symmetrically shielded microstrip or stripline. In both cases the effective dielectric constant will not be affected by a change in the strip width [19] and thus the phase velocities of all the lines will stay equal, even when the line widths change.

Equal phase response of the splitting lines' outputs, or in this case a complete matching transformer, still rely on all the ports being matched. Considering the coupling lines of the splitting junction, this will only be true if all the coupling lines have equal even mode impedances as calculated for the design.

It was however showed in section 3.3.1 that the manner in which the four lines coupled did not result in drastically different even mode impedances as was proved by the small phase shifts between lines.

To investigate the implementation of a junction in an environment where the effective dielectric constant stays constant, the same binomial matching transformer design is implemented in a stripline architecture with the strip in the middle of the two ground planes. The substrate dielectric constant is the same as for all the previous examples.

Figure 3.6 shows the calculated surface current of the junction as simulated with FEKO. Results of the junction implemented in the complete Microwave Office transformer design is given by Table 3.5.

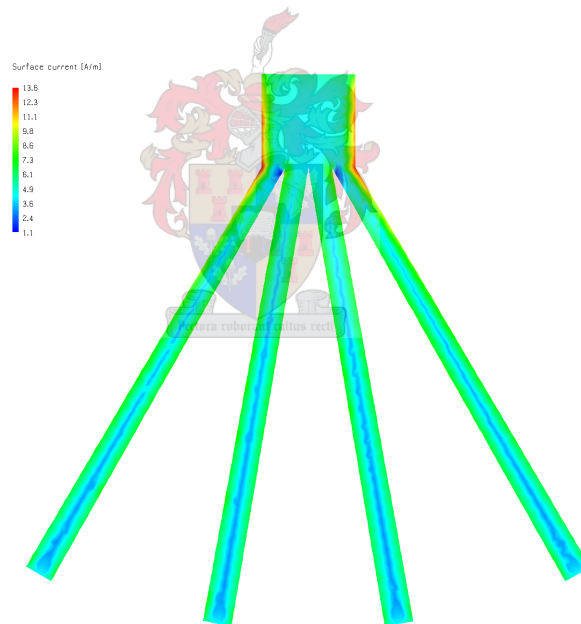


Figure 3.6: Surface current of a binomial transformer junction simulated in FEKO using a stripline architecture. Groundplane spacing = 3.048 mm and $\epsilon_r = 3$.

S-parameter	Magnitude (dB)	Phase (degrees)
S_{11}	-18.8	
S_{21}	-6.06	-178.7
S_{31}	-6.1	-179.5

Table 3.5: Analysis results of binomial transformer implemented in 3.048 mm thick stripline.

This transformer demonstrates better results when compared to the 1.524 mm microstrip case, with less than a degree in phase shift between ports and negligible difference in transmission loss. The input port reflection is almost 6 dB better and considering the thickness of the stripline example, results have improved significantly.

As good as the -18.8 dB reflection of this stripline example might seem in comparison to the previous simulations, it is still far from the performance one would expect from a good matching transformer.

3.3.3 Improved MATLAB Drawn Junction Implemented in Stripline

A new approach is considered to improve the matching of the junction. Until now the coupling lines have influenced the even mode impedances to such an extent that matching has deteriorated significantly. By decreasing the length over which the lines couple, better results should be achieved.

MATLAB code was written (Appendix A) to aid in the drawing of an one-to-four-way junction in the form of a AutoCAD standard DXF file, where lines are separated in such a manner that coupling between lines are kept to a minimum. This was accomplished utilizing MATLAB libraries supplied by [20]. A basic drawing of the junction is shown in Figure 3.7.

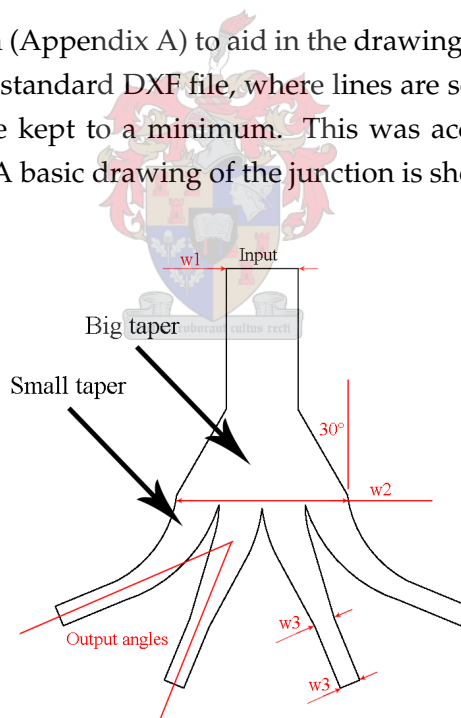


Figure 3.7: Basic junction drawn with the MATLAB code.

Figure 3.7 also shows the design parameters as used by the code: the input line width (w_1), the width in which the big taper ends (w_2), the output line widths (w_3) and the angles in which the outputs lines are directed.

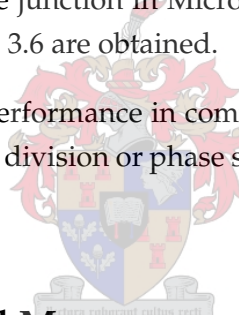
A key property of this design is the tapering system which is used to assist in the transition between the line impedances of the input section and the line impedances of the output sec-

tions. The input line is first tapered with a 30° angle to an impedance equal to all the output line impedances in parallel. It is then divided into four equal sections which are tapered with rounded bends to the correct output line impedances. The rounded bends have a radius of four times the width of the line and curves the lines outwards as quick as possible to ensure that the lines couple as little as possible.

The second order binomial matching transformer is again implemented in a stripline simulation example, this time using a MATLAB drawn junction. The angle of direction between the output ports are chosen to be 45° which makes it perfect if a large isolation network such as a Gysel isolation network should be implemented between the output lines. Figure 3.8 shows the surface current of the junction as simulated with FEKO. This figure provides a clear picture of how the surface current is distributed. The surface current in the centre of all the lines are nearly identical, while the surface current near the edges of the lines show dissimilar reactions due to the effect of the lines coupling. The surface current distribution of this junction would be difficult to predict without the use of electromagnetic simulation software.

Using the FEKO simulation of the junction in Microwave Office to analyse a complete transformer design, the results in Table 3.6 are obtained.

The analysis shows exceptional performance in comparison to all the simulations considered. No problems with unequal power division or phase shifts are present and the input port match is excellent.



3.4 Practical Design and Measurement

During the performance investigations of the various junctions in section 3.3, an L-band second order Chebyshev matching transformer consisting of four outputs was designed, built and measured (Figure 3.9). This divider is implemented in shielded microstrip with the ground-plane spacing twice the height of the substrate. Gil substrate with a thickness of 1.524 mm and a dielectric constant of 3.05 was used for the design.

The Chebyshev transformer matches the 50Ω input port to four 50Ω output ports, is designed for a reflection coefficient magnitude of -45 dB in passband ripple and a bandwidth of 210 MHz around a centre frequency of 1.3 GHz. The first quarter-wave section has an impedance of 35.26Ω while all the second quarter-wave sections have impedances of 70.91Ω . These values are almost the same as the values used in the previous examples because of the extremely small passband ripple. The electrical distance of the output lines are kept the same by putting bends in the lines with radii of no less than three times the width of the line to keep discontinuity to a minimum. A taper is used to simplify the transition between the 35.26Ω input line and the 70.91Ω output lines.

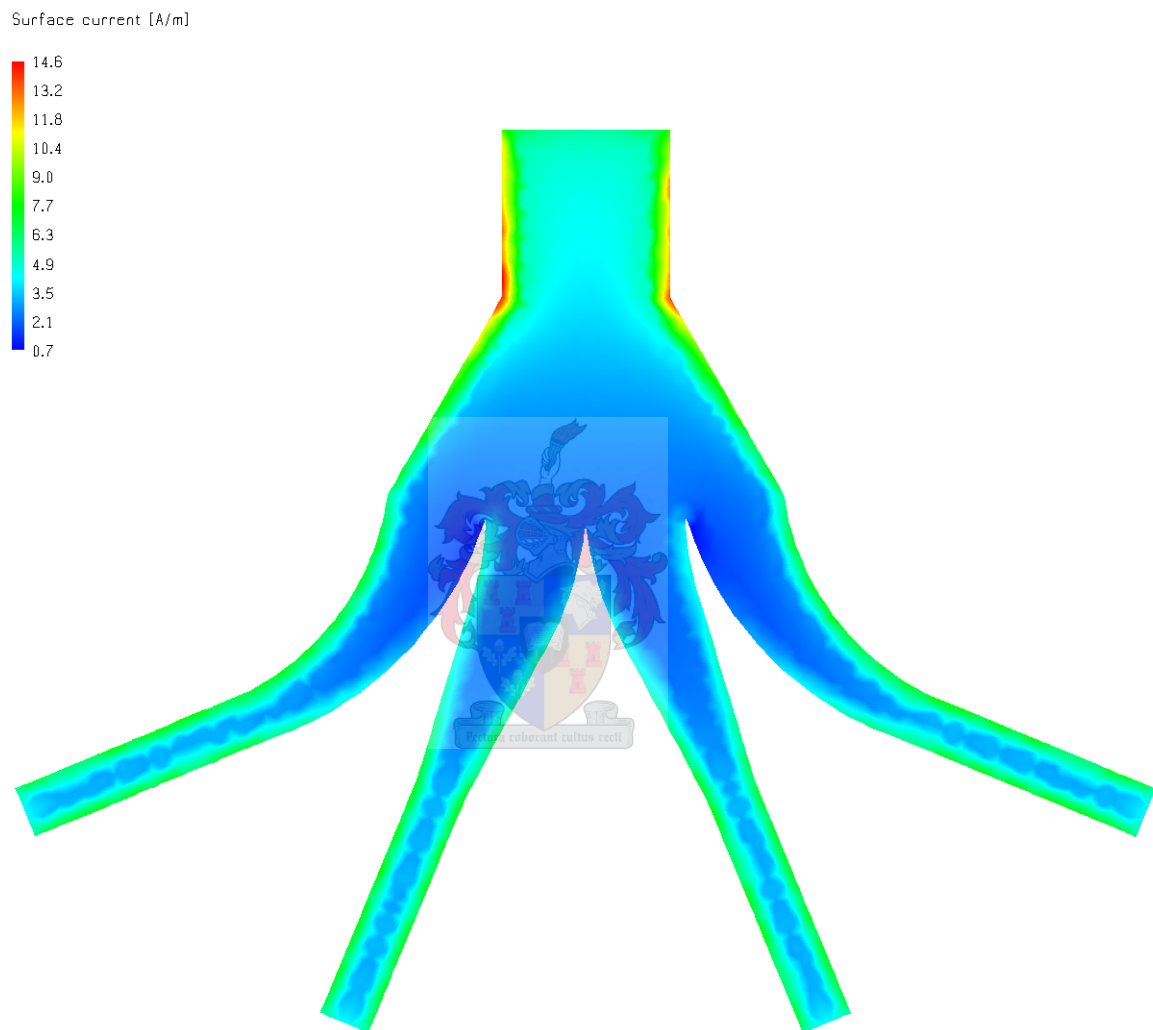


Figure 3.8: Surface current of a binomial transformer junction drawn with MATLAB and simulated in FEKO.

S-parameter	Magnitude (dB)	Phase (degrees)
S_{11}	-31	
S_{21}	-6.02	-179.3
S_{31}	-6.02	-179.5

Table 3.6: Analysis results of binomial transformer implemented in stripline with a ground plane spacing of 3.048 mm using a junction drawn using MATLAB code.

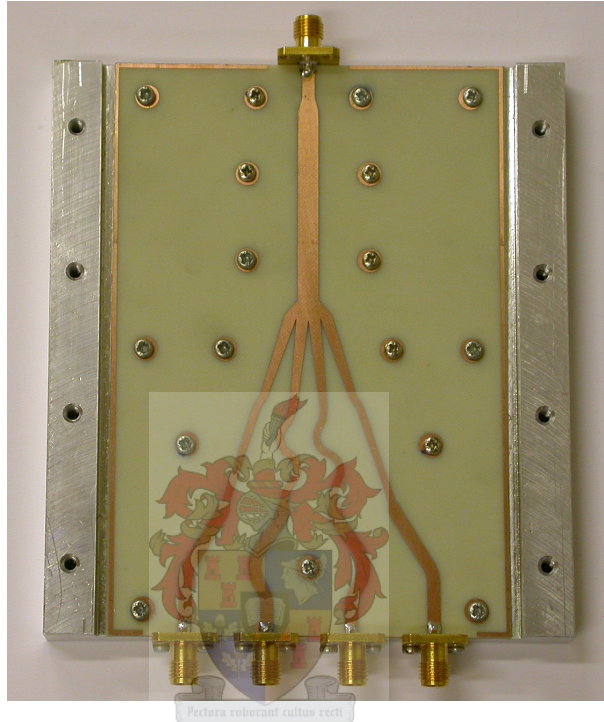


Figure 3.9: Four-way divider with the top shield removed.

CST Microwave Studio was used to simulate and calculate the S-parameter junction after which it was imported into Microwave Office where the rest of the lines were added for circuit analysis. Figure 3.10 shows the structure simulated in CST Microwave Studio using discrete measurement ports at the outputs. This simulated junction includes most of the bends used in the design.

The layout of this test design was quite difficult. All the output lines need to end in the same plane for the purpose of attaching the connectors while maintaining equal electrical length. MATLAB code was written to fit curved lines with specific electrical lengths within a determined offset. Another negative aspect of the design was the simulation time needed by CST to accurately model the junction. FEKO seems to be a better option for these kind of simulations because of the use of Green's functions which speeds up the simulation time considerably.

Figures 3.11 and 3.12 show a comparison between the measured and analysed design with Table 3.7 providing a summary of all the results.

A very good comparison is found between the measured and simulated results. These results

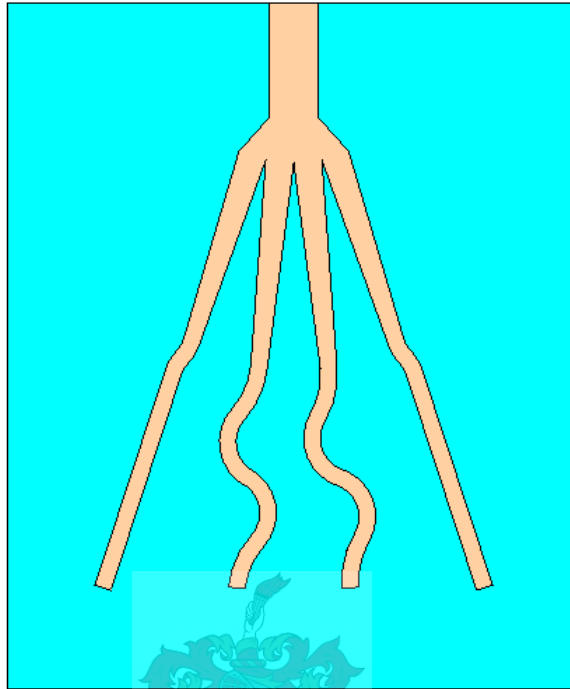


Figure 3.10: Four-way junction simulated in CST Microwave Studio using discrete ports at the outputs.

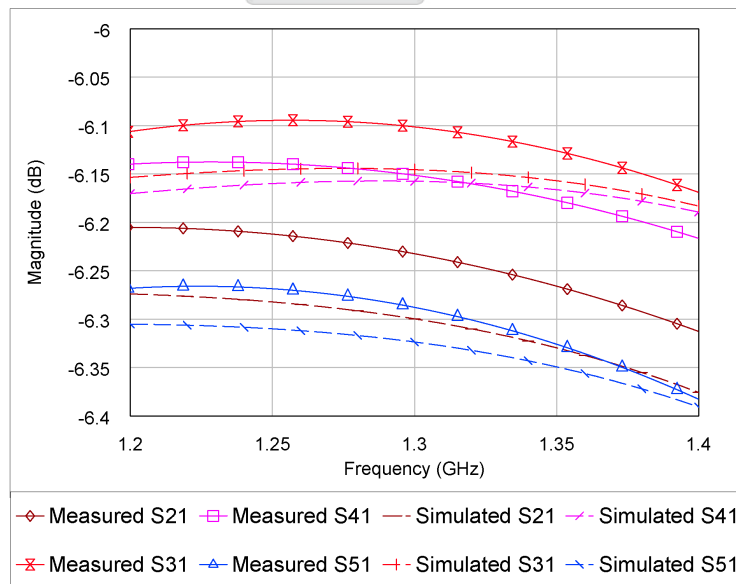


Figure 3.11: Transmission response comparison between a measured and simulated four-way divider.

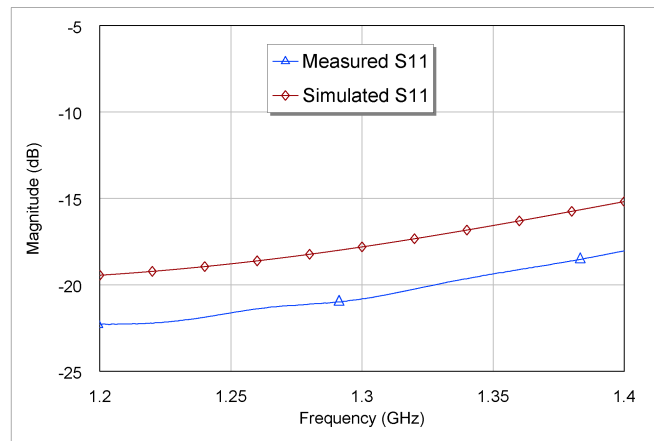
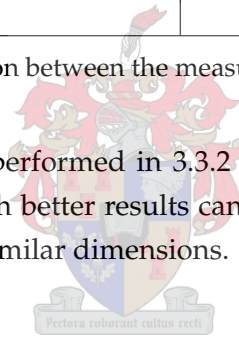


Figure 3.12: Input reflection comparison between a measured and simulated four-way divider.

	Maximum Magnitude Difference (dB)	Maximum Phase Difference (degrees)	Maximum S_{11} (dB)
Analysed	0.21	1.1	-15.2
Measured	0.22	1.7	-18

Table 3.7: Performance comparison between the measured and simulated matching transformer.

also agree with the simulations performed in 3.3.2 where a similar configuration was used. This experiment proves that much better results can be achieved through the use of shielded microstrip than microstrip with similar dimensions.



3.5 Conclusion

Interesting conclusions have been made in this chapter regarding junctions consisting of more than two outputs.

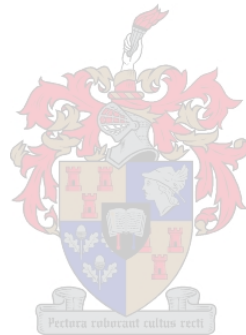
The output power difference between inner and outer lines of the various one-to-four-way junctions, was found to be smaller than initially expected. Only the port reflections were found to be poor due to the effect of the junction. Coupling between lines causes the even mode impedances to be different from the ideal case and is the reason for the poor performance.

When lines split with a relatively large angle between them, as was done with the examples, it seems that coupling does not result in major even mode impedance differences and thus equal power division existed.

It was also found that the substrate thickness determines the length over which the lines couple and is thus also a factor in the performance of the junctions. Junctions implemented in thick substrates give substantially inferior results.

Junctions implemented in stripline and shielded microstrip provide better performance than microstrip due to the unchanging dielectric constant with changes in effective linewidth.

The best performance of a one-to-four-way junction was obtained through the use of a MATLAB drawn junction implemented in stripline. This junction uses tapers to create a good transition between the input and output lines and divides the lines quickly to keep coupling to a minimum.



Chapter 4

Power Handling Capability

4.1 Introduction

The power handling capability (PHC) of components play a critical role in the successful design of a high power power combiner. Heating caused by ohmic and dielectric losses, as well as the ambient temperature, sets the limit of the average power the device can handle, while high voltage dielectric breakdown will limit the peak amount of power it can handle. The voltage breakdown is also dependent on the air pressure of the working environment. Components operating above their maximum specified operating temperatures will have a significant decrease in performance, or in severe cases may even fail completely. Voltage breakdown, whether it is partial discharge or complete discharge, will have a serious effect on performance. Corona discharges add noise to signals and will cause a loss of power. When full voltage breakdown occurs, dielectric materials may be destroyed completely.

Specifications for the 10 kW combiner state a maximum ambient temperature of 65°C and a maximum operating altitude of 3000 m above sea level.

Despite popular belief, microstrip lines can handle several kilowatts of power with careful design [5],[7],[6]. However, stripline and shielded microstrip are best suited for high power applications due to their physical configuration. Although a stripline design is a bit more difficult to implement, it allows for excellent heat flow due to the conduction of heat in an upwards and downwards direction. Shielded microstrip is easier to implement and has, like stripline, the advantage that it is shielded from its environment.

In this chapter the power handling capabilities of various components are presented. Section 4.2 covers the theory of the peak PHC of shielded microstrip and provides data for the design of lines operating above the breakdown voltage. The average PHC of shielded microstrip is investigated in Section 4.3 through the calculation of the temperature rise in the transmission lines. The influences of substrate parameters are also considered with a few examples. Sections

4.4 and 4.5 discuss the PHC of connectors and resistors and terminations.

Only stripline and shielded microstrip transmission lines are investigated as they provide essential electrical shielding between the high power transmission lines and the environment.

4.2 Peak Power Handling Capability of Shielded Microstrip

Very little literature covers the peak PHC of shielded microstrip transmission lines. Theoretical values for the breakdown voltage of shielded microstrip are provided by [21] while [1] provides a design graph based on a model for breakdown voltage for shielded microstrip. It is also shown by [1] that the measured breakdown voltage of shielded microstrip is more than three times higher than the theoretical values of [21]. Strip transmission lines normally do not have the problem with dielectric breakdown due to substrates which can handle several kilovolts without breakdown occurring.

With air having the lowest breakdown voltage, it is necessary to know the peak voltage shielded microstrip can handle without voltage breakdown.

The breakdown electrical field strength of air at microwave frequencies at a pressure of one atmosphere (760 Torr) is usually taken to be about $2900 V_{peak}/mm$ (or $2000 V_{r.m.s.}/mm$ for a sinusoidal wave). This is only true for flat uniform surfaces and does not apply to shielded microstrip lines where in theory the electrical field strength will approach infinity at the sharp edges and corners of conductors. Despite this, shielded microstrip lines can handle several kilowatts of microwave power without arcing.

The reason for this dissimilarity between the theory and practical application can be explained as follows [1]. Kinetic gas theory shows that ionization by electron impact can lead to breakdown of gases. Free electrons within a field gain kinetic energy as they move along the mean free path in the direction of the field. When a free electron with sufficient energy collides with an air molecule, the molecule may get ionized creating another free electron. If this freed electron also gains enough energy another collision is possible. A chain reaction can follow causing a flash over.

The voltage breakdown process, however needs certain conditions which may not always be met when, for instance, considering the sharp edges of a strip. For voltage breakdown to occur, a certain volume of air must exist in which the electric field is strong enough to accelerate electrons to the required energies. When low voltages are considered, the electric field strength decreases rapidly at the edges and the field does not exceed the threshold level for breakdown in a sufficiently large volume of air. As the voltage is increased, the field strength will also increase until it exceeds the critical field strength resulting in breakdown.

It should be noted that inaccurate results are obtained when using classical kinetic gas theory

to calculate breakdown voltages within a small volume such as sharp corners and edges.

Using the data supplied by [1], practical predictions of breakdown voltage for a wide variety of symmetrically shielded microstrip transmission line dimensions can be found. The shielded microstrip dimensions, as defined by [1], are shown in Figure 4.1 and can be used together with Figure 4.2 to predict the voltage breakdown.

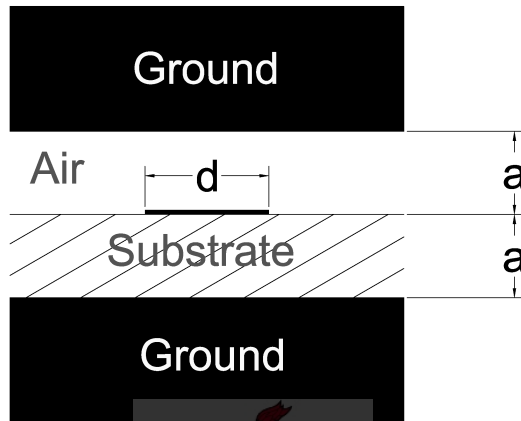


Figure 4.1: Shielded microstrip dimensions as defined by [1].

For altitudes higher than sea level it is necessary to adjust the value for breakdown voltage. A decrease in air pressure will cause a decrease in breakdown voltage as a result of the electron mean free path increase [22]. According to the International Standard Atmosphere, air pressure will decrease by a factor of 0.69 at an altitude of 3000m above sea level. For design purposes this pressure ratio can be used as the ratio for change in breakdown voltage.

4.3 Average Power Handling Capability of Stripline and Shielded Microstrip

The average PHC of stripline or shielded microstrip is determined by the temperature rise of the strip conductor and substrate. Good substrates are usually rated with a maximum operating temperature of 150°C.

Parameters that play major roles in the calculation of the average power handling capability of these lines are given by [23] as: (i) transmission line losses; (ii) thermal conductivity of the substrate material; (iii) surface area of the strip conductor; and (iv) ambient temperature. By taking all these factors into account, the theoretical temperature increase of the centre conductor relative to the ground planes can be calculated [24].

Section 4.3.1 gives the formulas with which the dielectric and conductor losses can be calculated while Section 4.3.2 looks at the impact of the conductor's surface roughness on losses. After the

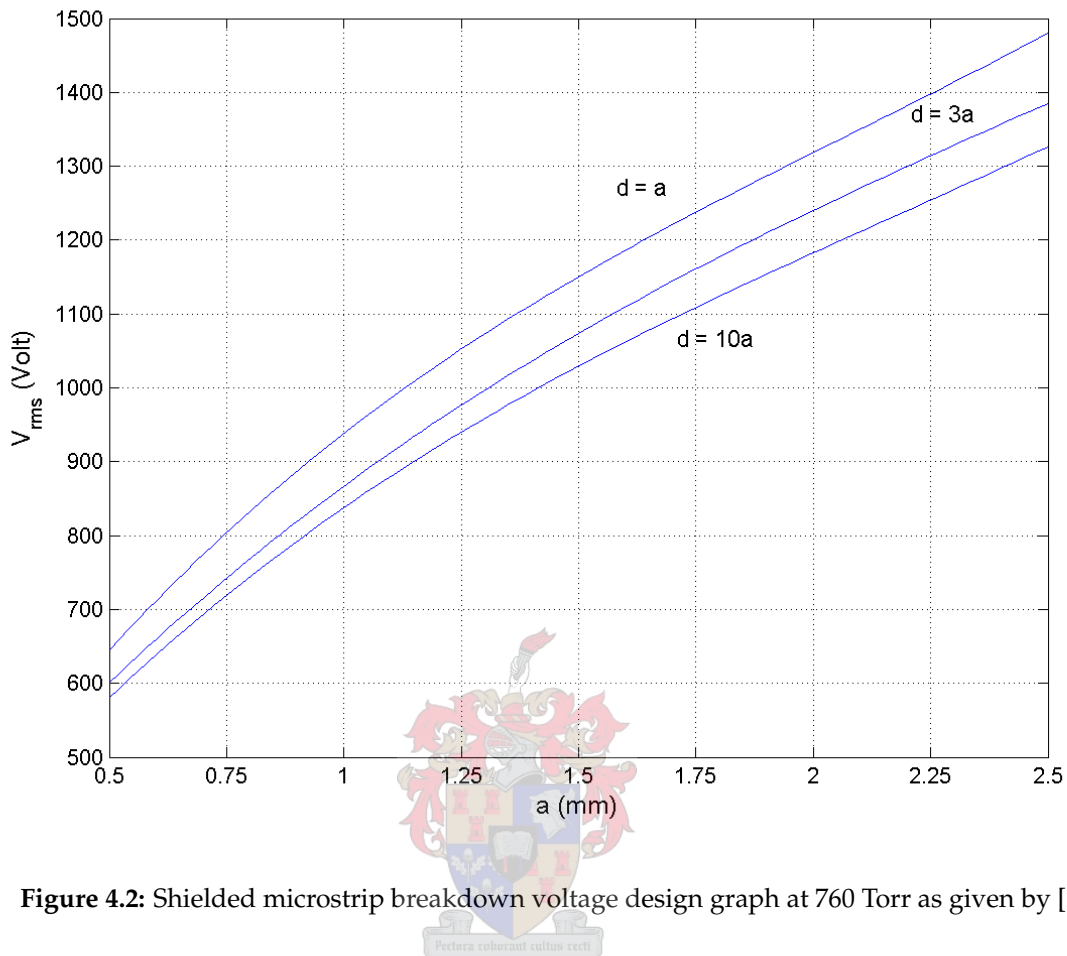


Figure 4.2: Shielded microstrip breakdown voltage design graph at 760 Torr as given by [1].

losses are known, the temperature rise of the centre conductor is calculated with the formulas provided in Section 4.3.3.

Section 4.3.4 provides a comparison between the thermal performance of two different Taconic substrates as well as the effect of surface roughness on centre conductor heat rise.

4.3.1 Stripline Transmission Line Losses

To calculate the thermal performance of stripline it is necessary to know the losses of the transmission line. Dielectric losses are calculated with

$$\alpha_d = \frac{F_d}{2} \frac{2\pi}{\lambda} \quad (Np/unit\ length) \quad (4.3.1)$$

where F_d represents the dielectric dissipation factor ($\tan\delta$) specified by substrate manufacturers.

The centre conductor losses are calculated through the use of Wheeler's incremental inductance rule [25] which states that the change of reactance caused by the penetration of magnetic flux into the conductor, is related to the effective resistance in the line. By calculating the change in

characteristic impedance from the lossless to the lossy scenario caused by the skin depth (δ_s), the conductor loss can be calculated.

Attenuation due to conductor losses are given by ([15],p97) as

$$\alpha_c = \frac{R_s \Delta Z_0}{\delta_s \eta Z_0} \quad (Np/unit\ length) \quad (4.3.2)$$

where ΔZ_0 is the change in characteristic impedance when all conductor walls are receded by a distance $\delta_s/2$, δ_s is the skin depth (meters), $\eta = \sqrt{\mu_0/\epsilon}$ is the intrinsic impedance of the dielectric (Ω) and R_s is the surface resistivity of the conductor in ($\Omega/square$).

4.3.2 Impact of Conductor Surface Profile

The impact of the conductor surface profile on transmission line attenuation should be considered when designing high power circuits [26]. In printed circuit boards, the conductor is supplied as copper foil which is laminated to the substrate material and for the purpose of adhesion, the bottom side of the foil is made to have a surface profile (roughness). This profile is important for the mechanical strength of the dielectric/conductor interface and has a significant influence on the thermal stability and reliability of the circuit.

Several grades of profile are available and surface roughness can vary between as little as 0.3 and as large as 2 microns. A trade-off should be made between better surface roughness, meaning less loss, and mechanical strength.

An empirical formula exists [27] which corrects the conductor loss for the inclusion of the conductor surface roughness. The correction formula is given by

$$\alpha_{cond,rough} = \alpha_{conductor} \left(1 + \frac{2}{\pi} \arctan \left(1.4 \left(\frac{R_{RMS}}{\delta_s} \right)^2 \right) \right) \quad (4.3.3)$$

where

$\alpha_{conductor}$ = attenuation due to perfectly smooth conductors (Np/unit length)

$\alpha_{cond,rough}$ = attenuation corrected for surface roughness (Np/unit length)

R_{RMS} = rms surface roughness (m)

δ_s = skin depth of the conductors (m)

4.3.3 Strip Transmission Line Heating

An approximation for the temperature rise of the centre conductor in stripline as used by [24] is

$$\Delta\theta_c = \frac{0.23\sqrt{\varepsilon_r}A_cP}{k\eta_0} \quad (^\circ\text{C}) \quad (4.3.4)$$

where $A_c = 8.69\alpha_c$ (dB/unit length), k is the thermal conductivity (W/(Km)), ε_r is the permittivity of the stripline substrate, η_0 is the characteristic impedance of free space (Ω) and P the average power the line is carrying (W). This equation is only valid for lines without any standing waves and when this is not the case, the centre conductor dimensions will determine how fast the heat is conducted along the axial direction of the conductor. This implies that when conductors are very thin, standing waves may give rise to hot spots.

The temperature rise in the dielectric is given by

$$\Delta\theta_d = \frac{\omega\varepsilon_0\varepsilon_rF_dV_0^2}{2k} \quad (^\circ\text{C}) \quad (4.3.5)$$

where V_0 represents the rms voltage.

4.3.4 Thermal Performance Comparison

To simplify the design process of strip transmission lines for adequate thermal performance, all the equations from the previous sections were implemented in MATLAB code (Appendix B). The characteristic impedance of stripline used in the equations is calculated with a formula derived by Cohn[28] and is only valid for line dimensions satisfying the following equation:

$$w/(b-t) \geq 0.35 \quad (4.3.6)$$

where

- w = conductor width (m)
- b = substrate thickness (m)
- t = conductor thickness (m)

Thermal calculations done with the MATLAB code were tested against values given by [24] and were identical. The effect of substrate characteristics, conductor surface profile, power and stripline dimensions on thermal performance can now clearly be investigated.

To investigate the influences of some of the substrate parameters on heat rise, the thermal performance of two Taconic substrates are calculated and compared to each other. Taconics' TLY-5 and RF-30 substrates (datasheets shown in Appendix C) with 18 μm copper cladding differ only in their specified dielectric constant, dissipation factor and thermal conductivity.

The TLY-5 substrate has an extremely low dissipation factor of 0.0009 and a very low dielectric constant of 2.2 in comparison to the 0.0014 dissipation factor and dielectric constant of 3 for the RF-30 substrate. For both these cases the dissipation factor is very good. The thermal conductivity of the TLY-5 substrate is a high 0.22 W/m/K while the RF-30 substrate is only 0.02 W/m/K less. Substrate thickness is chosen as 6.32 mm.

The calculations are performed for a 1.4 GHz, 1kW incident wave with a stripline impedance of 50Ω , with the ambient temperatures taken to be zero. Table 4.1 shows the parameters and thermal performance of the two substrate materials.

Substrate	TLY-5	RF-30
Composition	PTFE and Woven Glass	PTFE Ceramic and Woven Glass
Dissipation Factor	0.0009	0.0014
Dielectric Constant	2.20	3.00
Thermal Conductivity (W/m/K)	0.22	0.20
Surface Roughness (μm)	0.7	0.7
Substrate Thickness (μm)	6.32	6.32
Conductor Thickness (μm)	18	18
Conductor Width (mm)	5.18	4.03
Conductor Loss (dB/m)	0.23	0.28
Dielectric Loss (dB/m)	0.17	0.31
Total Loss (dB/m)	0.4	0.59
$\Delta\theta_c$ ($^{\circ}\text{C}$)	39	65
$\Delta\theta_d$ ($^{\circ}\text{C}$)	18	41
$\Delta\theta_{tot}$ ($^{\circ}\text{C}$)	56	106

Table 4.1: Thermal performance example comparison: 18 μm copper.

Although it may seem as if the differences between the material properties of the two substrates are subtle, the difference in temperature rise between them is an astounding 50°C . Considering that ambient temperature is not included in these calculations, which can be specified as high as 65° , temperatures can become problematic.

Repeating the calculation with the RF-30 substrate properties and changing the dielectric constant from 3 to 2.2, the calculated total temperature of the centre conductor drops from 106° to 73° . This proves that the dielectric constant of the substrate, which in turn determines the conductor width, has a significant effect on the thermal performance of the transmission line and should be considered when designing high power circuits.

The effect of the surface roughness on thermal performance is also worth looking at and is shown by Table 4.2. For this calculation set, the $18\mu\text{m}$ thick centre conductor is replaced with a $35\mu\text{m}$ conductor with a surface roughness of $1.6\mu\text{m}$ as specified by Taconic. The TLY-5 substrate shows an increase of 11°C while the RF-30 shows an increase of 18°C .

Substrate	TLY-5	RF-30
Composition	PTFE and Woven Glass	PTFE Ceramic and Woven Glass
Dissipation Factor	0.0009	0.0014
Dielectric Constant	2.20	3.00
Thermal Conductivity (W/m/K)	0.22	0.20
Surface Roughness (μm)	1.6	1.6
Substrate Thickness (μm)	6.32	6.32
Conductor Thickness (μm)	35	35
Conductor Width (mm)	5.13	3.98
Conductor Loss (dB/m)	0.293	0.368
Dielectric Loss (dB/m)	0.17	0.309
Total Loss (dB/m)	0.463	0.677
$\Delta\theta_c$ ($^{\circ}\text{C}$)	50	83
$\Delta\theta_d$ ($^{\circ}\text{C}$)	18	41
$\Delta\theta_{tot}$ ($^{\circ}\text{C}$)	67	124

Table 4.2: Thermal performance example comparison: 35 μm copper

The temperature calculations can also be performed for shielded microstrip with the shield height equal to the height of the substrate. Due to the poor thermal conductivity of air, temperature rise is taken as double that of the stripline case. The effective dielectric constant can be chosen as the average between the air and the substrate ([19], p350).

4.4 Power Handling Capability of Coaxial Connectors

As with transmission lines, the maximum PHC of coaxial connectors is determined by either dielectric strength or the thermal loading, depending on the particular application.

No theory is available to accurately predict the PHC of connectors and thus empirical formulas are used by manufacturers to rate their products. Therefore, published power ratings are typically conservative and results may vary from manufacturer to manufacturer due to design, materials and manufacturing.

Three popular type of coaxial connectors exist for use in high power applications. They are the SMA, N and 7/16-type connectors. Table 4.3 shows typical power and voltage ratings for these connectors [2].

While SMA-type connectors are only capable of handling a few hundred Watt of power, 7/16-type connectors can handle almost 2 kW average power and are preferred for high power applications.

When selecting an appropriate connector for a design, ambient temperature, altitude, frequency and the VSWR of the overall system should be taken into account as they will degrade

Connector Type	Working Voltage (V)	Power Rating at 1GHz (W)
SMA	335	190
N	1000	600
7/16	2700	1800

Table 4.3: Typical average power and voltage ratings of high power coaxial connectors [2].

the PHC of the connector. Derating graphs for ambient temperature are supplied by most manufacturers while some manufacturers even provide derating factors for altitudes. By using these derating factors, more realistic PHC values can be calculated, although they are not one hundred percent accurate.

As an example of the effect of the derating factor, consider a 7/16-type connector operating at 2 GHz at an ambient temperature of 60°C. According to Telegärtner [2], at 2 GHz the average power rating of the 7/16-type connector is now 1 kW and has to be multiplied by a temperature derating factor of 0.7. This results in a rating of 700 W and is much lower than the 1.8 kW given in Table 4.3.

4.5 Power Handling Capability of Resistors and Terminations

Power ratings of resistors and terminations are proportional to the size and thermal conductivity of the material used (Eq. 2.2.2). The most common substrate materials used are Beryllia (BeO) and Aluminum Nitride (AlN) with thermal conductivities of 2.5 and 1.7 watts/cm/°C respectively. Due to Beryllia's high thermal conductivity, it is still a popular choice for high power resistors and terminations. Although BeO terminations and resistors are much smaller for the same power rating than those manufactured with AlN, it should be remembered that BeO dust is classified as a hazardous substance and care should be taken when using it.

Top of the range high power resistors and terminations are capable of handling power up to the 250 W range and up to a standard 100 °C operating temperature.

4.6 Conclusion

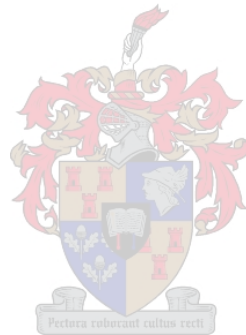
With the prediction of the peak PHC of shielded microstrip in the form of breakdown voltage, and the calculation of average power handling of stripline (shielded microstrip), excellent design considerations can be made to ensure satisfactory device operation.

The design graph provided by [1] serves as a reliable guideline for the prediction of voltage breakdown in shielded microstrip and was one of the few references that covered this topic. By

calculating the losses in the strip transmission lines, the temperature rise of the transmission lines can be calculated.

Examples of temperature measurements show the importance of a high quality substrate. A thick substrate with a low dielectric constant together with a low dissipation factor, is crucial for good thermal performance.

The selection of appropriate high power components are heavily based on the specifications given by the manufactures. For terminations and resistors the PHC is well defined, but for connectors manufacturers use a large safety margin due to the difficulty in predicting their their exact PHC.



Chapter 5

10 kW L-Band 8-Way Planar Power Combiner Design

5.1 Introduction

Before any combiner design can be considered as a practical option, considerations and decisions have to be made to ensure that it will meet the specified power requirements. These decisions include choosing the right components capable of handling the high power, as well as the layout and construction of the combiner.

In creating a good design, models of all components can be incorporated in a microwave analysis package, such as Microwave Office, capable of designing stripline circuits. These models should include connector-to-stripline transitions created by a 3D electromagnetic simulator such as CST Microwave Studio.

In Section 5.2 a basic combiner configuration is selected, chosen due to its fulfillment of critical requirements such as graceful degradation, low port mismatches and high isolation. Suitable components are chosen with regards to power handling capability in Section 5.3 and are then implemented in a complete design in Section 5.4. This section also looks at connector transitions and gives a complete circuit layout of the combiner.

All calculations and practical considerations use the design specifications for the combiner, which state a peak power rating of 10kW and an average power rating of 1kW. Maximum ambient temperature is taken as 65°C and maximum operating altitude is 3000 meters above sea level.

5.2 Basic Theoretical Design

A combination consisting of a four-way fork type combiner and four separate two-way Gysel combiners are chosen to make up the 8-way combiner as shown in the circuit diagram in Figure 5.1. The operation of these combiners is discussed in detail in Chapter 2 and makes use of Gysel-type isolation networks (Figures 5.2 and 5.3) capable of handling high power.

Unlike a corporate combiner using a network of only two-way combiners, this chosen configuration combines four signals in a single stage at the output. This implies that except for the high power, 1 kW average output section, the highest power level which has to be accommodated, is at the four-way combiner stage, carrying 250 W average power. If a corporate configuration is to be used, it will require that an additional 500 W section in between. The implementation of isolation networks, able to carry these levels of power, will be extremely difficult to achieve and are thus not a viable option.

This arrangement also has the distinct advantage of being smaller and more power efficient than a 8-way corporate power combiner and has better performance than a 8-way fork type power combiner. Figure 5.4 shows the transmission response, port reflections and isolation of the ideal 8-way power combiner. A practical high power design demonstrating this type of performance is extremely difficult to realize.

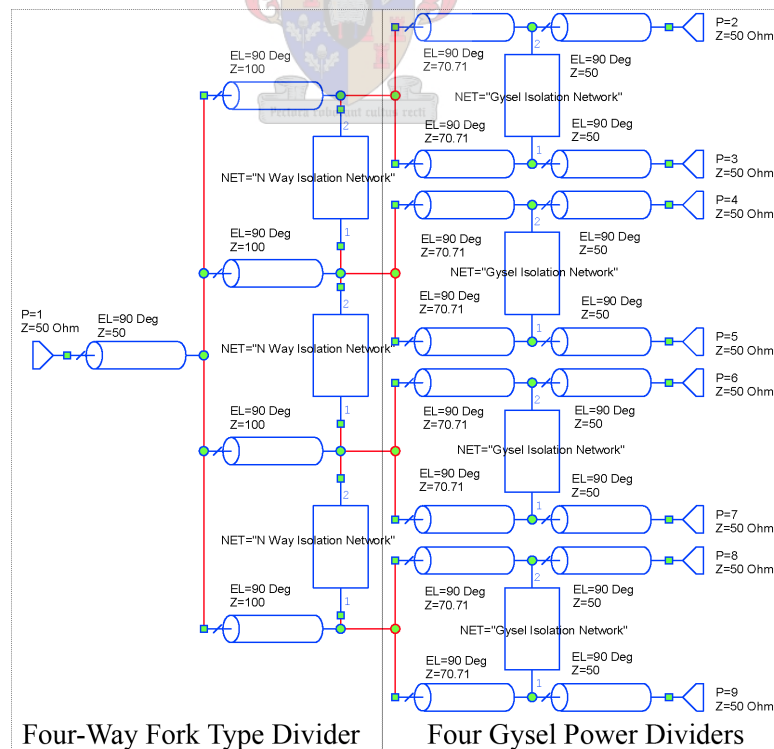


Figure 5.1: Circuit diagram of an ideal 8-way power combiner consisting of a four-way fork-type combiner and four two-way Gysel combiners.

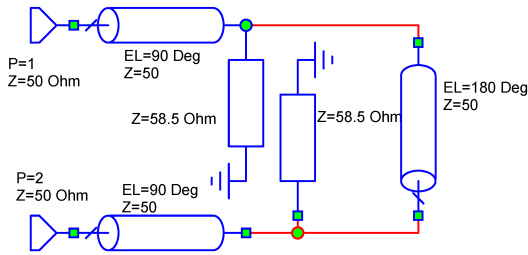


Figure 5.2: Optimised isolation network for a four-way fork-type combiner.

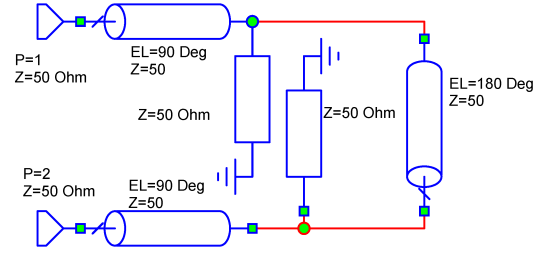


Figure 5.3: Isolation network for a Gysel combiner.

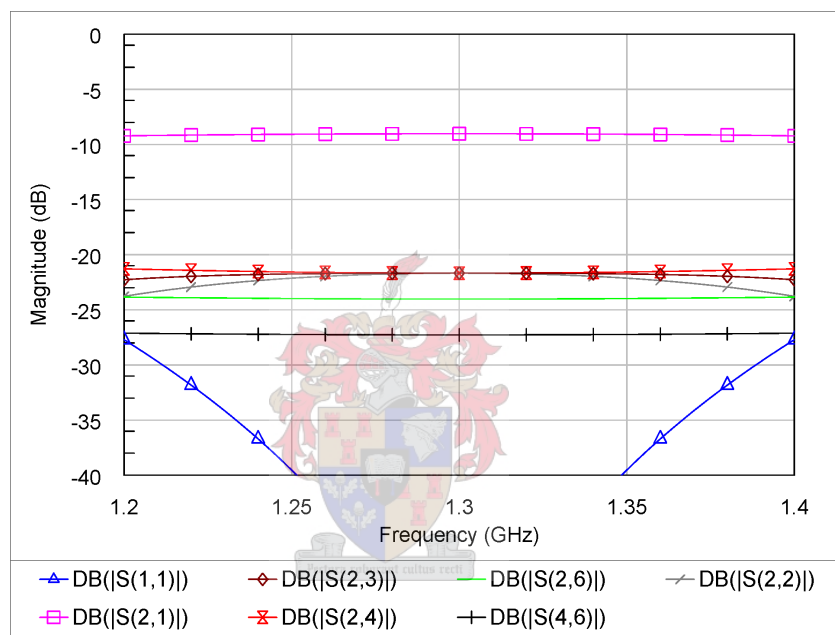


Figure 5.4: Transmission response, port reflections and isolation of an ideal 8-way combiner.

5.3 Practical Design Considerations

Many practical aspects have to be considered when designing high power circuits. These factors include power handling capability as discussed in Chapter 4 as well as the circuit layout and physical size of the combiner.

5.3.1 Substrate

Choosing the correct substrate is vital in high power applications. As illustrated in Section 4.3.4, only a low dielectric substrate with an extremely low dissipation factor and excellent thermal conductivity can be considered as an option for this design.

The power rating, together with the required size (specified design width in this case) of the

combiner, determines the choice of substrate thickness. Choosing a very thick substrate will increase the power handling capability of the transmission lines but might result in a design that is too large. Specifications for the combiner state a required design width of 420mm, which is the width of the stacking shelves where the unit amplifiers are situated.

For the basic combiner configuration chosen (Figure 5.1), four Gysel combiners are situated next to each other and thus decide the overall width of the design. Section 2.3.3 presented a shielded microstrip Gysel power combiner, designed with a Taconic TLY-5 1.58mm substrate resulting in a circuit width of about 100mm. This substrate has excellent electrical and good thermal properties (Table 5.1) and if implemented in the final design, will utilize the near maximum specified design width.

Therefore, Taconic TLY-5, 1.58 mm thick substrate with $18\mu\text{m}$ copper cladding for better surface roughness (Section 4.3.2) is chosen for the design.

Property	Value	Units
Dielectric Constant @ 10 GHz	$2.2 \pm .02$	
Dissipation Factor @ 10 GHz	0.0009	
Thermal Conductivity	0.22	W/m/K
Dielectric Breakdown	>60	kV
Dielectric Thickness	1.58	mm
Copper Thickness	18	μm
Surface Roughness RMS	0.7	μm

Table 5.1: Material and dimension properties of Taconic TLY-5 substrate to be used for the design.



5.3.2 Transmission Lines Configurations, Temperatures and Voltage Breakdown

It is decided that the combiner will consist of two types of transmission lines. The high power section, carrying the full 1 kW average power, will be implemented in strip transmission line, while shielded microstrip will be used for the lower power carrying sections.

For the sake of simplicity, the stripline section will use the same substrate as the shielded microstrip section of the design, but will consist of four substrate layers; two substrate layers above and two layers beneath the centre conductor. The two extra layers improves the power handling capability considerably and is a necessity as will be shown. Figure 5.5 shows the dimensions and implementation of the two transmission line types.

Different segments of the design carry different power levels as the eight inputs are systematically combined by the two types of combiners. The average power handling capability of each of these segments will be limited by the dimensions of the lines. With the decision of an appropriate substrate in section 5.3.1, the maximum line impedances capable of handling the power can now be calculated with the MATLAB code presented in Section 4.3 for every section

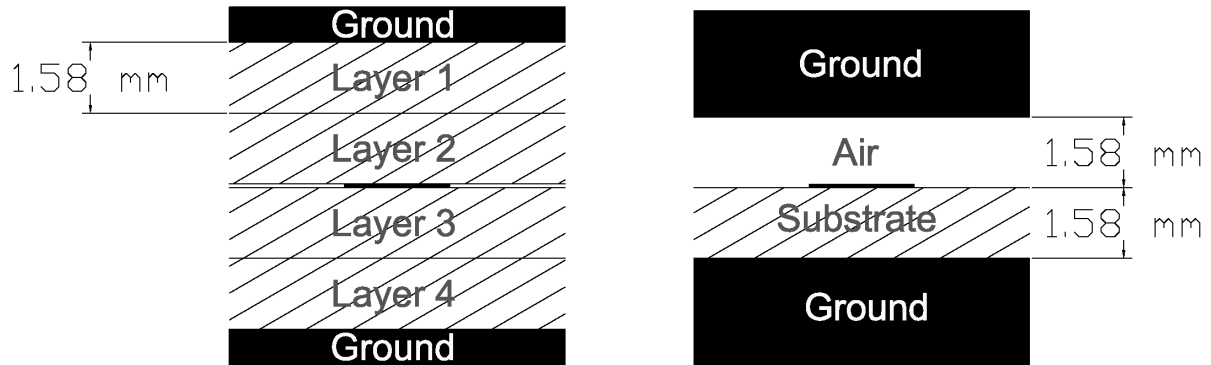


Figure 5.5: Stripline (left) and shielded microstrip (right) implementation and dimensions.

of transmission line, providing an important limit to the design. The dimensions shown in Figure 5.5 will be used for all the results to follow.

All calculations consider the worst case scenario implying an infinite VSWR at a maximum ambient temperature of 65 °C and a maximum transmission line operating temperature of 150 °C (supplied by Taconic). The infinite VSWR will have the same heating effect as double the incident power and although the infinite VSWR may seem extreme, it provides a very good and necessary safety margin. Table 5.2 gives the maximum calculated line impedance and corresponding line width for the different sections of the combiner carrying different power levels, assuming that the centre conductor may not get hotter than 150 °C. A 1.4 GHz signal is also assumed.

Transmission Line Type	Stripline		Shielded Microstrip	
Power (kW)	2	0.5	0.5	0.25
Maximum Impedance (Ω)	41	102	62	96
Linewidth (mm)	6.93	1.1	2.35	1.01

Table 5.2: Maximum line impedances capable of handling the power at the different combining sections.

Table 5.2 shows that the characteristic impedance of the stripline at the output of the combiner may not exceed 41 Ω . The basic theoretical design presented in Section 5.2, however implements a 50 Ω characteristic impedance at the output exceeding this value by a small margin. Using the MATLAB code presented in Section 4.3, it is calculated that the output strip transmission line will theoretically only be capable of handling 1.52 kW. For an incident wave of 1 kW this will imply a VSWR of 6.17 which may not be exceeded. In order to accommodate an infinite VSWR, the calculations show that the stripline substrate must be more than 10 mm thick to be able to handle a full 2 kW signal.

The calculations also show that the shielded microstrip section is not capable of handling a line impedance of more than 62 Ω for a 500 W (250 W if VSWR = 1) incident wave. According to Figure 5.1, a part of the shielded microstrip section is implemented in 100 Ω transmission lines,

also exceeding the calculated values from Table 5.2. An altered design is presented in Section 5.4.1 to improve the design with regards to these large impedance issues.

Specifications of the combiner design state that the combiner must be able to handle 10 kW of peak power and be able to operate up to a altitude of 3000 m above sea level. This information is especially important when considering the breakdown voltage of the shielded microstrip section carrying a peak power of 2.5 kW. Assuming that the minimum impedance at this section is 100 Ω (Figure 5.1), the peak voltage is calculated as

$$V_{peak} = \sqrt{2500 \times 100} = 500 \text{ V}$$

and thus 1000 V assuming an infinite VSWR.

The breakdown voltage at this section of the combiner is found through the use of the graph (Figure 4.2) from Section 4.2, giving the breakdown voltage as approximately 1670 V_{peak} at sea level. Using the derating factor of 0.69 from Section 4.2, the 3000 m altitude can be taken into account and results in a theoretically breakdown value of 1152 V. This value is 152 V higher than the infinite VSWR scenario and thus the shielded microstrip should be capable of handling the peak power.



5.3.3 Connectors

Eight connectors are needed at the 1.25 kW peak power inputs of the combiner while a single output connector is needed for the full 10 kW peak power. Only two types of connectors are considered as possible options for the design due to the large amount of power. Both the high power 7/16-type connector and N-type connector are capable of withstanding more than one kilovolt of peak power which is not the limiting factor in the design.

In general 7/16 and N-type connectors are capable of withstanding about 1.4 kW and 0.5 kW of average power respectively in the L-band frequency region. These values assume a VSWR of 1.0 and do not take ambient temperature or altitude into account and thus power derating graphs provided by manufacturers should be used.

Due to minimum quantity order regulations and availability from suppliers, a Telegärtner 7/16-type connector was chosen for the 10kW peak power output of the design. Telegärtner is however not the first choice when comparing specifications of connectors, due to much more stringent derating factors [2] when compared to other manufacturers such as Suhner [29].

Using the derating factor for an ambient temperature of 65 °C supplied by Telegärtner [2], admissible average power at 1.4 GHz is specified as about 800 W, 200 W below the desired design specification. Port mismatches will worsen the rating even more.

The power rating of a SMA-type connector plays it too close to the 125W rated inputs. Taking

the derating factor caused by the ambient temperature and altitude of operation into account [29], SMA connectors can handle about 170 W for a VSWR of 1. Assuming the same environmental conditions, N-type connectors can handle up to 340 W of average power. These larger connectors are much more robust than the SMA connectors and seem to be the better choice.

5.3.4 Solder

Lead free, high temperature solder wire with a 95% Sn, 3.8% Ag, 0.7% Cu metal composition is chosen for soldering the connectors and terminations. This alloy has a fairly high melting and solidus point of 217°C and is today's electronics industry standard, with features such as excellent thermal cycle fatigue resistance and greater strength than normal SnPb type solder.

5.3.5 Terminations

Terminations used for the design is the same as was used and modeled in Section 2.3.1. These 100 W terminations comfortably exceed the power rating needed for isolation when single input units fail. Table 5.3 gives the maximum power dissipation in isolation terminations calculated with Microwave Office for the basic circuit shown in Figure 5.1 when a single unit amplifier fails (becomes a floating input).

	Four-Way Fork Type	Gysel Type
Max Power Dissipation in Terminations (W)	22.5	39.2

Table 5.3: Maximum power dissipation in isolation terminations when a single unit amplifier fails.

It is also found that when the two adjacent units on the outer sides of the combiner fail (a whole two-way Gysel combiner), almost all the power of the adjacent two-way Gysel power combiner is dissipated in the terminations. Table 5.4 gives the maximum power dissipation in the isolation terminations when two adjacent outside units fail.

	Four-Way Fork Type	Gysel Type
Max Power Dissipation in Terminations (W)	116	0

Table 5.4: Maximum power dissipation in isolation terminations when two adjacent unit amplifiers situated on the outside fail.

This implies that the 100 W terminations will not be able to handle such severe fault conditions and 150 W terminations should rather be used. For the purpose of testing, 100 W terminations will suffice.

5.4 Prototype Design

With all the practical aspects of the design considered in Section 5.3 and suitable components chosen, a prototype is now designed.

5.4.1 Altered Theoretical Design

Although the theoretical design from Section 5.2 shows excellent performance, it is still slightly unpractical in the sense that there is not enough room for isolation networks and that some line impedances are exceeding the maximum line impedances calculated in Section 5.3.2. The $50\ \Omega$ stripline and $100\ \Omega$ shielded microstrip line impedances at the output side of the basic design (Figure 5.1) will not be able to handle the power according to Table 5.2.

These problems can be resolved by making a few adjustments to the design. By replacing the single transformer at the output with a second order Chebyshev transformer, the $50\ \Omega$ stripline output can be reduced to a lower impedance as shown in Figure 5.6. A second order Chebyshev transformer with a reflection coefficient magnitude in the passband ripple of $-45\ \text{dB}$ is used to adjust the $50\ \Omega$ line to an impedance of $35.26\ \Omega$.

To create more room for isolation networks at the four-way fork type combiner and to create a transition point between the stripline and shielded microstrip sections, $50\ \Omega$ 180° sections of transmission lines are added before and after the isolation networks. Figure 5.7 shows a circuit schematic with the implementation of the transformer as well as the added 180° transmission lines. The whole Chebyshev transformer can now be implemented in stripline while the rest of the circuit can be implemented in shielded microstrip without any impedance values exceeding the maximum calculated values.

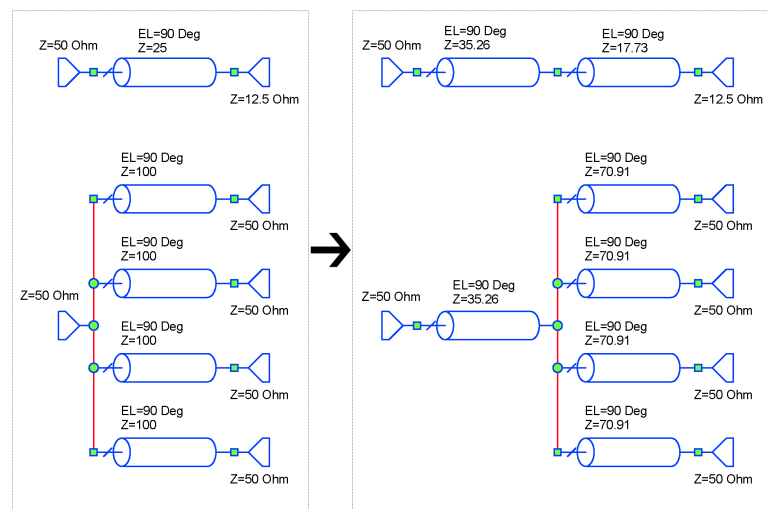


Figure 5.6: Lowering impedances with the use of a second order transformer.

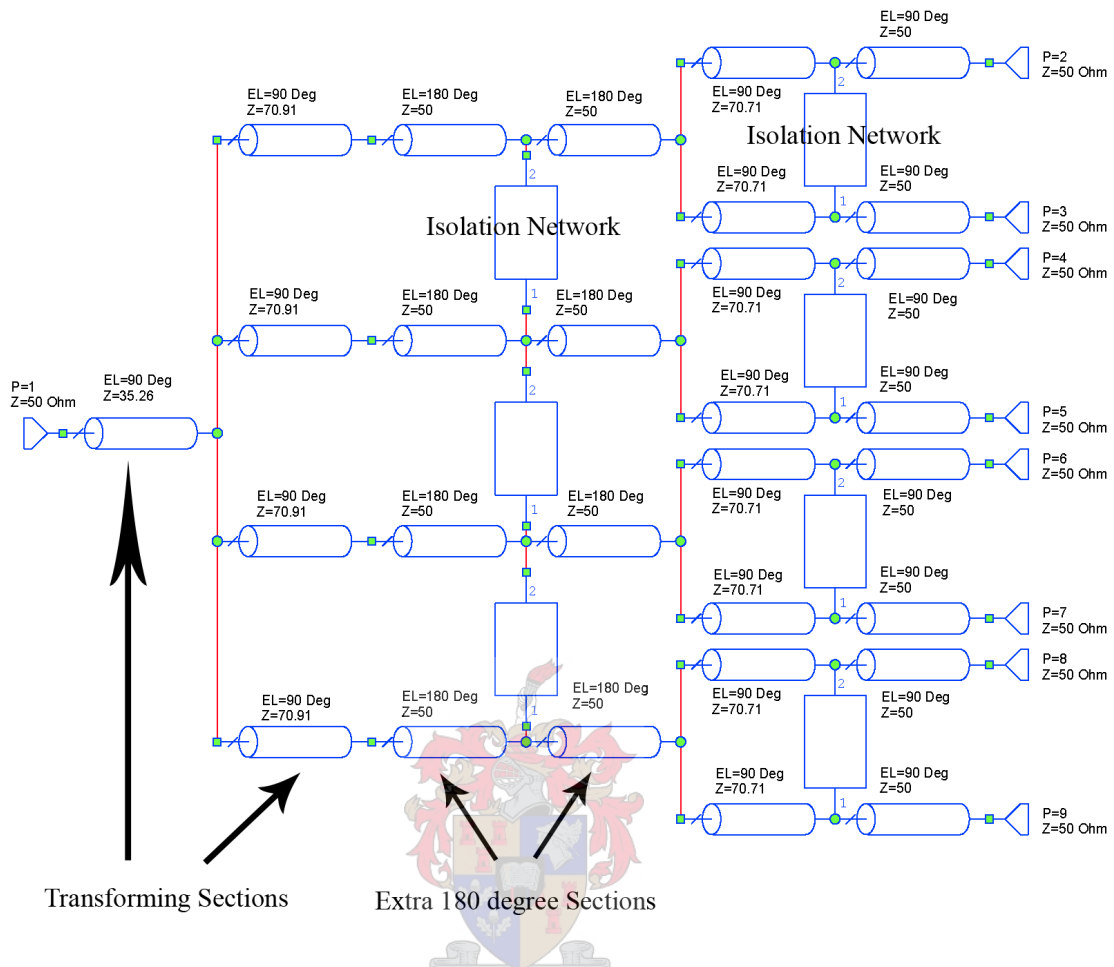


Figure 5.7: Practical theoretical design schematic using a second order transformer and 180° extension sections.

Although in theory this design may seem simple to implement, layout is still a major problem as will be shown in Section 5.4.5 where the circuit is implemented as real stripline models.

5.4.2 7/16-Type Connector Transition Design

An extremely good design is needed for the transition between the 10 W peak power coaxial connector at the output and the circuit transmission lines. Failure due to overheating or voltage breakdown are most likely to occur at this transition and thus special precaution must be taken. Good modeling of this transition will also aid in an accurate design.

CST Microwave Studio and Microwave Office are used for the design and modeling of all connector transitions.

Figures 5.8 and 5.9 show a simple representation of the 7/16-type connector that will be used together with a custom made contact pin. This particular version of the 7/16-type connector comes with a standard M3 thread for connecting a contact pin and for launching onto stripline

or other transmission line types. The endpoint of the contact pin is designed to fit tightly between substrate layers, keeping air to a minimum.

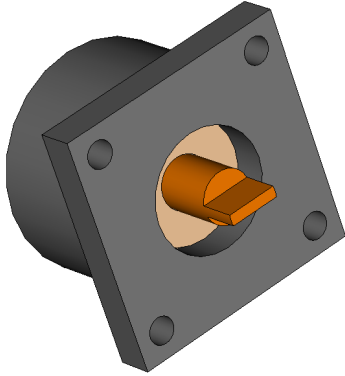


Figure 5.8: 7/16-Type connector representation with a custom made contact pin.

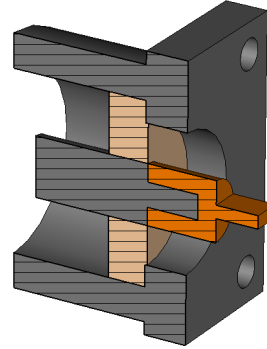


Figure 5.9: 7/16-Type connector centre cut-plane representation with custom made contact pin.

To avoid possible voltage breakdown caused by having the fairly large centre conducting pin too close to the surrounding ground planes of the stripline, an isolating section is designed which also acts as a transition between the connector and stripline circuit. This is accomplished through the use of a low permittivity foam ($\epsilon_r = 1.09$) and Teflon ($\epsilon_r = 2.04$) washer which surrounds the centre pin as shown in Figure 5.10. Both of these materials can handle tens of kilovolts and will ensure that no breakdown occurs at these points. A low permittivity foam is used to keep mismatch as small as possible as this area will normally be air. The washers are positioned within an aluminium enclosure which is designed for a low reflection transition. With the thermal conductivity of the Teflon washer (0.25 W/m/K), heat dissipation at the transition is improved.

The dimensions of the isolating washers and aluminium enclosure were found through optimisation with CST Microwave Studio to keep the connector setup 50Ω . Figure 5.11 shows the isolation network drawn with Microwave Studio with the port reflection in Figure 5.12. Port reflections of the voltage isolating section are very good, being less than -40 dB at 1.4 GHz .

The whole connector to 35.26Ω stripline transition is also simulated in CST Microwave Studio to be used as a S-parameter model in Microwave Office. This simulation also takes into account the effect of Silicon gel inserted in the open space surrounding the centre conductor of the connector to improve heat dissipation. Common Silicon gel has a typical thermal conductivity of 0.6 W/m/K and a dielectric constant of 11.9 . Figure 5.13 shows a cross section view of the simulated transition.

Figure 5.14 shows a photo of the 7/16-type connector with its manufactured voltage isolating section.

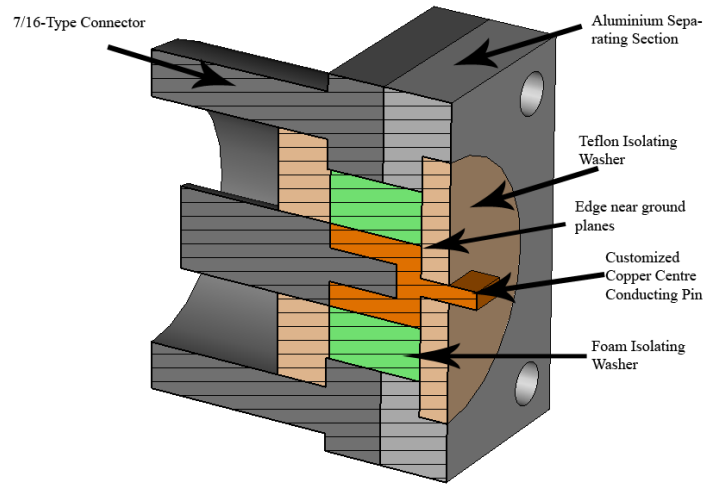


Figure 5.10: 7/16-Type connector implementation to avoid voltage breakdown and to ensure good heat flow.

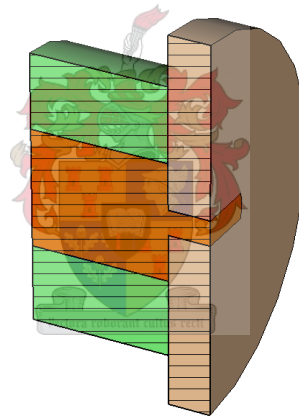


Figure 5.11: Foam and Teflon™ washer simulated with CST Microwave Studio.

5.4.3 N-Type Connector Transition Design

A S-parameter model of the N-type connector is also created with CST Microwave Studio, and as with the 7/16-type connector design, precaution is taken to ensure that there is enough distance between the centre conducting pin and the shielded microstrip ground planes to prevent voltage breakdown. This is achieved through cylindrical gaps which are inserted in the ground planes above and beneath the centre pin. Figure 5.15 shows the design in CST Microwave Studio with the port reflection in Figure 5.16. Dimensions of the ground plane gaps are established through optimisation giving port reflections of less than -33 dB at 1.4 GHz.

Port reflection of the simulated junction is very good with a magnitude of -34 dB at 1.4 GHz.

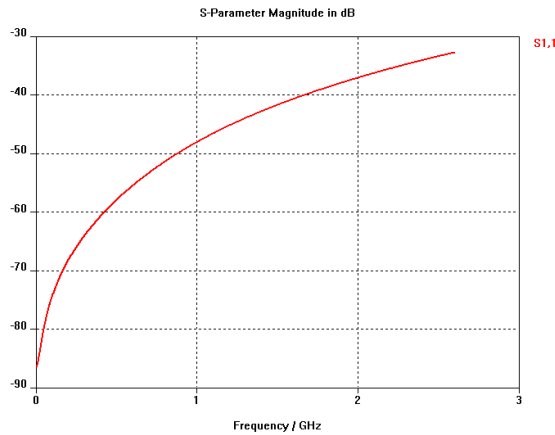


Figure 5.12: S_{11} of foam and TeflonTM isolation configuration.

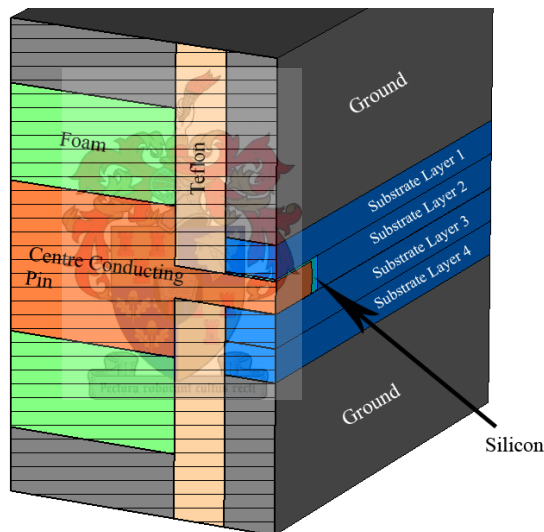


Figure 5.13: 7/16-Type connector transition simulated in CST Microwave Studio.

5.4.4 Junction Design

Using the design methods from Section 3.3.3, a S-parameter model of the four-way junction situated in the middle of the second order transformer can be created. This junction is implemented in stripline (Section 5.3.2) and uses the chosen design substrate as specified in Section 5.3.1. Figure 5.17 shows the four-way junction simulated in Feko with the meshing triangles used.

This junction gives excellent results regarding amplitude and phase difference with a difference in amplitude of less than 0.02 dB and less than 0.4 degrees for the phase. Figures 5.18 and 5.19 show the transmission response amplitude and phase of the junction.

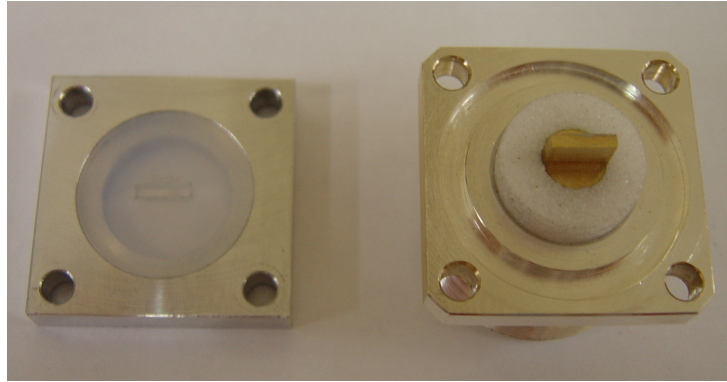


Figure 5.14: Isolating enclosure and Teflon™ washer (left). 7/16 Connector with foam washer and contact pin (right).

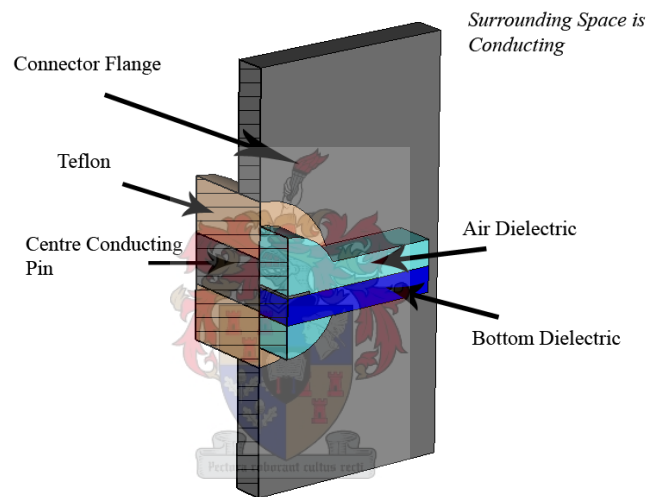


Figure 5.15: N-Type connector transition simulated in CST Microwave Studio.

5.4.5 Layout and Microwave Analysis

The simulated S-parameter models of the four-way junction and connector transitions, together with the measured S-parameter models of the isolation terminations, should assist in creating a thorough design.

Layout of the circuit was found to be the biggest limitation on the performance of the design. It is complex fitting the large isolation networks in the fork-type combiner section, as well as keeping sufficient distance between lines to avoid coupling. For the purpose of efficient heat flow, the substrate has to be mounted securely onto a large ground plane. This implies that several screws has to be used throughout the circuit without influencing performance.

With all these factors taken into account, a complete 8-way power combiner was designed with Microwave Office. The stripline as well as the shielded microstrip section of the design is analysed with the implementation of closed form stripline models. These models are also valid

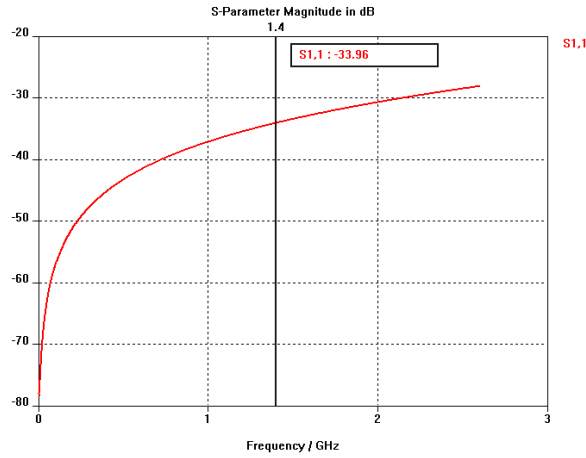


Figure 5.16: S_{11} of N-type connector transition simulated in CST Microwave Studio.



Figure 5.17: Four-way junction simulated in Feko with meshing triangles shown.

for the simulation of the symmetrically shielded microstrip section of the design due to the identical field distribution ([19],p349). For the shielded microstrip case, the average dielectric constant of the two layers is used for the stripline model (5.4.1).

$$\epsilon_{eff,stripline} = \frac{(\epsilon_{air} + \epsilon_{dielectric})}{2} \quad (5.4.1)$$

To manage the complex circuit layout, a general outline of the complete transmission line circuit is drawn and then optimized to give acceptable results. To ensure that lines do not overlap and connect seamlessly, all line dimensions are defined in terms of equations. These equations are

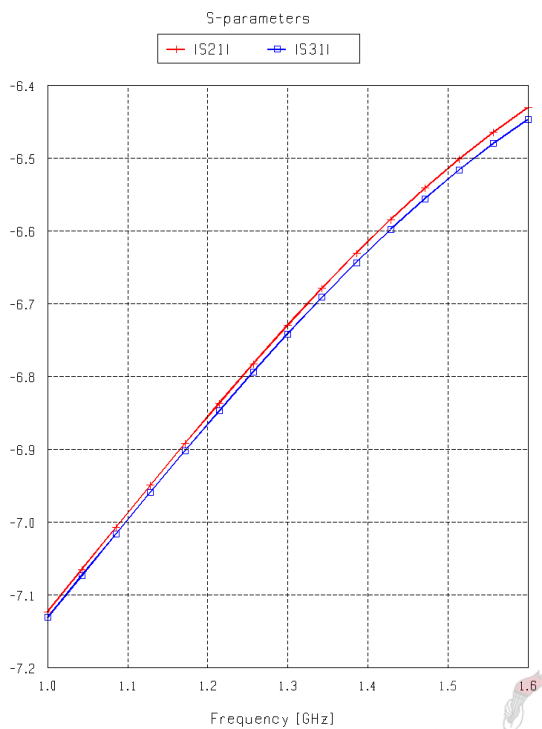


Figure 5.18: Transmission response of inner and outer strips.

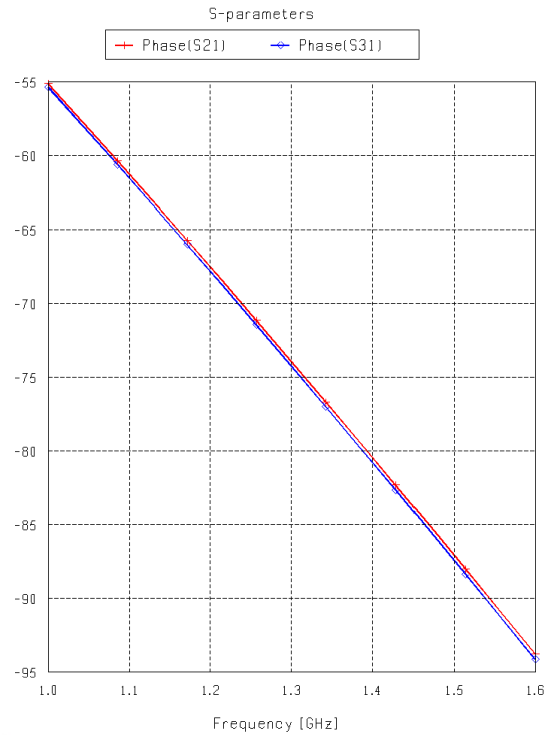


Figure 5.19: Phase response of inner and outer strips.

used to force the transmission lines to comply with the general outline shape chosen. Changing a single value, will thus change all other dimensions and ensure that intersections join correctly.

With all the component models put into place and with Microwave Office's optimizing tool used to aim for certain performance goals across the design frequency range, a satisfactory layout and circuit design is realised. Performance goals include a input port mismatch of less than -23 dB, output ports mismatch of less than -20 dB and a insertion loss of zero dB. Without the use of an optimizing tool, layout will be extremely difficult and will most likely result in a much larger system. Figure 5.20 shows the transmission line circuit layout after optimisation.

It should be noted that the extension lines between the fork-type combiner and Gysel combiners are not the same length which means that this phase difference should be compensated for when operating the unit amplifiers. For this particular design, phase difference at center frequency between the outer two-way Gysels and inner two-way Gysels are given by Microwave Office as 211.3° . Phase compensation at the input of the unit amplifiers is much easier to achieve due to the low power at this point and can be accomplished by the use of a power combiner where the length of the output lines compensates for the phase difference.

Microwave Office analysis results of the complete design implementing all component models are shown by Figures 5.21, 5.22 and 6.5. Port reflection at the output is less then -23.2 dB while reflections at all the input ports are less then -19.5 dB. Transmission response shows a

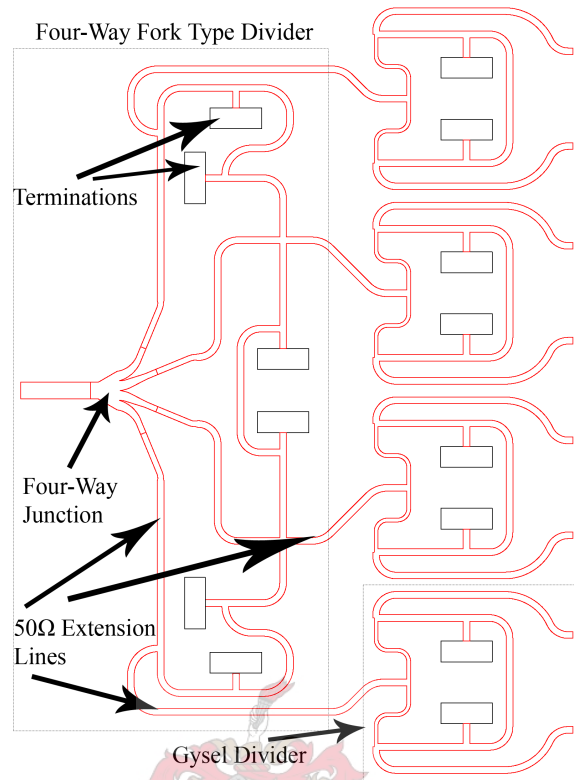


Figure 5.20: Circuit layout of the 8-way combiner design.

maximum loss of 0.8 dB and that minimum isolation between output ports is better than -18 dB. These theoretical results are found to be acceptable, when comparing them to the ideal case as depicted in Figures 5.4.

Graceful degradation is an important aspect of the design's performance. When one unit amplifier fails it should not radically affect the output power of the combiner. Before investigating the graceful degradation of the design, the efficiency of the combiner must be known for the faultless case. Figure 5.24 shows the output power of the design assuming that eight 125 W 50 Ω working unit amplifiers are connected to the inputs. Efficiency of the combiner is lowest at 1.4 GHz with a value of 86% and considering the size and complexity of the design, it is quite acceptable.

Unit amplifier failures are easily investigated in Microwave Office and are simulated by simply disconnecting that particular port. Figure 5.25 shows the average output power of the combiner when one of the center four unit amplifiers should fail, while Figure 5.26 shows the average output power when a unit amplifier of one of the outermost gysel sections should fail.

When a whole Gysel section fails, output power will fall to the levels shown by Figures 5.27 and 5.28.

Table 5.5 shows a summary of the effect of various faults on the performance of the combiner. When a single unit amplifier fails (becomes a floating input), combining efficiency decreases

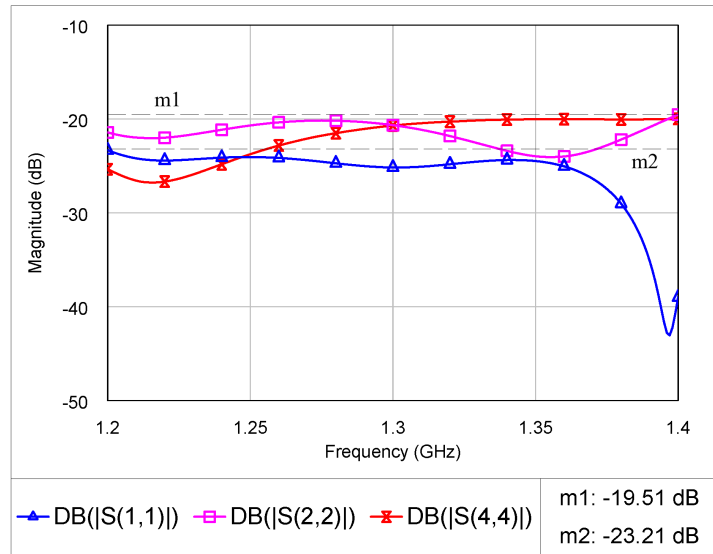


Figure 5.21: 8-Way combiner port reflections. Markers m1 and m2 give the maximum port reflections of the input ports and output port respectively.

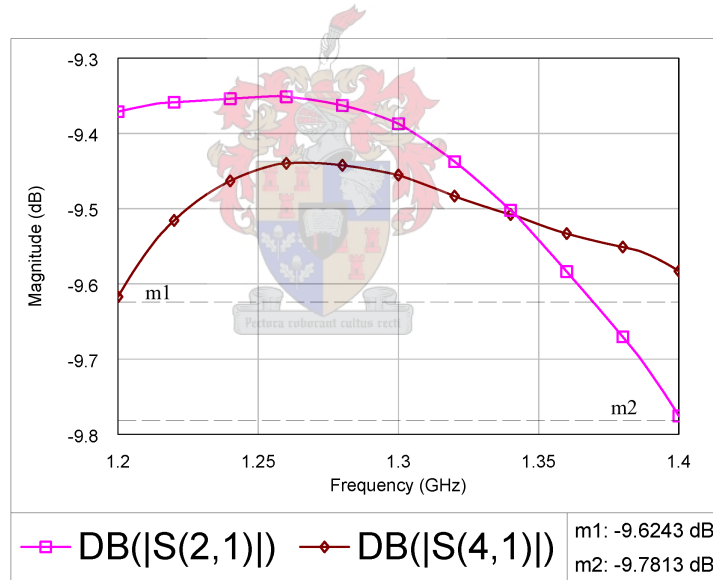


Figure 5.22: 8-Way combiner transmission response. Markers m1 and m2 give the minimum transmission response of the inner and outer Gysel sections respectively.

by up to 12%, and when two unit amplifiers of a whole Gysel combiner fails, efficiency can decrease by as much as 48%. Due to the combiner’s planar form, faults at the outsides of the combiner have more severe effects than those on the inside.

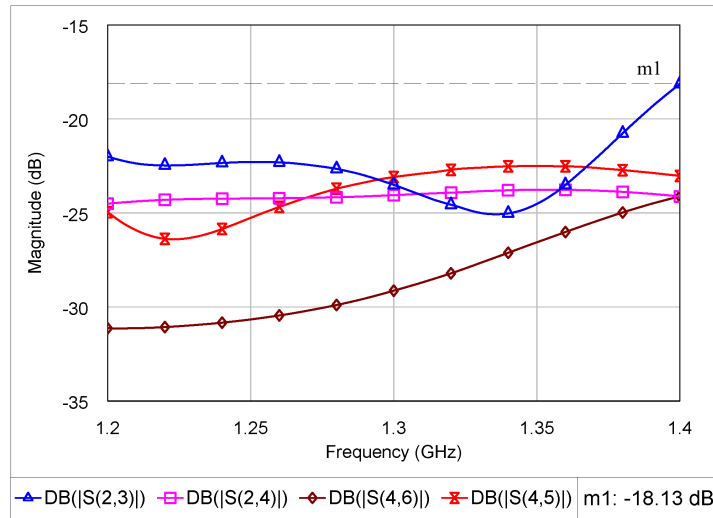


Figure 5.23: 8-Way combiner port isolation with marker m1 showing the minimum isolation mark.

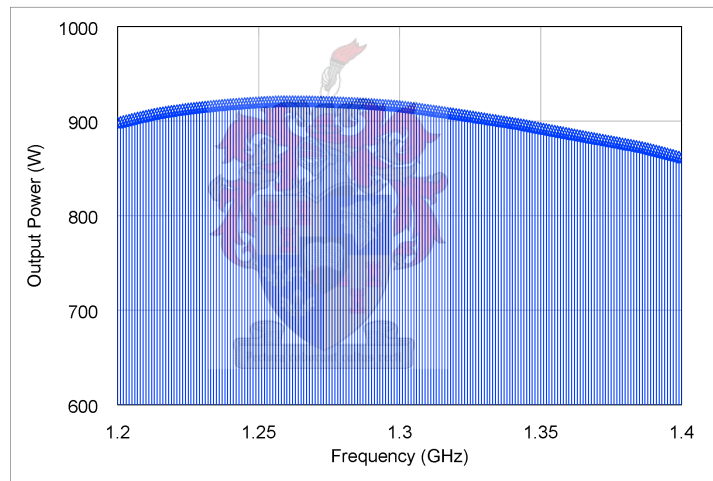


Figure 5.24: 8-Way power combiner design output power assuming 125 W unit amplifiers.

5.5 Conclusion

Although a good 8-way power combiner can easily be designed in theory, a vast number of practical aspects have to be considered. This is especially true when working with high power. The required power handling capability of connectors, terminations and transmission lines, set serious limits on the physical construction and layout of the design.

Layout of such a large combiner design is difficult due to the physical area required for isolation networks and substrate mounting screws, but can be accomplished with the help of a simulation and design package such as Microwave Office.

Models of all components and transitions can be implemented in a Microwave Office design where stripline models are used for the circuit. By defining the transmission line dimensions

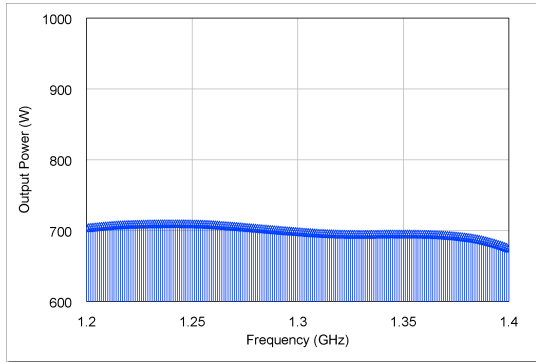


Figure 5.25: Average output power when a unit amplifier fails at one of the centre Gysel sections.

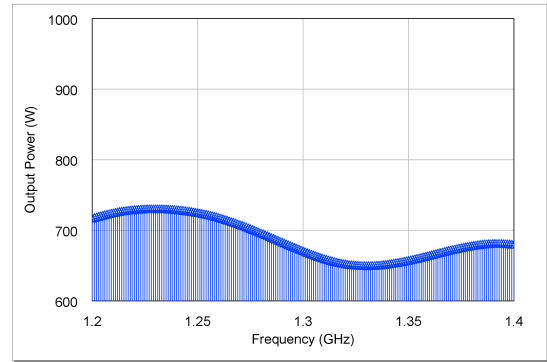


Figure 5.26: Average output power when a unit amplifier fails at one of the outer Gysel sections.

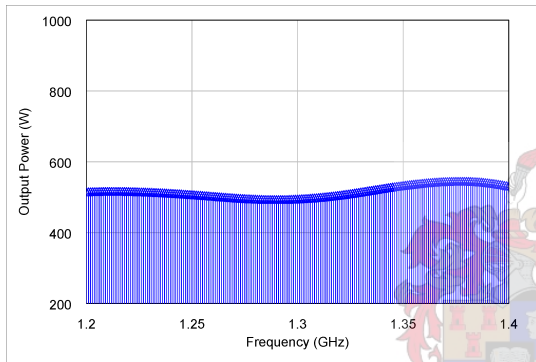


Figure 5.27: Average output power when a whole middle Gysel section fails.

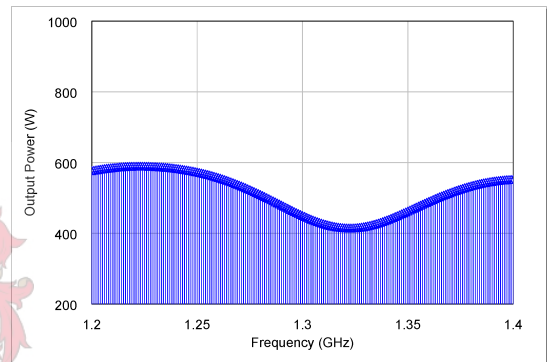


Figure 5.28: Average output power when a whole outer Gysel section fails.

Fault Condition	Combining Efficiency (%)	Output Reflection (dB)	Input Reflection (dB)
Single Middle Unit Amp	77	-15	-19.4
Single Outside Unit Amp	74	-14.8	-19.5
Two Inner Unit Amps From One Gysel	49	-10.4	-19.6
Two Outside Unit Amps From One Gysel	38	-9.9	-18.8
No Fault	86	-23.2	-19.5

Table 5.5: Simulated effect of various fault conditions on the performance of the designed power combiner.

as equations with certain constraints, the circuit layout can be forced to follow a general chosen shape where lines at intersections will always meet perfectly. This enables the effortless use of Microwave Office’s optimising tool to optimise lengths and widths of lines to some extent.

After the selection of appropriate components, an acceptable Microwave Office design was constructed which showed an efficiency of 86% when all unit amplifiers (inputs) are assumed to be working properly. The system allows for a certain level of graceful degradation and is

considered acceptable.

With all the practical aspects considered and satisfactory design-analysis results achieved, a prototype combiner can now be manufactured. Figure 5.29 shows a 3D representation of a complete power combiner with the top enclosure removed.

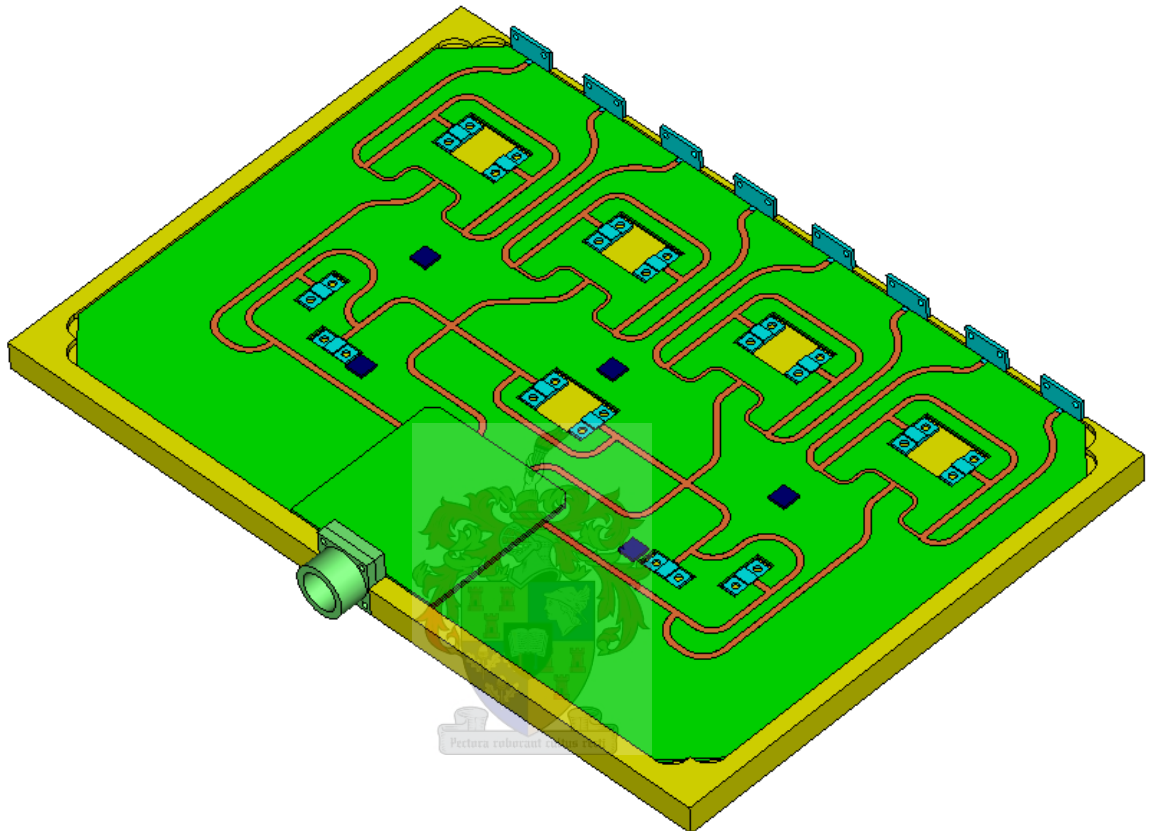


Figure 5.29: 3D Representation of the 8-way power combiner design with the top ground cover removed.

Chapter 6

Performance Evaluation

6.1 Introduction

To evaluate the complete performance of the constructed power combiner, a high power test and low power measurement has to be undertaken. A high power measurement will determine whether adequate heat flow is present in the design while a low power S-parameter measurement will measure properties such as matching, isolation and transmission response. The effects of different unit amplifier failures on the combiner can also be calculated from these measurements. No high power measurements were performed on the constructed power combiner due to time constraints and the limited availability of high power sources.

In Section 6.2 the low-power performance of the constructed combiner is measured under ideal working conditions which implies that all ports are always matched. Section 6.3 looks at the performance of the power combiner when unit amplifier failures are present.

Figure 6.1 shows a photo of an open view of the constructed 8-way power combiner with the port numbers shown as is defined in all the measurements performed. All the text in this chapter will refer to the ports as illustrated in this picture.

6.2 S-Parameter Measurement of the 8-Way Power Combiner During Normal Operation

S-parameter measurements of the combiner were performed with a Rohde and Schwarz ZVB network analyzer, consisting of various two-port measurements. During the measurements all the remaining ports are terminated with 50 Ω Huber+Suhner loads. These high quality loads have an excellent VSWR of less than 1.05 for frequencies up to 4 GHz.

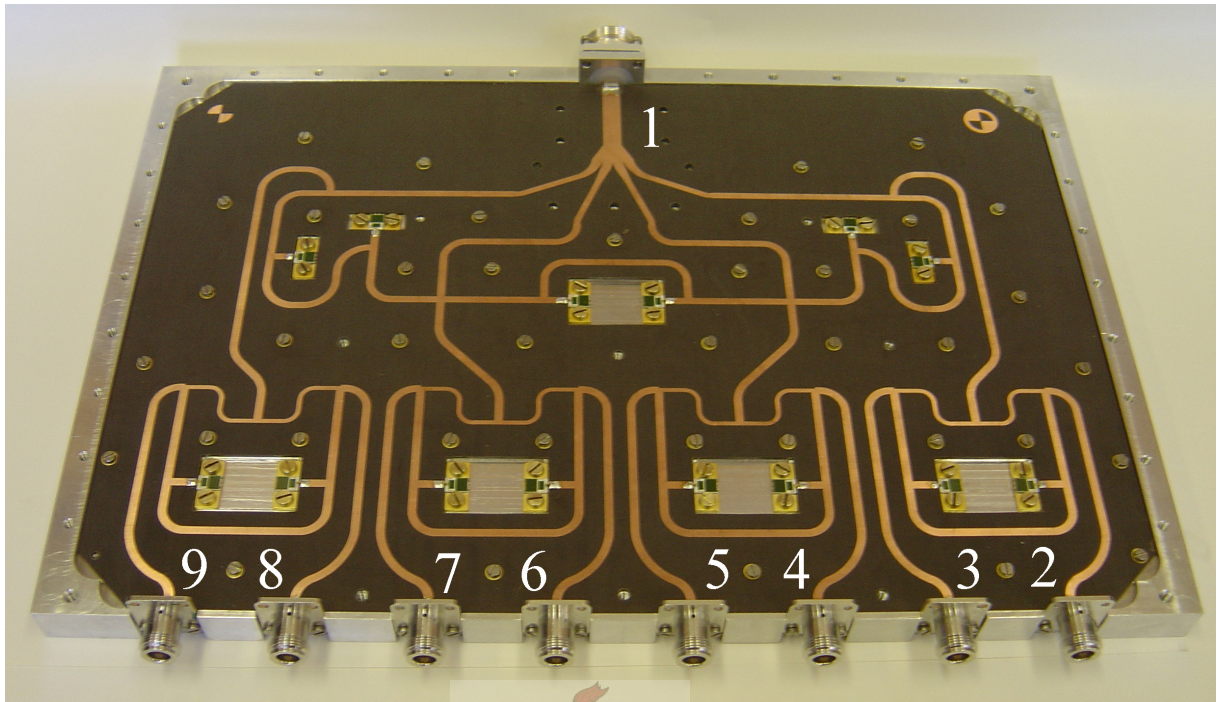


Figure 6.1: 8-Way power combiner circuit with top shield removed.

Due to the SMA calibration standards used for the calibration of the network analyzer and the use of SMA loads, all ports of the combiner have to be converted with adapters to the SMA standard. The 7/16-type output connector uses a 7/16-type to N-type adapter together with a N-type to SMA-type adapter. Both of these adapters have very good transitions with a VSWR of less than 1.07 over the combiner design frequency range and should not have a significant effect on the measurement of the device. The other 8 ports use the N-type to SMA-type adapters.

Measured port reflections give a good indication of the overall performance of the combiner and are shown in Figure 6.2. Table 6.1 gives the maximum port reflections over the designed frequency for all the ports.

Table 6.1 and Figure 6.2 show a slight imbalance between the left and right hand side of the combiner which is most likely caused by the tolerances in the manufacturing. Reflections at the input ports, especially the centre four ports (less than -21 dB), are very good, less than -16.9 dB for the worst case. Maximum input port reflections are 2.6 dB more than the values which were designed for. The output port reflection is -14.2 dB which is 9 dB larger than the designed target considered. This deviation is still acceptable when considering the large transmission line structure that was modeled. Every inaccuracy in modeling throughout the design will influence this single output reflection.

A comparison between the measured and simulated transmission response of the input ports are shown in Figure 6.3 while 6.4 shows the measured phase responses of the inputs.

The results show an unwanted resonant frequency point in the region of the 1.3 GHz centre fre-

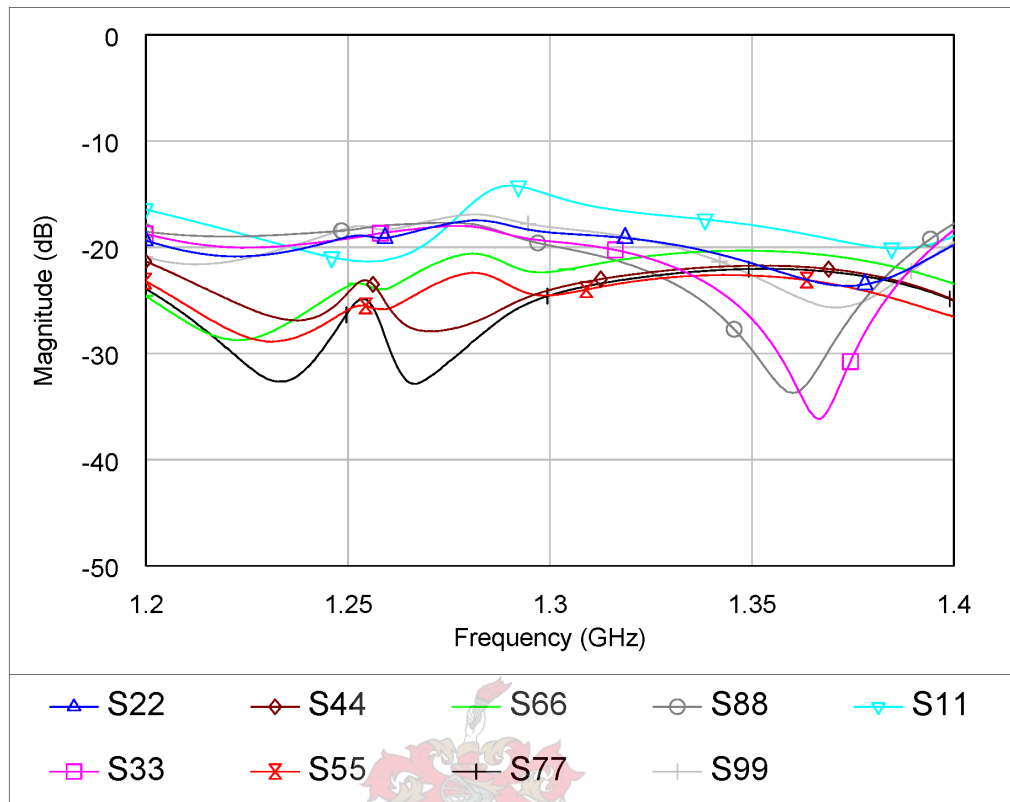


Figure 6.2: Measured port reflections of the 8-way power combiner.

	S_{11}	S_{22}	S_{33}	S_{44}	S_{55}	S_{66}	S_{77}	S_{88}	S_{99}
Port Reflection (dB)	-14.2	-17.5	-18	-21.3	-22.4	-20.3	-22	-17.7	-16.9

Table 6.1: Maximum port reflections of the 8-way power combiner.

quency as well as some port differences which should not occur. For the ideal design scenario, all measurements relating to ports 4,5,6 and 7 should be identical due to the symmetry within a two-way Gysel combiner and symmetry of the complete design, but this is not the case for the measurements. At 1.28 GHz the transmission response of ports 4 and 7 differ with 1.43 dB from ports 5 and 6 with regards to the output port 1. The difference in phase response between ports 4,5,6 and 7 is also greatest around 1.29 GHz with a value of 7 degrees. Coupling with the adjacent lines and manufacturing tolerances appears to be the only possible explanations for this phenomenon.

Initially it was thought that this effect is caused by the 210 degree phase difference between the outer Gysel combiners and the inner Gysel combiners. This means that the transmission line extensions situated at the centre ports (ports 5 and 6) effectively operate near even mode impedances, while the transmission line extensions situated at the outer Gysel ports (ports 8 and 7 together with 4 and 3) operate near odd mode impedance conditions. Using a line calculation program built into Microwave Office, it is however shown, as was designed for,

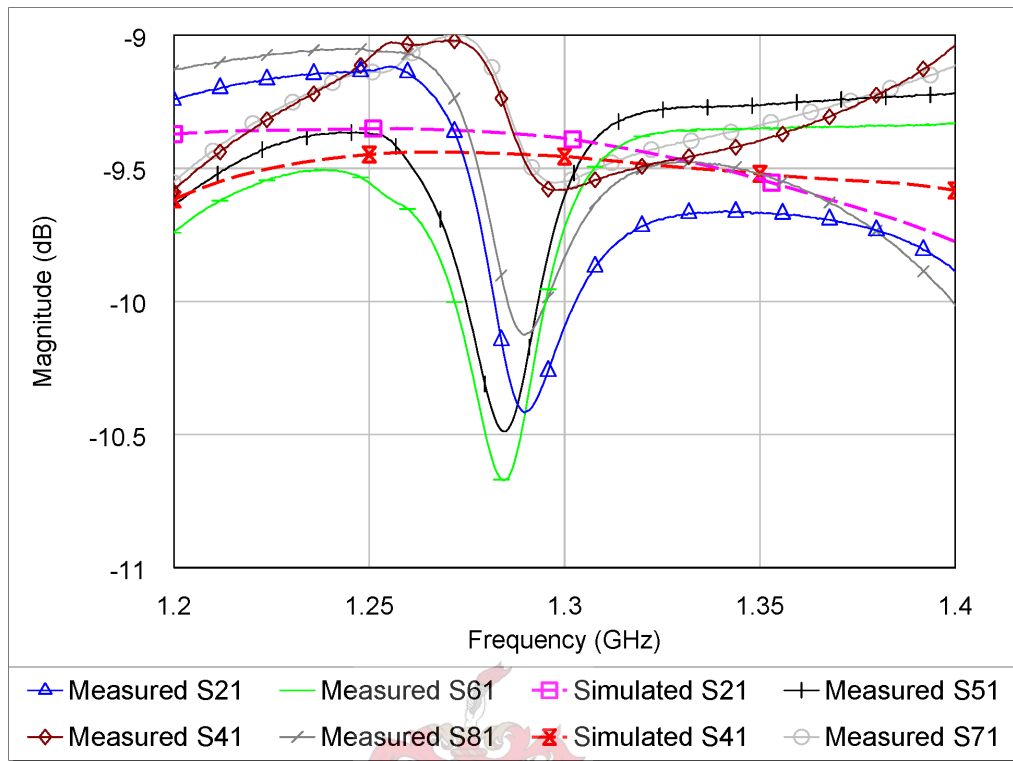


Figure 6.3: Comparison between measured and simulated transmission response of the 8-way power combiner.

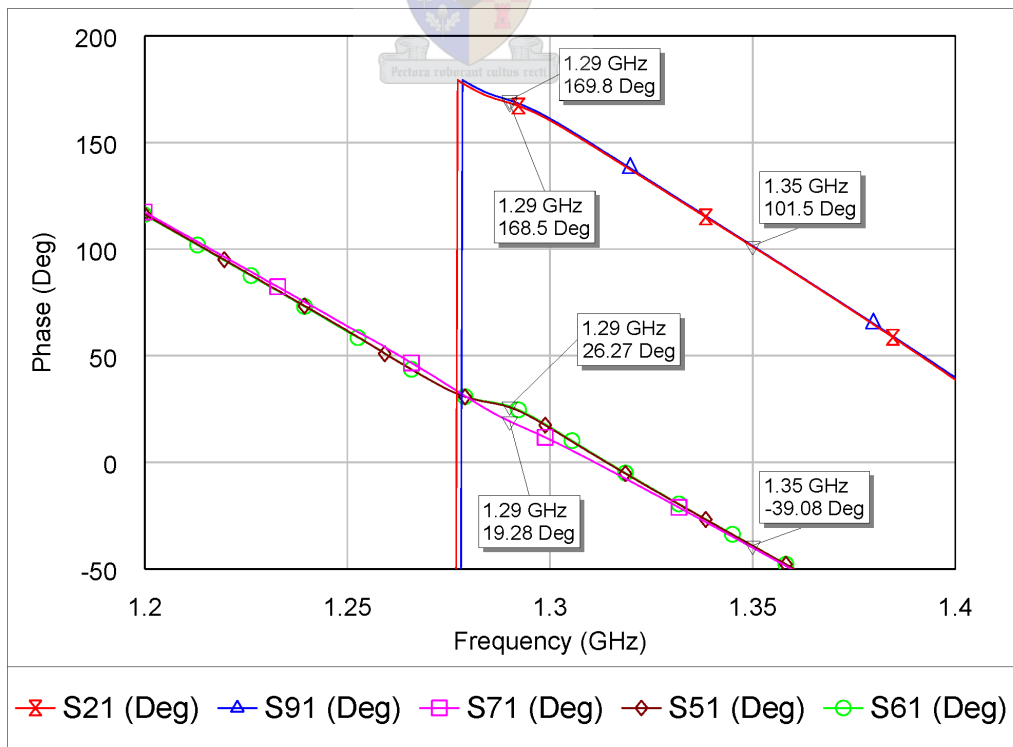


Figure 6.4: Measured phase response of the 8-way power combiner

that these lines do not couple in any way. The differences between the even and odd mode impedances of these lines are less than 0.03Ω and thus manufacturing tolerances seem to be the only logical cause for the difference.

A comparison between the measured and simulated input port isolation of the power combiner is shown in Figure 6.5. Although these values are slightly higher than designed for, isolation of 17.8 dB is still very good.

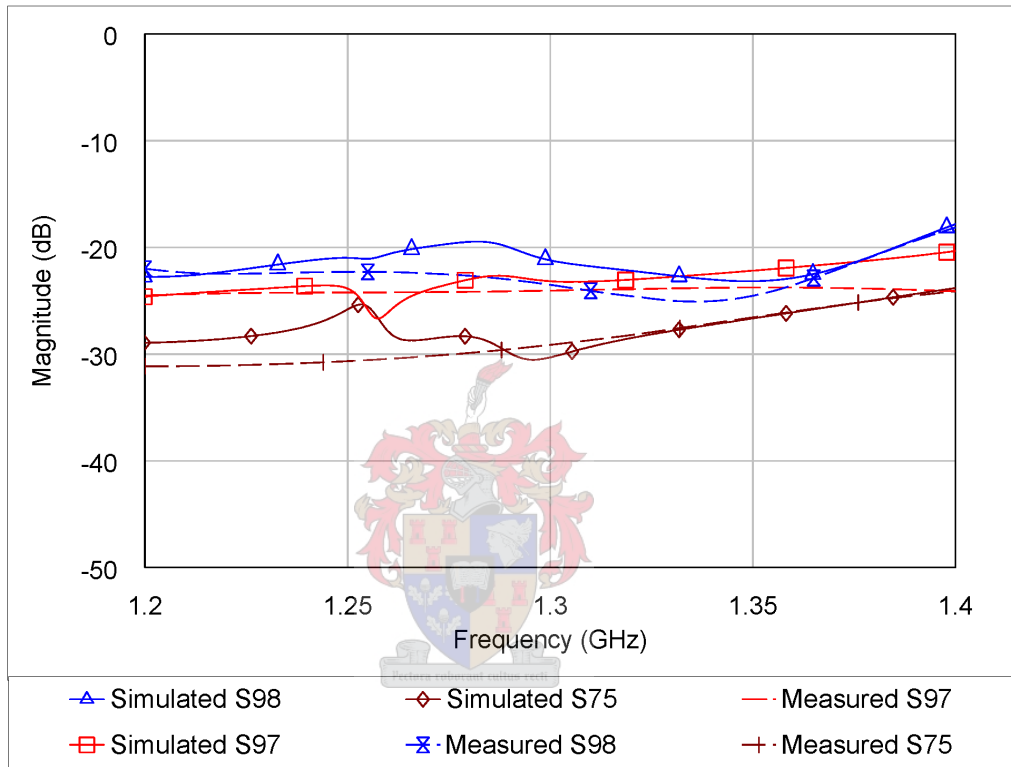


Figure 6.5: Comparison between the measured and simulated input port isolation of the 8-way power combiner

By implementing the measured S-parameters in Microwave Office, the theoretical combining efficiency of the constructed combiner can be calculated. Figure 6.6 shows a comparison between the total theoretical output power of the simulated combiner and the measured combiner assuming that 8 perfect 125 W unit amplifiers are connected to the inputs. The measured results are good, but the effect of the resonant point near the centre frequency can now be seen clearly. Power at this point drops to 781 W, implying a combining efficiency of 78% which is 8% less than the minimum combining efficiency of the simulated design. Overall combining efficiency however is quite good.

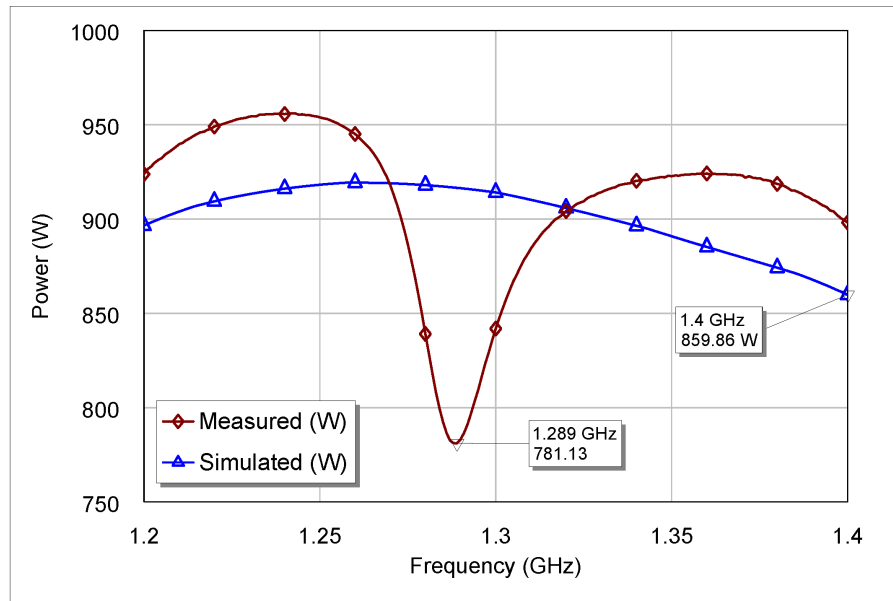


Figure 6.6: Comparison between the simulated output power and the calculated output power from the S-parameter measurement for the case where no Gysel combiner port fails.

6.3 S-Parameter Measurement of the 8-Way Power Combiner During Fault Conditions

The effect of unit amplifier failures on the performance of the power combiner is measured by removing the loads from the port or ports where the failures are supposed to occur. This is an important experiment and demonstrates the degree of graceful degradation that the combiner possesses.

The effect of four different fault conditions on the output power are investigated and consist of:

- Failure of a single outer Gysel combiner port
- Failure of a single centre Gysel combiner port
- Failure of two ports on an outer Gysel-combiner
- Failure of two ports on an centre Gysel-combiner

Figure 6.7 shows a comparison between the simulated output power and calculated output power from the S-parameter measurement for the case where an outer Gysel combiner port fails (becomes an open). Figure 6.8 shows a comparison between the simulated output power and calculated output power from the S-parameter measurement for the case where a centre Gysel combiner port fails (becomes an open).

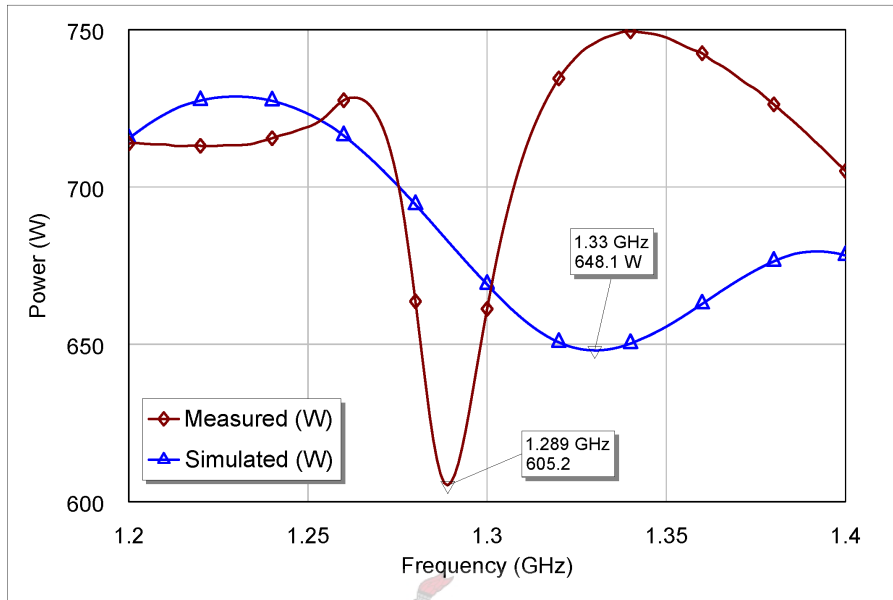


Figure 6.7: Comparison between the simulated output power and the calculated output power from the S-parameter measurement for the case where an outer Gysel combiner port fails.

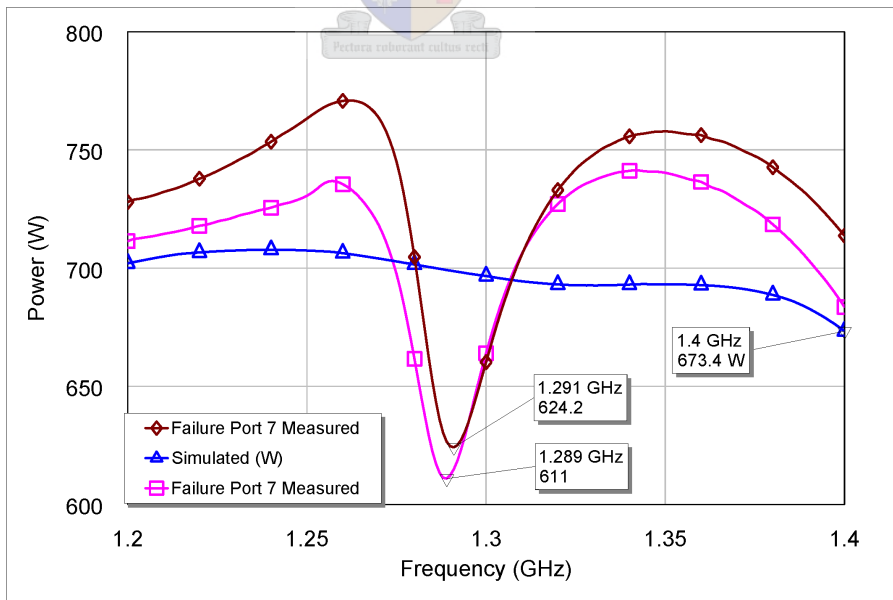


Figure 6.8: Comparison between the simulated output power and the calculated output power from the S-parameter measurement for the case where a centre Gysel combiner port fails.

Failures at an outer Gysel combiner have a larger impact on combining efficiency when compared to the centre Gysel combiner failure. The poorest combining efficiency of the combiner across the frequency range when a fault occurs at a middle Gysel combiner input is 70%, while for a fault at an outer Gysel combiner input it is 69%.

Figure 6.9 shows the effect of the serious fault conditions where the input ports of a whole outer or centre Gysel combiner fails. For the case where two unit amplifiers of an outer Gysel combiner fail and become open circuited, combining efficiency drops to 60% and for the event where two unit amplifiers of an middle Gysel combiner fail, combining efficiency drops to 63%.

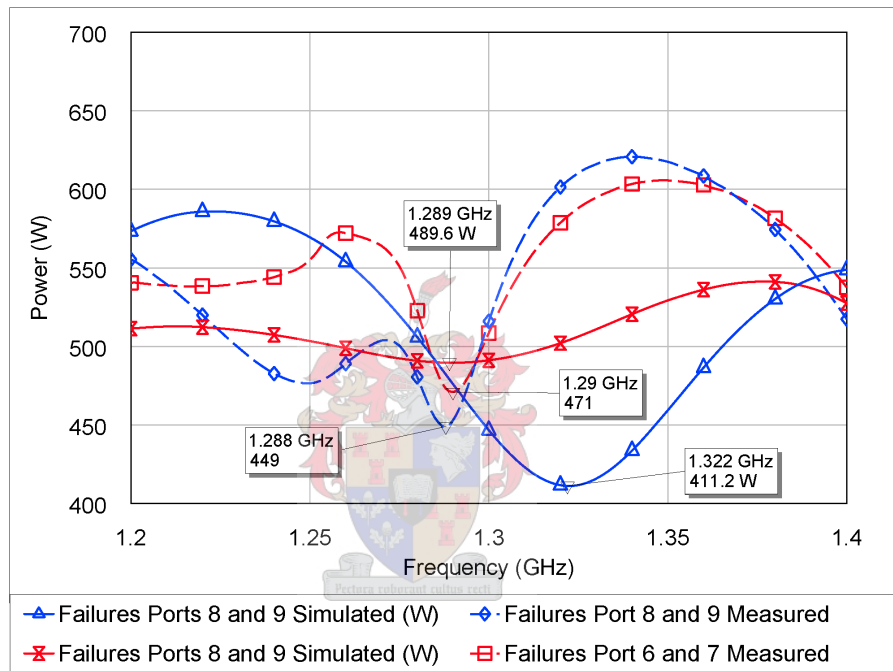


Figure 6.9: Comparison between the simulated output power and the calculated output power from the S-parameter measurement for the case where the input unit amplifiers of a whole Gysel section fails.

Table 6.2 provides a summary of the measured performance specifications and shows acceptable results although it is slightly below the predicted design performance (Table 5.5). For the scenario where a quarter of the unit amplifiers fail, combining efficiency does not drop below 60% and thus graceful degradation is achieved. Excellent input port reflections are achieved and do not drop below -15 dB, even when the output is disconnected.

6.4 Conclusion

The low power performance of the constructed 10 kW 8-way combiner is measured and compared to the Microwave Office simulated design. S-parameter measurements show satisfactory

Fault Condition	Combining Efficiency (%)	Output Reflection (dB)	Input Reflection (dB)
Single Middle Unit Amp	70	-11.7	-17
Single Outside Unit Amp	69	-11	-17.3
Two Inner Unit Amps From One Gysel	63	-8.4	-16.8
Two Outside Unit Amps From One Gysel	60	-7.5	-16.8
Output Fault			-15.8
No Fault	78	-14.1	-16.9

Table 6.2: Measured performance specifications of constructed combiner including various fault conditions.

similarity with the simulated design performance although a slight deviation around the centre frequency causes slightly poorer results. Manufacturing tolerances and construction of the design may contribute to these deviations. This assumption is made due to the fact that certain ports are not portraying the symmetry that they should.

The constructed power combiner shows, over the design frequency, very good matching (-16 dB) at all the input ports, no matter what fault conditions may occur and thus accomplishes the important goal of protecting the unit amplifiers at all times. Matching of the output port is found to be modest with a value of -14 dB.

The power combiner also shows satisfactory graceful degradation properties in the event of failing unit amplifiers. Combining efficiency decreases with only 18% when a quarter of the unit amplifiers fail.



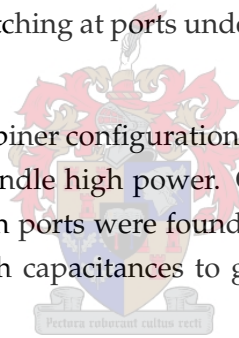
A high power measurement was not performed on the power combiner due to time constraints. To be able to test the power combiner at its full potential, extremely large power sources and extremely large loads are required.

Chapter 7

Conclusions

This study presents the design and measurement of a 10 kW L-band planar power combiner. It shows that a good 8-way, non-radial planar power combiner is realizable with properties such as graceful degradation, good matching at ports under all circumstances and acceptable power combining efficiency.

The performance of different combiner configurations was investigated with emphasis on their size, complexity and ability to handle high power. Only power combiners which implement terminations for isolation between ports were found to be adequate, due to the fact that high power resistors tend to have high capacitances to ground, causing a degradation in performance.



Various practical aspects were considered during the design. The power handling capability of components and circuit board layout were found to be major limiting factors in the combiner performance. Designing for peak power was primarily done through using experimental results from literature, while the average power handling capability of the circuit was predicted by heat flow theory. Circuit board mounting screws throughout the combiner and large isolation networks limited the freedom of the circuit board layout.

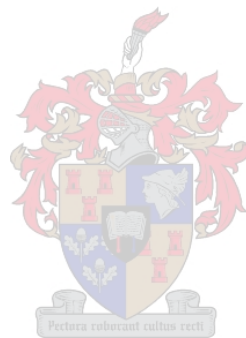
A simple, one to four-way junction design procedure was created after it was found that coupling between splitting lines are the main cause of a poor performing transmission line junctions.

Excellent microwave simulation packages exist, making it possible to model every aspect of the combiner design. Modeling of connector transitions specifically designed for high power applications was performed with CST Microwave Studio, where as FEKO was used to model the non-standard one to four-way stripline junction design.

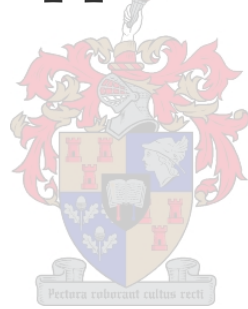
A complete combiner was designed through the implementation of these models in a Microwave Office design, where in the layout and transmission line analysis of the combiner

was performed.

The complete combiner design in Microwave Office was constructed and its performance measured at low power. Due to the lack of time and the resources, no high power tests could be performed. S-parameter measurements show an acceptable agreement between the simulated and measured results. It is felt that even better combiner specifications can be achieved through more accurate construction. Smaller tolerances concerning the manufacturing of the aluminium enclosure will ensure accurate ground plane spacing throughout the structure.



Appendices



Appendix A

MATLAB Code for Drawn DXF Junction



```
80 %Gert Fourie 2005
function [x,y] = junctiondraw(angle)

deg90 = 33.3; %length of 90 degree line

theta = deg2rad(angle); %output angles
w1 = 3.33; %output width 35.36 ohm
w2 = 7.99; %big taper input width 17.68 ohm
w3 = 1.03; %input width 70.71 ohm

L1 = w1/4;
L2 = w1/4;
L4 = w2/4;
L5 = w2/4;

length = L1 + L2; %(STARTING VALUE for optimizer)
L3 = length;
L7 = length;
L6 = length;
error = 1;
```

```

while abs(error) >= 0.01
    L3 = length;
    L7 = length;
    L6 = length;
    theta1 = pi - theta;

    L8 = sqrt(L2^2 + L3^2 - 2*L2*L3*cos(theta1));
    a = asin(L3/L8*sin(theta1));
    b = pi - theta1 - a;
    theta10 = acos((L7^2 - L4^2 - L8^2)/(-2*L4*L8));
    theta11 = pi - b - theta10 - (pi - pi/2 - theta);

    x1 = L1;
    x3 = x1 + L2;
    x4 = x3 + L3*cos(theta);
    x2 = x4 - L4*sin(theta11);

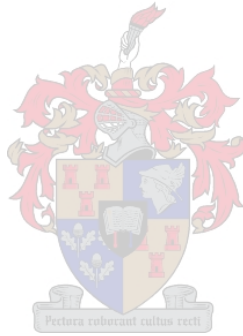
    y1 = -L3*sin(theta);
    y2 = y1 - L4*cos(theta11);
    y3 = -L6;

    L5true = sqrt((y3-y2)^2 + (x2)^2);
    error = L5 - L5true;
    if (sign(error) == 1)
        length = length + 0.01;
    end
    if (sign(error) == -1)
        length = length - 0.01;
    end
end

theta12 = pi - pi/2 - theta11;
theta13 = -atan((y3 - y2)/(x2));

anglecompout = deg2rad(247.5) - (3/2*pi-theta11)
anglecompin = deg2rad(202.5) - (pi+theta13)
lengthout = 3*L4*anglecompout;

```



```

lengthin = 3*L5true*anglecompin;
lengthratio = 1 + lengthin/lengthout

distdiff = lengthout - lengthin;

cxout = x2+3.5*L4*cos(theta12) %centre points of curve
cyout = y2+3.5*L4*sin(theta12)

cxin = 3.5*L5true*cos(theta13)
cyin = y3+3.5*L5true*sin(theta13)

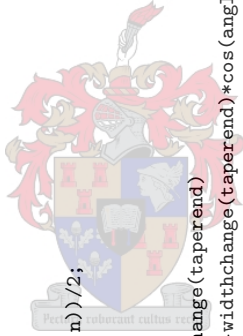
%*****Draws a discrete curves*****
n = 10; %number of increments
anglesteps = linspace(theta12,anglecompout+theta12,n);
anglesteps2 = linspace(theta13,anglecompin+theta13,n);
widthchange = (L4 - L4*linspace(1,w3/L4,n))/2;
widthchange2 = (L5true - L5true*linspace(1,lengthratio*w3/L5true,n))/2;

widthcor = L4/L5; %for unequal width divisions
taperend = round(lengthin/lengthout*n);
neighbour_1_xdiff=abs(cxout-3.5*L4*cos(anglesteps(taperend))+widthchange(taperend)
*cos(anglesteps(taperend)))-(cxout-2.5*L4*cos(anglesteps(taperend))-widthchange(taperend))*cos(anglesteps(taperend)));
neighbour_1_ydiff=abs(cyout-3.5*L4*sin(anglesteps(taperend))+widthchange(taperend)
*sin(anglesteps(taperend)))-(cyout-2.5*L4*sin(anglesteps(taperend))-widthchange(taperend))*sin(anglesteps(taperend)));
neighbour_1_diff = sqrt(neighbour_1_xdiff^2 + neighbour_1_ydiff^2) / widthcor; %dist between discrete points on outside line where inside line taper ends
inside_t_end_xdiff = abs(cxin - 3.5*L5true*cos(anglesteps2(n)) + widthchange2(n)
*cos(anglesteps2(n)) - (cxin - 2.5*L5true*cos(anglesteps2(n)) - widthchange2(n))*cos(anglesteps2(n)));
inside_t_end_ydiff = abs(cyin - 3.5*L5true*sin(anglesteps2(n)) + widthchange2(n)
*sin(anglesteps2(n)) - (cyin - 2.5*L5true*sin(anglesteps2(n)) - widthchange2(n))*sin(anglesteps2(n)));
inside_t_end_diff = sqrt(inside_t_end_xdiff^2+inside_t_end_ydiff^2);

widthchange2 = (L5true - L5true*linspace(1,neighbour_1_diff*L5true,n))/2;

for i = 1:n
    outcurve1(i) = cxout - 3.5*L4*cos(anglesteps(i)) + widthchange(i)*cos(anglesteps(i));
    outcurve1(i) = cyout - 3.5*L4*sin(anglesteps(i)) + widthchange(i)*sin(anglesteps(i));
    outcurve2(i) = cxout - 2.5*L4*cos(anglesteps(i)) - widthchange(i)*cos(anglesteps(i));
    outcurve2(i) = cyout - 2.5*L4*sin(anglesteps(i)) - widthchange(i)*sin(anglesteps(i));

```



```

incurvex1(i) = cxin - 3.5*L5true*cos(anglesteps2(i)) + widthchange2(i)*cos(anglesteps2(i));
incurvey1(i) = cyin - 3.5*L5true*sin(anglesteps2(i)) + widthchange2(i)*sin(anglesteps2(i));
incurvex2(i) = cxin - 2.5*L5true*cos(anglesteps2(i)) - widthchange2(i)*cos(anglesteps2(i));
incurvey2(i) = cyin - 2.5*L5true*sin(anglesteps2(i)) - widthchange2(i)*sin(anglesteps2(i));
end

%*****Draw straight taper*****
taperadjx1 = widthchange2(10)*cos(theta13 + anglecompin);
taperadjy1 = widthchange2(10)*sin(theta13 + anglecompin);

taperadjx2 = widthchange2(10)*cos(theta13 + anglecompin);
taperadjy2 = widthchange2(10)*sin(theta13 + anglecompin);

rectangle1 = cxin - 3.5*L5true*cos(theta13 + anglecompin) + taperadjx1;
rectangley1 = cyin - 3.5*L5true*sin(theta13 + anglecompin) + taperadjy1;
rectangle3 = cxin - 3.5*L5true*cos(theta13 + anglecompin) + taperadjx2;
rectangley3 = cyin - 3.5*L5true*sin(theta13 + anglecompin) + taperadjy2;

rectangle2 = cxin - 2.5*L5true*cos(theta13 + anglecompin) - taperadjx1;
rectangley2 = cyin - 2.5*L5true*sin(theta13 + anglecompin) - taperadjy1;
rectangle4 = cxin - 2.5*L5true*cos(theta13 + anglecompin) - taperadjx2;
rectangley4 = cyin - 2.5*L5true*sin(theta13 + anglecompin) - taperadjy2;

taperwidthdiff = (lengthratio*w3 - w3)/2;
xchange1 = taperwidthdiff * cos(theta13 + anglecompin);
ychange1 = taperwidthdiff * sin(theta13 + anglecompin);

%*****
%draw a DXF
[fid,err]=DXF_start('filename.dxf',1);

%Draw output strip
DXF_line(fid,x3,0,x3,0+deg90/10,0,0)

%Draw strip for equal lengths
DXF_line(fid,rectanglex3,rectangley3,rectanglex1+distdiff*sin(theta13 + anglecompin)

```

```
+ xchange1,rectangle1-distdiff*cos(theta13 + anglecompin) + ychange1,0,0)
DXF_line(fid,rectangle4,rectangle4,rectangle2+distdiff*sin(theta13 + anglecompin)
- xchange1,rectangle2-distdiff*cos(theta13 + anglecompin) - ychange1,0,0)

%Draw top line
DXF_line(fid,x3,0,x4,y1,0,0)

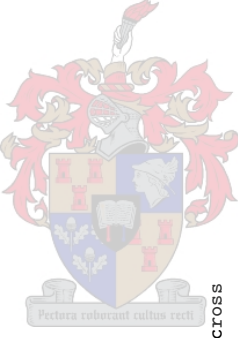
DXF_poly(fid,outcurve1,outcurve1,10,0,0)
DXF_poly(fid,outcurve2,outcurve2,10,0,0)
DXF_poly(fid,incurve1,incurve1,10,0,0)
DXF_poly(fid,incurve2,incurve2,10,0,0)

DXF_end(fid);
```



Appendix B

Thermal Performance Calculation MATLAB Code



```
51 %Gert Fourie 2005
%Heat due to dielectric loss and centre conductor loss
%Characteristic impedances are calculated by means of Cohn's large cross
%section impedance formula

function therperformC = therperformC(f,er,Fd,k,Z0,Pavg,b,t,SR)
%define constants
f = f*1e+9;
w = 2*pi*f;
P = Pavg;

e0 = 8.854e-12;
Vo = sqrt(P*Z0);
c = 2.9979e+8;
lamda = c/(f*sqrt(er));
sigma = 5.813e+7;
%b = lamda/15; %test value
b = b/1000;
%t = b/4; %test value
t = t/1000;

%rms voltage
```

```

thickness = t;
mu0 = 1.256637e-6;
roughness = SR*1e-6;
%roughness = 0;

%Calculate strip width
Cf = (0.0885*er/pi) * (2/(1-t/b) * log(1/(1-t/b)+1) - ( 1 / (1-t/b)-1 ) * log( 1/(1-t/b)^2 -1));
width = ( 94.15 / (Z0*sqrt(er)) - Cf / (0.0885*er) ) * ( 1 - t/b ) * b;

Test validity of Cohn's equations
validity = width/(b-t);
if validity <= 0.35
    valid = false;
else
    valid = true;
end

%skin effect; surface roughness is not taken into account
delta = 66/sqrt(f)/1000; %in meters

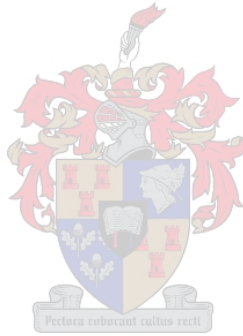
%*****
%new dimensions after skin effect on centre conductor
b2 = b ;%+ delta
t = t - delta;
width2 = width - delta;

%Work out new Z0; centre conductor loss
Cf = (0.0885*er/pi) * (2/(1-t/b2) * log(1/(1-t/b2)+1) - ( 1 / (1-t/b2)-1 ) * log( 1 / (1-t/b2)^2 -1));
Zodelta = 94.15 / ( sqrt(er) * ( width2 / b2 / (1 - t/b2) + Cf / (0.0885*er) ) );
deltaZ0 = Zodelta - Z0;

%*****
%new dimensions after skin effect on all conductors
b3 = b + delta;

%Work out new Z0; total conductor losses (includes ground losses)
Cf = (0.0885*er/pi) * (2/(1-t/b3) * log(1/(1-t/b3)+1) - ( 1/(1-t/b3)-1 ) * log( 1/(1-t/b3)^2 -1));
Zodelta = 94.15 / ( sqrt(er) * ( width2 / b3 / (1 - t/b3) + Cf / (0.0885*er) ) );

```



```

deltaZ02 = Z0delta - Z0;
%*****
eta = sqrt(mu0/(e0*er)); %Pozar page 97
Rs = 1/(sigma*delta);
beta = 2*Rs/(delta*eta); %Pozar page 97 (2.104) and (2.106)

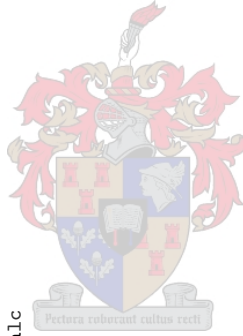
%Calculate attenuation
alphahc = beta*deltaZ0/(2*Z0);
alphahc = alphamc*(1 + 2/pi*atan(1.4*(roughness/delta)^2)); %p.98 pozar quasiempirical formula
alphan = beta*deltaZ02/(2*Z0);
alphan = alpham*(1 + 2/pi*atan(1.4*(roughness/delta)^2)); %p.98 pozar quasiempirical formula
Ad = 27.3*Fd/lambda;
Amc = alphamc*8.69;
Am = alpham*8.69;
Aground = Am - Amc;

%Calculate heat from loss using (14) and (16) PW paper
heatcentre = 0.23*sqrt(er)*Z0*Amc*P/k/(120*pi);
heatallcond = 0.23*sqrt(er)*Z0*Am*P/k/(120*pi);
heatground = heatallcond - heatcentre;
tempmax_inner_cond = (w*e0 * er * Fd * Vo^2)/(2*k); %(16)

%Display results
disp('-----Validity of Cohn's equation-----')
if (valid)
    disp(['Stripline parameters are valid ', num2str(validity), ' > 0.35'])
else
    disp(['Stripline parameters are invalid', num2str(validity), ' < 0.35'])
end

disp('-----Parameters-----')
disp(['er', num2str(er)])
disp(['f', num2str(f/1e+9), ' GHz'])
disp(['Fd', num2str(Fd)])
disp(['k', num2str(k), ' W/Km'])
disp(['b', num2str(b*1000), ' mm'])
disp(['t', num2str(thickness*1000), ' mm'])
disp(['Power', num2str(P), ' Watt'])

```



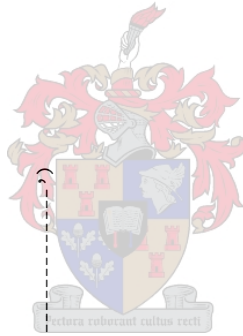
```

disp(['Voltage      ', num2str(Vo), ' Volt'])
disp(['ZO         ', num2str(ZO), ' ohm'])
disp(['width      ', num2str(width*1000), ' mm'])

disp('-----Thermal Performance-----')
disp(['Centre conductor attenuation: ', num2str(Amc), ' dB/m'])
disp(['Earthplane attenuation      : ', num2str(Amground), ' dB/m'])
disp(['Dielectric attenuation       : ', num2str(Ad), ' dB/m'])
disp(['Total attenuation            : ', num2str(Am+Ad), ' dB/m'])
disp(['Temperature increase from magnetic losses in centre conductor: ', num2str(ceil(heatcentre)), ' degrees C'])
disp(['Temperature increase from magnetic losses in earth planes      : ', num2str(ceil(heatground)), ' degrees C'])
disp(['Temperature increase from magnetic losses in all conductors     : ', num2str(ceil(heatallcond)), ' degrees C'])
disp(['Temperature increase from dielectric                            : ', num2str(ceil(tempmax_inner_cond)), ' degrees C'])
disp(['Total temperature increase (temp in earth planes are ignored): ', num2str(ceil(tempmax_inner_cond+heatcentre)), ' degrees C'])

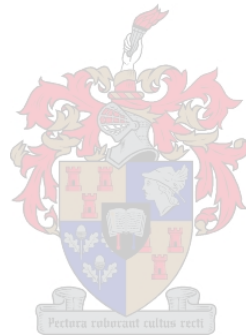
disp('-----')

```



Appendix C

Taconic Product Guide



Taconic High-Performance Material Properties

Part #	Composition	DK	DF	Volume Resistivity Mohm/cm	Surface Resistivity Mohm	Flexural Strength lbs/in ²		Moisture Absorption %	Thermal Conductivity W/m/K	Coefficient of Thermal Expansion ppm/°C			Peel Strength lbs/in 1 oz Cu	UL Rating
						Lengthwise	Crosswise			x	y	z		
TLY-5A	PTFE Woven Glass	2.17 ^(a)	0.0009 ^(a)	10 ⁷	10 ⁷	>12,000	>10,000	<0.02	0.22	20	20	280	12.0	94-V0
TLY-5	PTFE Woven Glass	2.20 ^(a)	0.0009 ^(a)	10 ⁷	10 ⁷	>12,000	>10,000	<0.02	0.22	20	20	280	12.0	94-V0
TLY-3	PTFE Woven Glass	2.33 ^(a)	0.0012 ^(a)	10 ⁷	10 ⁷	>12,000	>10,000	<0.02	0.22	20	20	280	12.0	94-V0
HT 1.5	Bonding Film	2.35	0.0025					0.005						
TLX-0	PI/E Woven Glass	2.45 ^(a)	0.0019 ^(a)	10 ⁷	10 ⁷	>23,000	>19,000	<0.02	0.14	9	12	140	12.0	94-V0
TLX-9	PTFE Woven Glass	2.50 ^(a)	0.0019 ^(a)	10 ⁷	10 ⁷	>23,000	>19,000	<0.02	0.14	9	12	140	12.0	94-V0
TLX-8	PTFE Woven Glass	2.55 ^(a)	0.0019 ^(a)	10 ⁷	10 ⁷	>23,000	>19,000	<0.02	0.14	9	12	140	12.0	94-V0
TLX-7	PTFE Woven Glass	2.60 ^(a)	0.0019 ^(a)	10 ⁷	10 ⁷	>23,000	>19,000	<0.02	0.14	9	12	140	12.0	94-V0
TLX-6	PTFE Woven Glass	2.65 ^(a)	0.0019 ^(a)	10 ⁷	10 ⁷	>23,000	>19,000	<0.02	0.14	9	12	140	12.0	94-V0
ILC-27	PTFE Woven Glass	2.75 ^(a)	0.0030 ^(a)	10 ⁷	10 ⁷	>40,000	>35,000	<0.02	0.24	9	12	70	12.0	94-V0
TLE-95	PTFE Woven Glass	2.95 ^(a)	0.0019 ^(a)	10 ⁷	10 ⁷	>35,000	>30,000	<0.02	0.20	9	12	70	12.0	94-V0
TLC-30	PTFE Woven Glass	3.00 ^(a)	0.0030 ^(a)	10 ⁷	10 ⁷	>40,000	>35,000	<0.02	0.24	9	12	70	12.0	94-V0
RF-30	PTFE Ceramic Woven Glass	3.00 ^(a)	0.0014 ^(a)	1.26 x 10 ⁹	1.46 x 10 ⁸	>13,000	>9,000	<0.02	0.20	11	21	125	>10.0	94-V0
TSM-30	PTFE Ceramic Woven Glass	3.00 ^(a)	0.0015 ^(a)	2.5 x 10 ⁸	5.6 x 10 ⁷	>6,900	>6,000	0.03	0.27	23	28	78	8	94-V0
TLC-32	PTFE Woven Glass	3.20 ^(a)	0.0030 ^(a)	10 ⁷	10 ⁷	>40,000	>35,000	<0.02	0.24	9	12	70	12.0	94-V0
TacPreg TP-32	Prepreg	3.19 ^(a)	0.0046 ^(a)					0.10						
TacLam TL-32-0040	PTFE Ceramic BT Woven Glass	3.19 ^(a)	0.0046 ^(a)	7.1 x 10 ¹⁴	10 ⁷	19,000	16,000	0.10	0.29	20	14	120	7.0	94-V0
TacLam TLG-32	PTFE Ceramic BT Woven Glass	3.20 ^(a)	0.0030 ^(a)	8.2 x 10 ⁷	1.5 x 10 ⁶	20,000	22,100	0.16	0.27	8	12	61	13	94-V0
TacLam TLG-34	PTFE Ceramic BT Woven Glass	3.38 ^(a)	0.0031 ^(a)	8.2 x 10 ⁷	1.5 x 10 ⁶	20,000	22,100	0.16	0.27	8	12	61	13	94-V0
TacLam TLG-35	PTFE Ceramic BT Woven Glass	3.50 ^(a)	0.0030 ^(a)	8.2 x 10 ⁷	1.5 x 10 ⁶	20,000	22,100	0.16	0.27	8	12	61	13	94-V0
RF-35	PTFE Ceramic Woven Glass	3.50 ^(a)	0.0018 ^(a)	1.26 x 10 ⁹	1.46 x 10 ⁸	>22,000	>18,000	0.02	0.24	19	24	64	>10.0	94-V0
RF-35A	PTFE Ceramic Woven Glass	3.50 ^(a)	0.0025 ^(a)	1.77 x 10 ⁸	2.3 x 10 ⁷	>7,600	>12,300	0.04	0.35	8	10	29	12	94-V0
RF-35P	PTFE Ceramic Woven Glass	3.50 ^(a)	0.0025 ^(a)	5.0 x 10 ⁸	3.5 x 10 ⁷	>28,000	>16,000	0.03	0.27	15	15	110	>10.0	94-V0
RF-60A	PTFE Ceramic Woven Glass	6.15 ^(a)	0.0028 ^(a)	9.0 x 10 ⁸	2.28 x 10 ⁸	>18,300	>14,600	0.02	0.54	9	8	69	8.0	94-V0
CER-10 (0.0620)	PTFE Ceramic Woven Glass	10.0 ^(a)	0.0035 ^(a)	2.1 x 10 ⁸	1.1 x 10 ⁸	>16,500	>15,500	0.02	0.63	13	15	46	>5.0	94-V0

^(a) Measured by IPC-TM-650 method 2.5.5.5 (stripline resonator) at 10 GHz
^(b) Measured by IPC-TM-650 method 2.5.5.5.1 (modified stripline) at 1.9 GHz
^(c) Measured by IPC-TM-650 method 2.5.5.5.1 (modified stripline) at 10 GHz
^(d) Measured by IPC-TM-650 method 2.5.5.6 (full sheet resonant)

All reported values are typical and should not be used for specification purposes. In all instances the user shall determine suitability in any given application.

Copper Cladding

Copper Designation	Surface Roughness R _{MS} Treated side		Surface Roughness R _{MS} Untreated side		Description	Thickness	
	Microinches	Microns	Microinches	Microns		Mils	Micrometers
RH	16	0.4	7	0.2	Rolled-Annealed 1/2 oz	0.7	17.5
R1	11	0.3	7	0.2	Rolled-Annealed 1 oz	1.4	35.0
CLH	13	0.3	20	0.5	Reverse treated Electrodeposited 1/2 oz	0.7	17.5
CL1	13	0.3	25	0.6	Reverse treated Electrodeposited 1 oz	1.4	35.0
CVH (CH)	27	0.7	11	0.3	Very Low Profile Electrodeposited 1/2 oz	0.7	17.5
CV1 (C1)	25	0.6	11	0.3	Very Low Profile Electrodeposited 1 oz	1.4	35.0
C2	77	2.0	8	0.2	Electrodeposited 2 oz	2.8	70.0

Omega Ply® and Gould Resistive foils available upon request. Please call for availability of other foils.

Heavy Metal Cladding

The following heavy metal claddings are also available upon request. Please call for availability and specification information.*

- Aluminum
- Copper
- Brass

*Taconic's heavy metals are supplied in metric measurements only.

Typical Sizes*

Typical Size		Long Laminates		Cut Sizes	
36" x 48"	914mm x 1220mm	36" x 60"	914mm x 1524mm	12" x 18"	304mm x 457mm
		36" x 76"	914mm x 1930mm	16" x 18"	406mm x 457mm
		36" x 102"	914mm x 2590mm	18" x 24"	457mm x 610mm
				16" x 36"	406mm x 914mm
				24" x 36"	610mm x 914mm

*Other sizes available upon request

List of References

- [1] P. W. van der Walt, "The breakdown voltage of shielded microstrip lines," *South African Symposium on Communications and Signal Processing, Cape Town, South Africa*, pp. 397–400, 1998. (Cited on pages xii, 39, 40, 41, and 46.)
- [2] Telegärtner, Karl Gärtner GmbH Lerchenstr. 35 D -71144 Steinenbronn, *Product Catalogue Coaxial Connectors*, 2005. (Cited on pages xv, 45, 46, and 53.)
- [3] R. A. York, "Some consideration for optimal efficiency and low noise in large power combiners," *IEEE Transactions on Microwave Theory and Techniques*, vol. 49, no. 8, pp. 1477–1482, August 2001. (Cited on page 1.)
- [4] Nai-Shuo Cheng, Pengcheng Jia, D.B. Rensch, and R.A. York, "A 120-w x-band spatially combined solid-state amplifier," *IEEE Transactions on Microwave Theory and Techniques*, pp. 2557–2561, December 1999. (Cited on page 1.)
- [5] K. J. Lee, "A 25kw solid state transmitter for l-band radars," *1979 IEEE MTT-S Int. Microwave Symp. Dig.*, pp. 298–302, April 1979. (Cited on pages 1 and 38.)
- [6] M. Hanczor and M. Kumar, "12-kw s-band solid-state transmitter for modern radar systems," *IEEE Transactions on Microwave Theory and Techniques*, vol. 41, no. 12, pp. 2237–2242, December 1993. (Cited on pages 1 and 38.)
- [7] U. H. Gysel, "A new n-way power divider/combiner suitable for high-power applications," *1975 IEEE MTT-S Int. Microwave Symp. Dig.*, pp. 116–118, May 1975. (Cited on pages 1, 3, and 38.)
- [8] A. A. M. Saleh, "Planar electrically symmetric n-way hybrid power dividers/combiners," *IEEE Transactions on Microwave Theory and Techniques*, vol. MTT-28, no. 6, pp. 555–563, June 1980. (Cited on pages 1, 17, and 23.)
- [9] K. J. Russell, "Microwave power combining techniques," *IEEE Transactions on Microwave Theory and Techniques*, vol. MTT-27, no. 5, pp. 472–478, May 1979. (Cited on pages 1 and 4.)
- [10] G. E. Nortje and P. W. van der Walt, "High performance five way power divider using shielded microstrip," *IEEE/SAIEE Symposium on Antennas and Propagation and Mi-*

- crowave Theory and Techniques AP MTTTS-90*, pp. 245–250, August 1990. (Cited on pages 1, 25, and 29.)
- [11] J. D. Hay, E. A. Kerstenbeck, D. G. Rahn, D. W. Halayko, and G. R. Painchaud, "The exploratory development of a high power s-band solid state radar transmitter," *Radar Conference*, pp. 135–140, May 1990. (Cited on page 1.)
- [12] Z. Galani and S. J. Temple, "A broadband planar n-way combiner/divider," *1977 IEEE MTT-S Int. Microwave Symp. Dig*, pp. 499–502, 1977. (Cited on pages 1, 3, 16, and 17.)
- [13] R. Lehmensiek and P. W. van der Wlat, "A compact, high-power, low-loss, l-band coaxial 18-way power divider/combiner," *Microwave and Optical Technology Letters*, vol. 16, no. 4, pp. 241–243, November 1997. (Cited on page 1.)
- [14] E. J. Wilkinson, "An n-way hybrid power divider," *IRE Transactions on Microwave Theory and Techniques*, vol. MTT-8, pp. 116–118, January 1960. (Cited on pages 1 and 3.)
- [15] D. M. Pozar, *Microwave Engineering*, Wiley, third edition edition, 2005. (Cited on pages 3, 4, 25, 26, and 42.)
- [16] R. L. Ernst, R. L. Camisa, and A. Presser, "Graceful degradation properties of matched n-port power amplifier combiners," *1977 IEEE MTT-S Int. Microwave Symp. Dig*, pp. 174–177, June 1977. (Cited on page 4.)
- [17] C. A. Engen and G. F. Hoer, "'thru-reflect-line': An improved technique for calibrating the dual six-port automatic network analyzer," *IEEE Transactions on Microwave Theory and Techniques*, vol. MTT-27, no. 12, pp. 987–993, December 1979. (Cited on page 6.)
- [18] R. Chadha and K. C. Gupta, "Compensation of discontinuities in planar transmission lines," *IEEE Transactions on Microwave Theory and Techniques*, vol. MTT-30, no. 12, pp. 2151–2156, December 1982. (Cited on page 24.)
- [19] R. K. Hoffmann, *Handbook of Microwave Integrated Circuits*, Artech House, Inc., 1987. (Cited on pages 25, 29, 45, and 61.)
- [20] James Trevelyan, "www.mech.uwa.edu.au/jpt/matlab-dxf/dxf.html," . (Cited on page 31.)
- [21] G. Matthaei, L. Young, and E.M.T Jones, *Microwave Filters, impedance-matching networks, and coupling structures*, Defam, MA: Artech, 1980. (Cited on page 39.)
- [22] E. Kuffel, W.S. Zaengl, and J. Kuffel, *High Voltage Engineering: Fundamentals*, Newnes, second edition edition, 2000. (Cited on page 40.)
- [23] K. C. Gupta, R. Garg, I. Bahl, and P. Bhartia, *Microstrip Lines and Slotlines*, Artech House, INC., second edition, 1996. (Cited on page 40.)

- [24] P. W. van der Walt, "The average power rating of single and broadside coupled striplines," *IEEE/SAIEE Symposium on antennas and propagation and microwave theory and techniques AP/MTTS-90, Somerset West*, pp. 223–230, August 1990. (Cited on pages 40 and 43.)
- [25] H. Wheeler, "Formulas for the skin effect," *Proc. IRE*, vol. 30, pp. 412–424, September 1942. (Cited on page 41.)
- [26] S. J. Normyle, T. F. McCarthy, and D. L. Wynants, "The impact of conductor surface profile on total circuit attenuation in microstrip and stripline transmission lines," *Taconic Advanced Dielectric Division*. (Cited on page 42.)
- [27] T. C. Edwards, *Foundations for Microstrip Circuit Design*, John Wiley & Sons, N.Y., 1987. (Cited on page 42.)
- [28] S. Cohn, "Problems in strip transmission lines," *IEEE Transactions on Microwave Theory and Techniques*, vol. MTT-3, no. 2, pp. 119–126, March 1955. (Cited on page 43.)
- [29] Suhner, HUBER+SUHNER AG Coaxial Connector Department 9100 Herisau Switzerland, *Suhner Coaxial Connectors General Catalogue*, 2005. (Cited on pages 53 and 54.)

